Melanocyte proliferation in wounded skin *in vitro*: a histological and immunohistochemical analysis

Morea Petersen

(PTRMOR003)

Supervisor: Prof. S.H. Kidson

Thesis presented for the degree of Master of Science in Medicine

Division of Cell Biology

Department of Human Biology

Faculty of Health Sciences

University of Cape Town

19 July 2017

Declaration

I, Morea Petersen, hereby declare that the work on which this dissertation is based is my original work (except where acknowledgements indicate otherwise) and that neither the whole work nor any part of it has been, is being, or is to be submitted for another degree in this or any other university.

I empower the university to reproduce for research either the whole or any portion of the contents in any manner whatsoever.

Signed by candidate

Signature:

Date: 19 July 2017

Acknowledgements

I would like to express my sincere gratitude to the following people for their invaluable assistance. This dissertation would not have been completed without their invaluable input:

Professor Susan Kidson, thank you for giving me the opportunity to learn new skills and to discover a newfound respect for effective scientific communication. Your passion and commitment as a mentor is exemplary. Thank you for your expert guidance, your belief in my abilities, extraordinary patience throughout this long journey and for giving me the freedom to grow and develop at my own pace.

Dr. John Common of A*Star Institute in Singapore, a special thank you for providing the cultured skin sections and for your collaboration in this project.

Mr. Declan Lunny, thank you for arranging for the samples to be couriered to SA and for so willingly providing additional information.

A/Prof. Dirk Lang, Ms Susan Cooper, and Dr. Liz van der Merwe, thank you all for your encouragement and support, and for technical assistance and training in the imaging facility.

Dr. Robea Ballo and Ms Toni Wiggins, for being such terrific friends and colleagues and for the moral and emotional support.

Thank you to Mr. Charles Harris in the HUB workshop, for making the awesome metal rack insert for me. I'm sure that future students working in the Histology Laboratory will be using it for years to come.

Thank you to all the postgrad labsters on Level 6 for your friendship and support.

A special thank you goes to the HSF Library staff, a huge thank you to all of you for assisting me with my endless requests for journal articles. To Mary and Tamzyn, a special thank you for your friendship and expert assistance. Your friendly faces and positive attitudes made the walk across to the library worthwhile.

Many thanks to NRF Grant holder bursary (Prof Susan Kidson) and UCT for provided funding for this study.

And last, but not least, a big thank you to my children, Firdoze, Ashraf, Imãn and Hanã. Thank you for being my beacons of inspiration and for your infinite support and encouragement throughout this enriching experience.

Dedication

وَمَا تَوْفِيقِي إِلاَّ بِاللهِ

My success is only by Allah

Abstract

Wounding of skin initiates a complex series of overlapping cellular events that culminates in the formation of a scar. The negative consequence of most cutaneous scars is the lack of adequate repigmentation of the neoepidermis. In order to effect successful wound healing by restoration of effective skin barrier function, keratinocytes must proliferate and migrate to cover the gap created by the wound in an efficient and timeous manner. Melanocytes are not thought to actively participate in wound repair and closure, since they are primarily responsible for maintenance of normal skin pigmentation. Mechanisms of keratinocyte migration during the re-epithelialisation phase of cutaneous wound healing have been well documented. However, it is not clear how melanocytes contribute to neoepidermis formation and repigmentation. Provision of an optimal epidermal milieu would enable restoration of pigmentation of cutaneous scars for a satisfactory cosmetic outcome. This dissertation contributes to the understanding of melanocyte participation and proliferation during re-epithelialisation of skin using an *in vitro* skin organ culture model of wound healing.

To determine whether the culture model used in this study was reliable, skin explants were cultured over a period of 12 days, fixed and processed for histological analysis. By measuring the lengths of the developing epidermal tongues, it was noted that epiboly was the initial event that occurred at the wound edges. After day two of culture, growth of the epithelial tongues was observed from the wound edges, which peaked at day five. The length of the epidermal tongues remained constant for the remaining culture period up to day twelve, at which stage complete wound closure was observed in some samples. Histological analysis of the tongues revealed that the cultured skin remained viable for the duration of culture period.

To establish to what extent keratinocyte proliferation contributed to the growth of the tongues, immunohistochemical staining using the proliferation marker, Ki67, was used. Results show that after an initial lag phase, with no detectable cell proliferation at the wound edges, dividing keratinocytes were seen at day two post-wounding. The number of dividing keratinocytes peaked at day five, where after the numbers remained constant until day twelve of culture. This result supports the validity of the culture model.

To uncover whether melanocytes re-enter the neoepidermis during wound during re-epithelialisation, the number of melanocytes per unit of basement membrane was determined using immunohistochemical staining. The melanocyte-specific marker, MART-1/MelanA, was used in conjunction with the proliferation marker, Ki-67, in an optimised dual immunolabelling protocol (Petersen et al., 2012) to establish whether melanocytes proliferate during re-epithelialisation of wounds. Melanocytes along the basal layer of the epithelial tongues and in the normal epidermis were located and counted. Basal melanocytes (MelanA+) were seen from day two onwards in the normal epidermis and from day five onwards in the developing epidermal tongues. However, at days ten and twelve of the culture period. dividing melanocytes (Ki67+/MelanA+) were seen in the epidermis in locations: proximal to the wound area, at the wound edge and in the developing tongues. This result suggests that melanocyte entry into the wound is delayed until after keratinocyte proliferation has brought about the

beginning of neoepidermis formation and growth. This result also demonstrates the proliferation potential of differentiated melanocytes and that de-differentiation of melanocytes can occur under favourable culture conditions as can be seen in this culture model.

Table of Contents

List of Figures

List of Tables

List of Abbreviations

µg	microgram
µl	microlitre
µm	micrometre
°C	degrees Celsius
BrdU	bromodeoxyuridine
BSA	bovine serum albumin
cm	centimetre
DAB	3,3'-diaminobenzidine
DAPI	4',6-diamidino-2-phenylindole, dihydrochloride
Dct	dopachrome tautomerase (see TRP-2)
ddH_2O	double distilled water
DMEM	Dulbecco's Modified Eagle's Medium
DNA	deoxyribonucleic acid
EDTA	ethylene-diamine-tetra acetic acid
EMU	epidermal melanin unit
FCS	foetal calf serum
FFPE	formalin-fixed paraffin-embedded
g	grams
G_0	gap zero phase or resting phase
G1	gap 1 phase or post-mitotic phase
H&E	Haematoxylin and Eosin
HCl	hydrochloric acid
HIER	heat induced epitope retrieval
HREC: REF	Human Research Ethics Committee Reference
IHC	immunohistochemistry
JPEG	Joint Photographic Experts Group
KCl	potassium chloride
KGF	keratinocyte growth factor
l	litre/s
M	molar

MART-1	Melanoma Antigen recognised by T-cells (see MelanA)
MelanA	Melanoma antigen (see MART-1)
mg	milligrams
MiTF	Micropthalmia-associated transcription factor
min/s	minute/s
ml	millilitres
mM	millimolar
MRC	Medical Research Council
MW	molecular weight
NDS	normal donkey serum
nm	nanometres
PBS	phosphate buffered saline
PBST	phosphate buffered saline/Tween 20
PFA	paraformaldehyde
RT	room temperature
SEM	standard error of mean
TIFF	Tagged Image File Format
Tris	Tris-hydroxymethane
TRP-1	Tyrosinase-related protein-1
TRP-2	Tyrosinase-related protein-2 (also known as Dopachrome
TYR	Tyrosinase
U	Unit
UCT	University of Cape Town
UV	ultraviolet
UVR	ultraviolet radiation

CHAPTER 1
INTRODUCTION AND LITERATURE REVIEW

1 Introduction and Literature Review

1.1 Introduction and Aims

Cutaneous wound repair is a mechanism whereby adult tissues attempt to speedily restore normal tissue structure and function following an external insult, whether it be physical, mechanical, biological, or chemical. Following cutaneous injury, restoration of blood supply, barrier function, elimination of infection and restoration of mechanical integrity to wounded site is of paramount importance. During mammalian embryogenesis, wound healing is a rapid and scar free process (Lorenz and Adzick, 1993, Richardson et al., 2013) whereas in adults, wound healing is a complex multi-step process which results in a scar (Xue and Jackson, 2015). The cosmetic and sometimes functional outcome of the actual scar itself is often not optimal due to diminished structural and tensile integrity when compared to that of normal uninjured skin (Adzick and Lorenz, 1994). In addition, these scars may be either hypo- or hyperpigmented, and factors governing both these outcomes are not well understood. The ongoing development of new cellular and molecular strategies that can recapitulate cutaneous repair, can potentially elucidate better means for improvement of patient outcomes for quality of post-surgical healing and mitigation of impaired wound healing.

Animal models have been extensively used in dermatological research but these differ from human skin both physiologically and histologically (Lebonvallet et al., 2010). Researchers therefore continuously seek alternative methods that could translate into clinical application. For example, two-dimensional monocellular culture systems or three-dimensional co-culture systems have been developed which provide relatively inexpensive and uncomplicated alternative methods to investigate certain aspects of cutaneous wound healing (Lars Steinstraesser, 2009). However, these culture systems lack all the necessary skin cell types and do not reproduce the three-dimensional histologic structure of skin. On the other hand, reconstructed skin models have the basic three-dimensional structure of skin but do not usually include all the appendages and cellular components typically found in human skin (Kataranovski and Karadaglic, 1999, Lebonvallet et al., 2010). The human skin explant model, which utilises ex vivo skin organ culture, is designed to obviate the shortcomings mentioned above.

Typically, explants are skin biopsies obtained during surgical procedures that are cultured with appropriate media under various conditions (Companjen et al., 2001). Because they lack functional nervous and vascular tissues, such tissue explants cannot entirely reproduce *in vivo* conditions. Nevertheless, skin explants have shown great potential in dermatologic research to perform *in vitro* studies that focus on the three-dimensional structure of skin, and interactions between different types of cutaneous cells (Lebonvallet et al., 2010). A robust experimental model that can recapitulate each phase of wound healing is thus essential for the development of biological strategies for clinical use. Explant culture of human skin closely resembles *in vivo*

conditions because normal skin structure and cellular elements are maintained, as well as dermal elements such as fibroblasts and collagen.

Keratinocyte participation during the re-epithelialisation phase of wound healing has been extensively studied, but the participation of melanocytes in this phase has yet to be elucidated. Little is known whether melanocytes are indeed participants during the re-epithelialisation phase of wound healing, or whether they participate only after epithelial integrity has been restored. It is also unclear whether melanocytes proliferate during this phase, along with the keratinocytes, which are primarily responsible for closing the wound or, how melanocytes enter the newly formed epidermis. To this end, a human *ex vivo* skin explant culture was utilised to investigate the role of melanocytes during the re-epithelialisation phase of wound healing.

1.2 Structure of the Skin

The human skin is the largest multifunctional organ in the human body and serves as a biological shield to protect the body from external insults such as ultraviolet radiation (UVR), infection, trauma, temperature fluctuations, and toxic chemical agents. The skin also provides an effective moisture barrier, preventing water loss and preserving internal homeostasis. Histologically, the skin is divided into three main layers: the epidermis, the dermis and the hypodermis or subcutaneous layer. The postnatal epidermis is a keratinising, stratified squamous epithelium which undergoes constant self-replenishment by the processes of epithelial regeneration and epidermal differentiation (Fuchs and Raghavan, 2002, Pincelli and Marconi, 2010). Keratinocytes, the major cellular constituent of the epidermis, are arranged in five distinct layers (Fig.1.1 a and b below) - the basal (stratum basale), spinous (stratum spinosum), granular (stratum granulosum), stratum lucidum (a clear, thin layer of flattened dead cells - thought to occur only in thick skin), and the outer corneal layer (stratum corneum). Cell proliferation actively occurs in the basal layer where the newly divided epidermal cells displace the older, more differentiated cells, which in turn, move upwards towards the outer skin surface. Other cellular residents of the epidermis include melanocytes, the pigment-producing cells, and mechanoreceptor cells, called Merkel cells, which are found along the basal layer of the epidermis (Kierszenbaum, 2012). In addition, bone marrow-derived, migratory Langerhans' cells enable immune surveillance of the skin and are found in the stratum spinosum and other suprabasal layers, although they are not exclusively confined to the epidermis (Wolff and Stingl, 1983).

Because the epidermis is ectodermal in origin, and the dermis mesenchymal, they are separated by a highly specialised extracellular matrix, the basement membrane, at the dermal-epidermal interface or the dermo-epidermal junction (Fig. 1.1 c below). Since the epidermis does not have its own blood supply, the blood vessels and cells at the dermo-epidermal junction provide nutrients to the epidermal layers (Zaidi and Lanigan, 2010). The dermo-epidermal junction comprises of several interconnected layers: the plasma membrane connects via hemidesmosomes to the lamina densa, which consist of type IV collagen fibres; the lamina densa in turn is connected to dermal collagen fibres via anchoring fibrils, that are made of type VII collagen.

In the dermis, mesenchymally-derived fibroblasts both synthesise and degrade the extracellular matrix during normal skin homeostasis and wound healing. Collagen, produced by the fibroblasts, provides structural and tensile support to the dermal components. Dermal appendages include the hair follicles and their associated sebaceous glands, sweat glands and mammary glands, which are only found in breast tissue (Romrell, 1989). Migratory cells, such as fibroblasts, macrophages and mast cells, are found throughout the dermis.

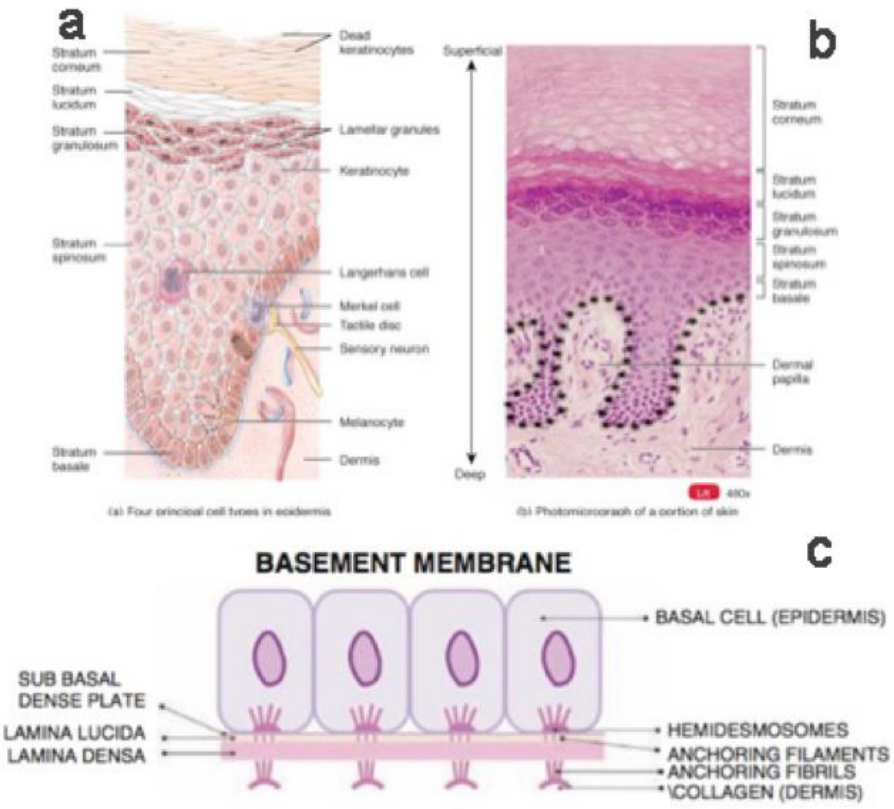

Figure 1.1 Structure of the skin.

(a) Diagrammatic representation of skin showing the cellular architecture of the epidermis with resident skin cells. (b) H&E photomicrograph of normal skin illustrating the five skin layers. Layers of the skin consist of: the dermoepidermal junction that separates the epidermis from the underlying dermis, the proliferative basal layer, and the four differentiation keratinocyte stages: spinous layer, granular layer, lucidum layer and outermost stratum corneum. (c) The dermo-epidermal junction provides nutrients to the epidermis and comprises several layers that anchor the basal cells to the basement membrane.

An additional component enabling anchorage to the extracellular matrix is provided by transmembrane receptors, called integrins. Epidermal integrins include type I hemidesmosomes that consist of plectins, tetraspanin CD151, and the bullous pemphigoid (BP) antigens 180 (also called BPAG-2 or type XVII collagen) and 230 (BPAG-1), (Margadant et al., 2010), which are transmembrane proteins, that project beneath hemidesmosomes in basal keratinocytes, thus facilitating stable anchorage to the underlying basement membrane (Masunaga et al., 1997, Powell et al., 2005, Simpson et al., 2011).. Integrins bind loosely to the extracellular matrix, but at a high concentration on the surface of the cell (Fig. 1.2 a and b). This unique binding arrangement facilitates cell movement in response to extracellular cues. If the binding affinity were increased, then cell movement would be greatly hindered or even become impossible.

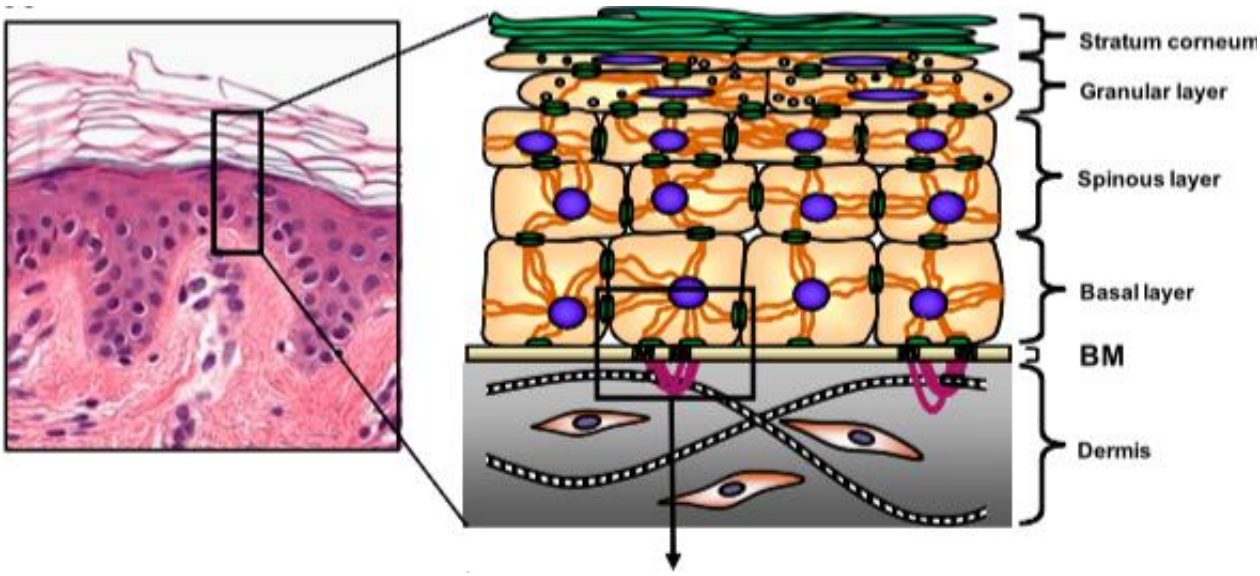

Figure 1.2 Schematic representation of epidermal integrins.

(a) Integrins link basal epidermal cells to the dermis at the dermo-epidermal junction. (b) Boxed area in (a) shows how integrins provide anchorage to basal cells at the dermo-epidermal junction in a schematic diagram at increased magnification.

1.3 Melanocyte Biology

Melanocytes are specialised, neural crest-derived, dendritic skin cells. During embryogenesis, they migrate to specific sites within the human body. Upon reaching their target sites, melanocyte precursor cells, called melanoblasts, differentiate to become mature melanocytes, which can synthesise the pigment, melanin. Melanocytes are found in the skin (basal layer of epidermis), the hair matrix, and the eye (uveal tract), where they provide cutaneous and ocular pigmentation, as well as protection against the detrimental effects of ultraviolet radiation. Melanocytes are also found in the inner ear, heart and leptomeninges of the brain, where they are thought to be essential for the normal development and functioning of these organs.

1.3.1 Melanocyte development and survival in the epidermis

Melanocyte development and survival depend on numerous signalling systems and transcription factors *for their survival and migration*. The most important signalling pathway that regulates melanocytes is the Wingless-related integration site or Wnt signalling pathway (Dorsky et al., 1998); (Dorsky et al., 2000). Wnt signalling plays a critical role in melanocyte development and is involved in the triggering of melanocyte stem cell proliferation (Guo et al., 2016, Nishimura, 2011). The G-coupled endothelin B receptor (EDNRB) and its ligand endothelin-3 (EDN3) together are also responsible for development of epidermal melanocytes (Baynash et al., 1994) (Lee et al., 2003). However, the differentiation, migration and survival of melanocytes is controlled by microphthalmia-associated transcription factor (MITF) (Hemesath et al., 1994); (Levy et al., 2006). MiTF is a basic-helix-loop-helix-leucine zipper transcription factor, that ensures the survival of melanocytes in mammalian epidermis by modulating the tyrosine kinase receptor, KIT, and its ligand, KIT-ligand (KITL)

(Wehrle-Haller, 2003, Grichnik, 2006). KIT and MiTF are closely associated in that MiTF is necessary for the maintenance of KIT expression in precursor melanocyte cells or melanoblasts. MiTF can interact directly with β-catenin, which is the key mediator of the canonical Wnt-signalling pathway and together, through a complex feedback mechanism, MiTF can modulate Wnt-signalling to control the number of genes regulated by β-catenin (Schepsky et al., 2006). Melanocyte precursor cells or melanoblasts express both KIT and MiTF (Opdecamp et al., 1997) which are both mutually exclusive genes, whereby each regulates the others expression or activity. Moreover, the presence of MiTF alone is not sufficient for the expression and activation of tyrosinase (TYR), a melanogenic protein (see section 1.2.3.1), and TYR activation requires the participation of KIT-ligand during melanogenesis (Peters et al., 2003). Therefore, the proliferation and survival of melanoblasts (melanocyte precursor cells) and their differentiation to become mature melanocytes, is dependent on KIT signalling. Furthermore, paired box-3 or PAX3 and SRY box-10 or SOX10 are two important genes which by acting together, activate MITF transcription (Kubic et al., 2008).

1.3.2 Melanin biosynthesis

Melanin is produced within melanosomes, which are specialised membrane-bound vesicles which bud off from the endoplasmic reticulum and form part of the lysosomal pathway within the melanocyte (Raposo et al., 2001) (Fig.1.1 a below). Each stage of the melanosome maturation process relates to a specific ultrastructural morphology and also to the amount of melanin synthesised. Stage II melanosomes are non-melanised, immature melanosomes, whereas stage III melanosomes are partially-melanised, but still immature. The internal matrix of these immature melanosomes is a protein-based lamellar structure with longitudinal striations, which become increasingly pigmented as the organelle matures. Fully melanised mature Stage IV melanosomes have an internal matrix that is completely masked by melanin pigment (Seiji et al., 1961, Marks and Seabra, 2001).

Melanocytes maintain close contact with neighbouring keratinocytes through cytoplasmic processes called dendrites, whereby melanin pigment (within melanosomes) is transferred to keratinocytes in the upper epidermal layers via these dendrites. The melanosomes localise over the keratinocyte nucleus, forming a supranuclear cap, thus providing photoprotection against ultraviolet radiation (Ando et al., 2012). Melanin biosynthesis begins when the key enzyme, tyrosinase catalyses the hydroxylation of tyrosine, an amino acid substrate, to L-3,4-dihydroxyphenylalanine (DOPA) (Borovansky and Riley, 2011, Hearing, 2011), followed by the oxidation of DOPA to DOPAquinone (see Fig.1.3 (b) below). In the presence of cysteine, conversion of DOPAquinone occurs, which results in the formation of pheomelanin, a reddish-yellow polymeric pigment. For eumelanin to be synthesised, two further enzymes are needed: (i) tyrosinase-related protein-1/ TRP-1 and (ii) Dopachrome tautomerase or DCT (also known as tyrosinase-related protein-2/ TRP-2). These two proteins are responsible for molecular rearrangement of DOPAchrome, which is spontaneous cyclic oxidation of DOPAquinone, to form to a stable intermediate, 5,6-dihydroxyindole-2-carboxylic acid (DHICA). Further

oxidation and polymerisation results in the formation of soluble, brown DHICA-melanin (Solano and García-Borrón, 2007). When TRP-2 is absent, catalytic activity of TYR results in the conversion of DHI to indole-5,6-quinone, which polymerises to form black, insoluble DHI-melanin (Ito and Wakamatsu, 2003, Yamaguchi et al., 2007).

1.3.3 Melanocyte-keratinocyte interaction in the epidermis

To maintain normal homeostasis of human skin pigmentation, proper melanin synthesis and the transfer of melanin to surrounding keratinocytes is crucial (see Fig. 1.3 b below). In 1963, the concept of the' epidermal melanin unit' was first proposed by (Fitzpatrick and Breathnach, 1963), whereby one basal melanocyte interacts with approximately thirty to forty neighbouring keratinocytes (Figure 1.3 a below). Through the epidermal-melanin unit, keratinocytes regulate melanocyte proliferation, dendrite formation, and rate of melanin synthesis and transfer.

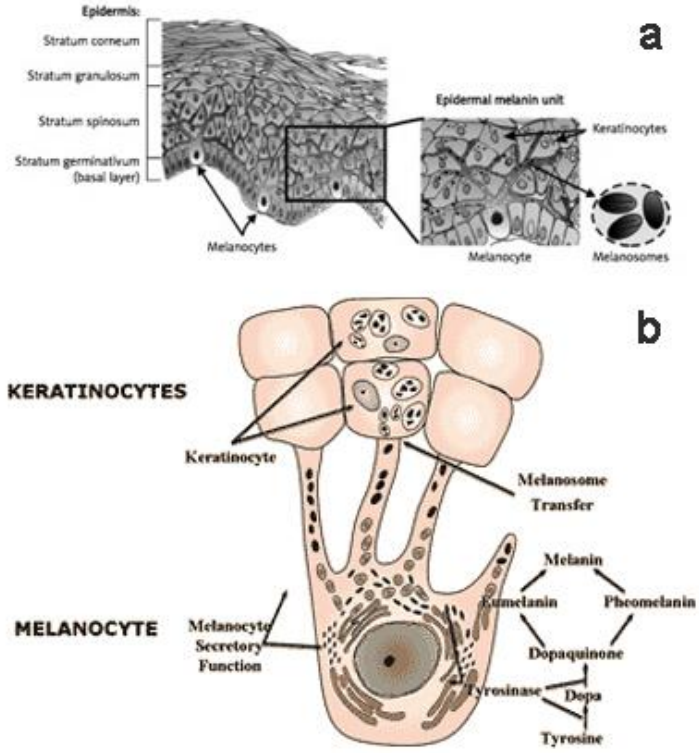

Figure 1.3 Diagrammatic representation of the epidermal-melanin unit and the melanin biosynthetic pathway.

(a) Melanocytes reside in the basal layer with a 1:10 ratio to keratinocytes and synthesise the pigment melanin within melanosomes, which are transferred to keratinocytes to provide photoprotection from UV radiation (image from Cichorek et al. (2013)). (b) Melanin biosynthesis occurs within melanosomes leading to the production of eumelanin and/or pheomelanin. Melanosomes transported to the tips of dendrites where they are transferred to keratinocytes.

Normal skin pigmentation is dependent on the amount, composition (eumelanin/pheomelanin ratio) and distribution of melanin within the skin (Alaluf et al., 2002). The number of melanocytes found in human skin differs amongst individuals (dark versus light skin), but also within the same individual, and in different sites on

the same individual (Szabo, 1954), although the underlying reasons for this variation are not clear (Whiteman et al., 1999). Moreover, there is a high degree of variation between the corresponding areas in different individuals, even though, according to Tadokoro et al. (2003), melanocyte density in any given area of skin is maintained irrespective of skin colour. Individuals with fair- or lighter skin colour have small, immature melanosomes that produce less melanin and are localised in clusters around the nucleus. In contrast, dark-skinned individuals have larger, mature, more pigmented melanosomes that have a diffuse distribution throughout the cytoplasm of melanocytes, and are more dendritic than those found in fair-skinned individuals (Kidson et al., 1993, Minwalla et al., 2001, Taylor, 2002, Thong et al., 2003).

1.3.4 Melanogenesis-related proteins

At least three main melanogenic enzymes regulate the melanin biosynthetic pathway within melanosomes: tyrosinase (TYR), tyrosinase-related protein 1 (TRP-1) and tyrosinase-related protein 2 (TRP-2), also known as dopachrome tautomerase (DCT) (Marks and Seabra, 2001). In addition, several structural proteins are also important for proper regulation of melanosome formation, melanogenesis and/or melanosome development. These include Pmel17/gp100, a eumelanosomal structural protein that regulates melanosomal biogenesis (Berson et al., 2001), the P protein, involved in pH regulation within melanosomes and for proper transit of TYR from the endoplasmic reticulum (Chen et al., 2002), the oculocutaneous albinism-1 (OA-1) protein, which regulates melanosome biogenesis via signal transduction between the lumenal and cytoplasmic compartments within the melanosome (Schiaffino and Tacchetti, 2005), and melanoma antigen recognised by T cells-1 (MART-1), also known as MelanA , that regulates melanosomal protein Pmel17/gp100 (Hoashi et al., 2005, Kawakami et al., 1996). Using several methods including mass spectrophotometric analysis, (Basrur et al., 2003) identified 68 proteins associated with Stage I-II melanosomes obtained from cultured melanocytes. Of these proteins, the 6 known melanosomal proteins were identified, as well as 56 proteins shared with other organelles and 6 novel melanosomal proteins.

1.3.4.1 Tyrosinase

Mammalian pigment production is dependent on the enzymes produced in melanosomes. The key enzyme is Tyrosinase (TYR), a copper-containing protein complex, and the rate-limiting enzyme in the melanogenic pathway (Korner and Pawelek, 1982). The TYR gene is melanocyte-specific and mutations of this gene can lead to cessation/loss of tyrosinase enzyme activity, as in the condition known as type 1 oculocutaneous albinism (Spritz et al., 1997), which leads to a lack of melanin pigment in the hair, skin and eyes of affected individuals. Tyrosinase activity is initiated in Stage II melanosomes and minimal tyrosinase activity continues to occur throughout melanosomal maturation to the final developmental stage, i.e. Stage IV melanosomes.

1.3.4.2 Tyrosinase-Related Protein 1 and 2

TRP-1 and TRP-2 (also known as dopachrome tautomerase or DCT) are Type 1 membrane glycoproteins that belong to the tyrosinase gene family (Oetting and Setaluri, 2007). They are structurally similar to TYR and their biosynthetic, processing and trafficking pathways have considerable overlap. TRP-2/ DCT acts as a DOPAchrome tautomerase by catalysing the tautomerisation of DOPAchrome to DHICA which results in eumelanin formation (Panzella et al., 2011). TRP-2/ DCT activity *in vivo* is therefore responsible for increased DHICA/DHI ratios in natural eumelanins. Importantly, TRP-2/ DCT is one of the first proteins expressed by developing melanocytes/melanoblasts and can thus be detected in both melanocytes and melanoblasts (Steel et al., 1992). Although it was originally thought that TRP-1 also catalysed DHICA transformation by functioning as a DHICA-oxidase (Kobayashi et al., 1994), it has since been shown to be only true for the murine homologue (Boissy et al., 1998). TRP-1 acts as a chaperone-like protein during TYR processing by ensuring the proper folding of TYR within the ER, and targeting to melanosomes during melanin synthesis (Jimbow et al., 2000a).

1.3.4.3 Melan-A/MART-1

The melanocyte differentiation antigen, Melan-A/MART-1 (hereafter referred to as MelanA), was originally identified in melanoma patients who expressed MART-1-reactive T lymphocytes (Kawakami et al., 1996). Kawakami et al. (1997) later demonstrated that although MelanA localised to the melanosomal membrane during melanosome biogenesis, MelanA expression inversely correlated with melanosomal maturation. Using quantitative immunoelectron microscopy methods, DeMaziere (2002) showed that increased levels of cellular MelanA content was found in vesicles and tubules throughout the cell, and that the maximum concentration was seen in the Golgi region, particularly the trans-Golgi network. In addition, he showed that MelanA was also present in the melanosomes, endosomes, ER, nuclear envelope, and plasma membrane in considerable amounts. Furthermore, since MelanA was also localised to the limiting membrane of less mature melanosomes, MelanA expression decreased as melanosomes matured. It was shown by (Hoashi et al., 2005) that MelanA formed a complex with the eumelanosomal structural protein, Pmel17 (also known as gp100), thus regulating its expression and function. MelanA is therefore important for proper melanosome biogenesis and maturation (Raposo and Marks, 2007)

1.4 Wound healing as a model to study *in vitro* melanocyte proliferation

Adult cutaneous wound healing occurs in response to disrupted tissue homeostasis. Wound repair is a well-orchestrated and highly coordinated process and comprises a series of overlapping phases (Martin, 1997, Heng, 2011), which includes haemostasis and inflammation, cell proliferation, matrix deposition, and tissue remodeling and maturation (Janis and Harrison, 2014) (see Fig. 1.4 below). Cellular protagonists involved in the wound repair process arise from several different cell lineages. These include epidermal keratinocytes,

dermal fibroblasts and the cells derived from the skin appendages, such as the sebaceous and sweat glands and the hair follicles. Besides the cellular elements involved in wound repair and tissue regeneration, other major role players include soluble inflammatory mediators such as cytokines, growth factors, and proteases (Borena et al., 2015, Olczyk et al., 2014). Adult wound healing therefore involves several overlapping but distinct mechanisms, which culminate in the development of a fibrotic tissue mass, commonly known as a scar.

1.4.1 Haemostasis and inflammation

The immediate response following damage to adult mammalian skin is the activation of the blood clotting mechanism, whereby platelet activation and aggregation results in the formation of a fibrin clot to control local bleeding. In addition to plugging blood vessels, the released coagulation factors provide a temporary matrix to enable binding of growth factors to their receptors, such as transforming growth factor (TGF)-β, fibroblast growth factor (FGF), and epidermal growth factor (EGF). Fibroblast and inflammatory cell migration is also expedited until a more stable, permanent matrix is formed. The inflammatory phase is characterized by the chemotactic migration of inflammatory neutrophils, macrophages and lymphocytes into the wound area (Gosain et al., 2006). While neutrophils clear the wound area of invading bacteria and other cellular debris, macrophages release cytokines that promote the inflammatory response and are responsible for mopping up apoptotic cells (Meszaros et al., 2000). Moreover, by modulating their phenotype, macrophages promote the switch to the proliferative phase of wound healing by stimulating keratinocytes and fibroblasts and promoting angiogenesis (Brancato and Albina, 2011).

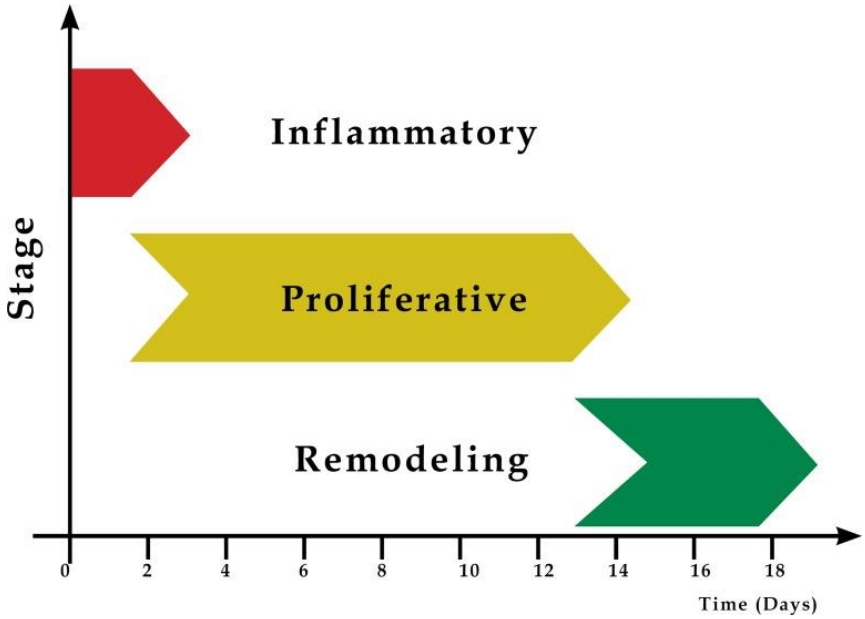

Figure 1.4 Phases of acute wound healing.

Schematic representation of normal wound healing shows three distinct but overlapping phases (image from (Gonzalez et al., 2016); https://www.ncbi.nlm.nih.gov/pmc/articles/PMC5087220/figure/f8/).

1.4.2 Proliferative phase

Epithelial proliferation and migration of cells over the provisional matrix signals the beginnings of the proliferative phase. The proliferative phase of wound repair heralds the start of actual closure of the wound gap and replenishment of lost tissue (Shaw and Martin, 2009). Re-epithelialisation of a wound by keratinocytes is achieved by a combination of migration and proliferation of epithelial cells in the damaged area in a collective migration process (Martin, 1997).

This collective migration of cells, which is central to the wound healing process (Murawala et al., 2012, Mort et al., 2015) occurs by three main mechanisms for the collective migration of epithelial cells during re-epithelialisation have been previously identified:

- the "purse string" mechanism in which an actin-myosin tract develops along the wound edge, and wound closure is accomplished by contraction of the actin belt around the wound (Martin and Lewis, 1992, Bement et al., 1993, Gonzalez et al., 2016).
- active spreading and migration of cells at the wound edge, known commonly as "lamellopodial crawling." Lamellopodial extension is mediated by Rac and Rho GTPases and possibly occurs due to cellular forces exerted by adjacent cells and/ or "pulling" forces exerted by the leading edge cells (Fenteany et al., 2000, Farooqui and Fenteany, 2005). This mechanism is more commonly seen during *in vitro* culture experiments using the scratch wounding assay.
- Using fluorescent time-lag staining in organotypic skin cultures, Safferling et al (2013) revealed a novel extending shield mechanism of re-epithelialisation, whereby the suprabasal cells provided a stable scaffolding compartment with the basal layer actively migrating as a collective. Interestingly, the suprabasal layer did not come into contact with the basement membrane or extracellular matrix at any stage of the re-epithelialisation process.

At a cellular level, several transformations occur that facilitate their migration (Ilina and Friedl, 2009): epithelial cells in the front rows of the migrating sheet extend their lamellipodia and alter their integrin expression so that the epidermal sheet can attach and drag itself forward over the wound substratum, which is further aided by the assembly of actin-rich lamellopodia for crawling (Mitchison and Cramer, 1996), and upregulation of matrix metalloproteinases (Pilcher et al., 1998). This enables them to bore a pathway at the boundary between the newly-formed scab and adjacent uninjured tissue. Mechanisms underlying these cytoskeletal transformations are therefore dependent mainly on cell polarity, cell-cell junctional integrity and structural modifications that drives the movement of cells across or through tissue matrix. Recently, the molecular mechanism that drives the coordinated movement of epithelial cells was uncovered (Das et al., 2015). Using epithelial monolayer culture and three-dimensional human skin explants, Das et al (2015) showed that merlin, a membrane-cytoskeleton scaffolding protein, that provides linkage between actin filaments and the cell membrane, firstly

relocates to the cytoplasm, then initiates a mechanical pulling on the leading cell, followed by orchestration of Rac1 activation and lamellopodial movement in migrating cells.

1.4.3 Tissue remodelling and maturation

Following dynamic cellular proliferation and synthesis of the extracellular matrix, the wound healing process enters the final remodelling or maturation phase, which can last for months to several years (Gurtner et al., 2008). The tissue remodelling phase aims to restore the skin architecture to a pre-injury state. Within the wound bed, fibroblasts produce collagen, glycosaminoglycans and proteoglycans, which are extracellular matrix constituents. Granulation tissue formation, ongoing collagen deposition and reorganisation, and resolution of granulation tissue occurs until the wound epidermis closely resembles that of normal skin. Complete restoration can, however, never be achieved and research into optimal wound healing solutions is ongoing.

1.5 Melanocyte proliferation in adult skin during wound healing

Although proliferation of adult melanocytes *in vivo* is infrequent, it is well established that under favourable conditions melanocytes can undergo mitosis *in vitro* (Eisinger and Marko, 1982, Kippenberger et al., 1997, Halaban, 2000). For melanocytes to proliferate *in vitro*, the presence of mitogens and growth factors such as basic fibroblast growth factor, hepatocyte growth factor, mast/stem cell factor (M/SCF), endothelins and melanotropin (MSH) is essential (Halaban et al., 1988, Gordon et al., 1989, Yaar and Gilchrest, 1991, Halaban et al., 1993, Hara et al., 1995). The mechanism whereby melanocytes undergo mitosis *in vitro* was uncovered by Kippenberger et al. (1997), by performing time-lapse studies of melanocytes during *in vitro* culture. These studies revealed that melanocytes undergo a change in morphology whereby the cell, after retraction of its dendrites, becomes rounded and detaches itself from the support medium. Further, mitosis occurs while the cell is in suspension and the two resultant cells then re-attach to the support and produce new dendrites.

While the migratory pathways of melanocytes during embryogenesis have been described in detail (Erickson, 1993), the mechanism of melanocyte migration in adult skin is not well understood. Broadly, there are three situations where replenishment is needed: (i) during expansion of the total skin surface during childhood and (ii) during re-epithelialisation following a skin insult, or (iii) when loss of melanocytes occurs e.g. in vitiligo. Upon activation by appropriate signalling, detachment from the basement membrane and from neighbouring keratinocytes is essential for both melanocyte division and migration (Tang et al., 1994). In addition, effective control of cell proliferation is essential. Under the influence of several cytokines and growth factors present in the local environment, melanocytes start by retracting their dendrites, and then undergo mitosis and migrate along the basement membrane to their destination location. Re-attachment to the basement membrane and to neighbouring basal keratinocytes follows with re-establishment of the epidermal melanin unit (Haass and Herlyn, 2005).

In adult human skin, melanocytes are generally quiescent cells and proliferation in the normal epidermis is an infrequent event (Haass and Herlyn, 2005). Following melanocyte inactivation or loss (e.g. in vitiligo) or during repigmentation of adult skin during wound healing, melanocytes must overcome many hurdles during their migration into areas that are devoid of melanocytes (Birlea et al., 2016). Stem cells resident in the epidermis and the bulge region of hair follicles, can also be recruited by the regenerating epidermis in response to injury (Fuchs and Horsley, 2008). These bulge stem cells commit to an epidermal keratinocyte phenotype and then migrate into the epidermis to participate in the repair process (Ito et al., 2005). Chou et al (2013) demonstrated the migration and proliferation of melanocyte stem cells out of the follicular niche after skin wounding or UVB irradiation in response to activation by the MC1R–ACTH-α-MSH signalling pathway. Before they can navigate through an unyielding epidermis, proliferation of melanocytes, or melanocyte precursor cells (melanoblasts) must firstly occur. However, it is not known exactly where they divide *en route* to the epidermis to achieve this repigmentation. It may occur either within the epidermis, and/or along the basement membrane and/or in the dermis (Li et al., 2010, Petit and Larue, 2016). Further, it has been shown that migration of melanocyte stem cells occurred before melanocyte proliferation (Chou et al., 2013). In addition, it was earlier shown using fate-mapping experiments, that hair follicle bulge stem cells contribute to acute wound repair, but they do not become activated under normal epidermal homeostatic conditions (Ito et al., 2005). However, it has recently been shown that activation of niche stem cells only occurs during the later stages of wound repair, which might be a safeguarding mechanism against depletion of the niche (Garcin et al., 2016). Control of melanocyte proliferation is also modulated by the oncogene Bcl2, an anti-apoptotic protein which is highly expressed by melanocytes and which allows melanocytes to bypass programmed cell death: this therefore enables them to survive in the epidermis (Klein-Parker et al., 1994).

1.6 The participation of melanocytes during repopulation of wounds

Despite numerous studies involving melanocytes and wound healing, there remains a paucity in the literature around the participation of melanocytes during wound healing. One of the earlier studies that investigated wound healing in partial-thickness wounds in guinea-pig skin, showed that wound healing occurred through neoepithelial formation and extension from the wound edge, as well as from hair follicles that remained in the dermis (Pepper, 1954). The results of a study made by Breathnach (1960) using DOPA-stained sheets of human epidermis, showed that melanocytes were present in the proximal area of a three-week old scar, but were fewer in number than the melanocytes that were seen in the normal adjacent epidermis. His results did not show any melanocytes present “in the epidermis covering a more centrally lying area of the scar”. Breathnach (1960) further reported that in the two-week old scar from the same study, the results were similar, but the “distance in from the edge at which melanocytes could not be detected was less”. Since, the descriptions of the location of melanocytes in the Breathnach (1960) study are vague, one can only deduce that the proximal area that is referred to must be the epidermis proximal to the wound edge or even at the

actual wound edge, since he did not find any melanocytes in the central parts of the scar. A later study done by Snell (1963) found that re-epithelialisation occurred from the wound edges only, which corroborates the previous findings, notwithstanding the fact that this was in full-thickness wounds. In addition, these investigators also found that melanocytes were carried along with the advancing neoepithelium and did not give any account of how they might have gotten there. Observations of melanocyte repopulation during wound healing (in guinea-pig skin full thickness wounds) by Cox et al. (1989) disagreed with the previous studies undertaken by Pepper (1960) and Snell (1963), whereby they showed that melanocyte division occurred between thirty-six and fifty days in their study, with a finding of increased numbers of melanocytes in their ninety-nine-day sample. However, they did not find any dividing melanocytes in the adjacent epidermis, nor in the healing wounds, but they do suggest that melanocyte division must have occurred in the developing neoepidermis. All these studies have found that melanocytes either lagged behind the migrating epithelial tongue, and/ or migrated with the developing tongues and/ or migrated into wounds once the neoepidermis had formed.

1.7 Study rationale, aims and specific objectives

To our knowledge, there have been few studies on melanocyte proliferation during wound healing. Little is known about whether melanocytes participate in the re-epithelialisation of a wound and how and when repigmentation occurs. There are two possibilities on how repigmentation might occur *in vivo*:

a) Either the melanocytes form part of the growing neoepidermis, proliferating as part of the migrating epithelial tongue, or
b) The melanocytes enter the newly formed epidermis only after complete re-epithelialisation has occurred, i.e. a complete neoepidermis is present.

The broad aim of this study was to explore the role of melanocytes in the wound healing process. An improved understanding of hyper- and hypopigmentation in some scars and in hypopigmentary disorders such as vitiligo, would contribute to improved treatment for a successful cosmetic outcome following wound repair.

1.7.1 Specific Objectives

i) To determine whether the wound healing in the cultured skin in this study reasonably mimics the *in vivo* wound healing process (including the pattern of keratinocyte proliferation)
ii) To develop and optimise a double-labelling protocol to detect melanocytes and dividing melanocytes in the wound area in cultured skin
iii) To utilise this double-labelling to screen “wounded” skin samples, cultured for between two to twelve days, for the presence of melanocytes (dividing and non-dividing melanocytes), to answer the question of:
    a. Whether melanocytes participate in re-epithelialisation stage of the wound healing processor,

b. Whether they only appear in the wound after complete formation of the neoepidermis.

CHAPTER 2
MATERIALS AND METHODS

2 Materials and Methods

2.1 Human skin biopsy collection and preparation

Normal skin samples were obtained for use as control tissue and for optimisation of immunostaining protocols. Adult skin samples were obtained from consenting patients undergoing elective plastic surgery at Groote Schuur Hospital, Cape Town and from neonatal foreskin samples from circumcisions obtained from the Maternity Unit of Kingsbury Hospital, Cape Town. All procedures and protocols were officially approved by the University of Cape Town Ethics Committee (UCT Ethics REC REF 493/2009) (see Appendix C). Samples were placed in sterile specimen bags and transported directly to the Department of Human Biology laboratory on ice. All subsequent work was performed in a Bio-Flow Biological Safety Cabinet Class II and gloves were always worn. The skin samples were aseptically trimmed of excess dermal fat and cut into 2mm^2 blocks and washed in PBS to remove all traces of blood. Skin samples were then incubated in a 5mM 3,5-bromodeoxyuridine (BrdU) solution in Dulbecco's Modified Eagles Medium (DMEM) with 10% foetal calf serum (FCS) and 100 IU/ml Penicillin / 100 µg/ml Streptomycin solution added, for 24 hours at 37ºC in a 5% CO_2 / 95% O_2 humidified incubator (see Appendix B1.3).

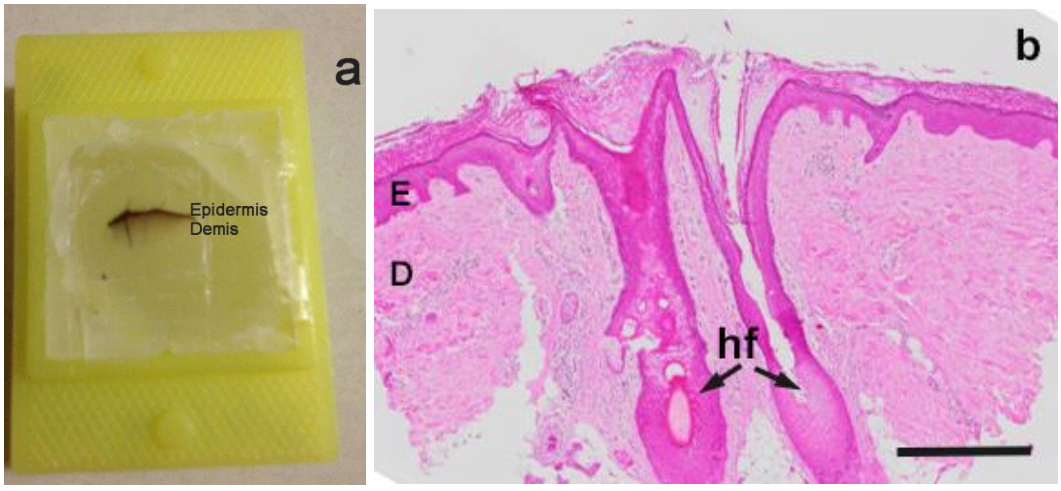

Figure 2.1 Representative images showing results of optimisation of anti-Ki67.

(a) Digital image of hair-bearing human skin embedded in paraffin wax with longitudinal orientation. The pigmented epidermis is clearly distinguishable from the dermis below. b) An H&E stained section from the block shown in (a). Two hair follicles are visible in the dermis in this section. hf = hair follicle; E = epidermis; D = dermis. Bar = 500 µm.

2.2 Fixation and processing

Following incubation in BrdU solution, the skin samples were rinsed with three changes of PBS, followed by fixation in a 4% formaldehyde solution from paraformaldehyde (w/v) in PBS (Appendix B 1.5) at 4 ºC for 4 hours (hrs). Individual tissue samples were then placed into Tissue-Tek® Uni-Cassettes® (Sakura; Labotec) and processed to paraffin wax according to the standard protocol (Bancroft and Gamble, 2005). Briefly, the tissue samples were processed on an overnight schedule using an automatic tissue processor (Shandon Automatic Tissue Processor, model SE400, Shandon Scientific Co. Ltd; England) (see Appendix A.1 for detailed processing schedule). Dehydration of tissues was carried out by continuous agitation in increasing grades of ethanol. Clearing of tissues was achieved by immersion in xylene, followed by impregnation with molten paraffin wax (Histosec® wax pastilles; Merck, 111609) in a wax bath heated to 60 ºC. Tissues were subsequently embedded in paraffin wax. Care was taken with orientation of the skin biopsies in the wax block to obtain longitudinal sections of the epidermis and dermis of the skin (see Fig.2.1 a above).

2.3 Microtomy

2.3.1 Normal skin for use as control tissue sections and for optimisation of immunostaining protocols

Tissue blocks were sectioned at 4 micrometres (µm) thickness on a rotary microtome (Leica, model RM 2125RT, SMM Instruments Ltd., Cape Town) and floated out onto a waterbath (Leica, model HI 1210, SMM Instruments Ltd., Cape Town). Two or three consecutive sections were placed onto Superfrost Plus® microscope slides (ThermoScientific, Menzel Gläser; Labotec (Pty) Ltd.) for immunohistochemistry. Positively-charged Superfrost Plus® slides electrostatically attract tissue sections, thus preventing section loss during immunostaining procedures. Sections were left to drain in a vertical position, before heating in a 60º C drying oven (Memmert, model B30) overnight to complete drying.

2.3.2 Sections obtained from human skin organ culture wound healing model

Several slides with 4 µm sections were kindly provided by Dr John Common, A*Star Institute, Singapore). These serial sections were cut from blocks of normal human skin explants, which were cultured over a period of 288 hours, which is equivalent to 12 days (Fig. 2.2 below). Please refer to Appendix A.2 for details of human skin explant culture of samples used in this study (kindly provided by Dr John Common - personal communication). Briefly, tissue samples were removed from the culture medium at various time points, fixed in 10% neutral buffered formalin (Appendix B.1.4) and processed to paraffin wax according to the standard protocol. Serial sections were cut at 4µm thickness, placed

onto Superfrost Plus® microscope slides and allowed to dry. Sections were then carefully packaged and dispatched via courier to the Cell Biology Laboratory, Department of Human Biology, UCT. Two boxes of slides were received containing several slides cut from blocks at different time points for routine H&E stain and immunofluorescent staining.

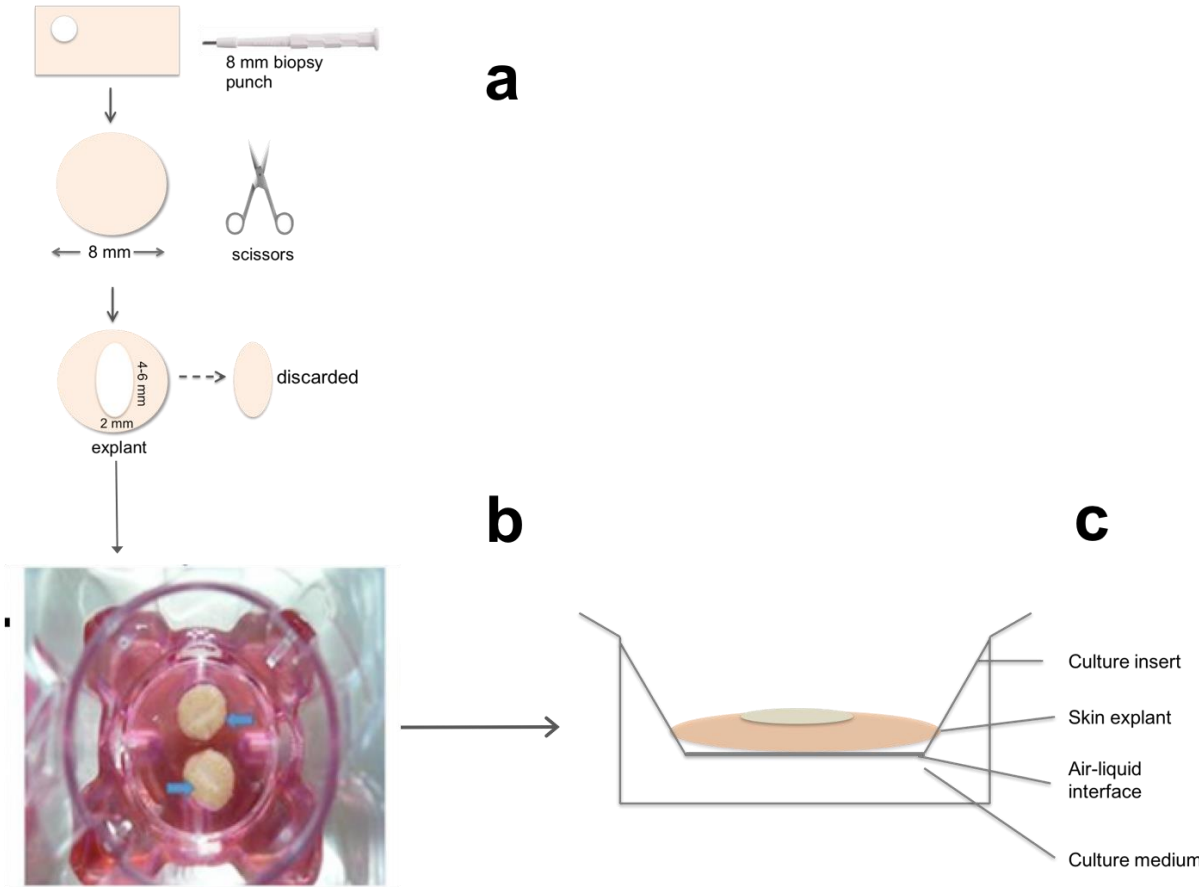

Figure 2.2 Human skin explant culture model

(a) Schematic of skin explant culture model showing that 8 mm diameter punch biopsies from human skin were used to make elliptical cuts (~2mm in width). (b) Representative image of the wounded punches were cultured at the air-liquid interface in DMEM at different time points over a 10 day period (aerial view). Wound created on skin punch biopsies is shown by small blue arrows (this is a modified image from the original kindly provided by Dr. John Common). (c) Schematic representation showing a side view of (b).

2.4 Staining of sections for light microscopy

Sections were selected from the boxes of slides received and stained with the H&E stain according to standard protocol (Appendix A.3).

2.5 Immunohistochemistry of FFPE tissue sections

2.5.1 Approach and selection of markers

To identify both proliferating cells and melanocytes within the epidermis and the neoepidermis of the wound healing samples, a double-immunolabelling approach was used. This dual-labelling strategy relies on nuclear labelling of dividing cells (both melanocytes and keratinocytes) with a proliferation marker, and cytoplasmic labelling of melanocytes with a melanocyte-specific marker. Thus, true double-immunopositivity would only be detected in dividing melanocytes (Ki-67+/ MelanA+) (see Figure 3.1 below). Antibodies to both proliferation markers and melanocyte-specific markers are widely available, thus making it possible to identify the expression of these proteins in tissue sections by utilising fluorescent immunolabelling techniques. To this end, two proliferation markers and several melanocyte-specific markers were investigated for suitability for this study.

Figure 2.3 Schematic representation of dual immunolabelling strategy using anti-Ki-67 and anti-MelanA.

(a) The cell with a blue nucleus is a non-dividing cell stained with the DAPI nuclear counterstain. (b)The nuclei of dividing cells stain green with the proliferation marker, anti-Ki-67. (c) The cytoplasm of melanocytes stain red with the melanocyte-specific marker, MelanA. (d) A dual-labelled cell showing green/ yellow nuclear staining and red cytoplasmic staining is considered to be a dividing melanocyte (Ki-67+/ MelanA+). Note that this schematic depicts only the cell bodies of the epidermal cells and melanocytes.

Antibodies to BrdU and anti-Ki-67 were investigated to select the best cell proliferation marker. Bromodeoxyuridine (BrdU), a thymidine analogue, is incorporated with nuclear DNA during cell division, and can thus be detected by immunohistochemical means (Leif et al., 2004). The use of anti-BrdU as a proliferation marker is restricted to mitotic cells during the S-phase of cell division. Pre-incubation of tissue samples with BrdU is necessary and introduces an additional step in the staining protocol. The Ki-67 protein is a proliferation marker expressed throughout all stages of the cell cycle except for G_0, when it cannot be recognised by the Ki-67 antibody (Scholzen and Gerdes, 2000). Ki-67 localises to the nucleus where it is predominantly located in the perinucleolar region in the G1 phase, and in the later phases, provides a more diffuse pattern by dispersing throughout the nuclear matrix. BrdU and Ki-67

antibodies were therefore utilised to optimise immunohistochemical protocols for identifying proliferating cells in the epidermis of cultured skin.

The melanocyte differentiation antigen, Melan-A (MART-1), plays an important role in eumelanogenesis by regulating the expression, stability and trafficking of the eumelanosomal structural protein Pmel17/gp100 (Hoashi et al., 2005) . Melan-A is explicitly expressed in melanocytes present in normal skin, melanomas and retinal pigment epithelium, but is not demonstrable in other tissues. It is a highly sensitive and specific marker of cells of melanocytic lineage, and antibodies against this antigen are widely used in dermatological research to detect melanocytes and melanoma cells by immunohistochemical means (Busam and Jungbluth, 1999, Snyder and Paulino, 2002).

Tyrosinase (TYR) is the rate-limiting enzyme in the melanogenic pathway, and in the skin, it is considered a specific marker for differentiated melanocytes. Melanin biosynthesis is initiated by the catalytic oxidation of tyrosine to DOPA by tyrosinase. Tyrosinase then catalyses the dehydrogenation of DOPA to dopaquinone (Korner and Pawelek, 1982). As discussed previously, TRP-2 /DCT is expressed early in the neural crest migratory pathway and can thus be deemed a marker of immature/undifferentiated melanocytes i.e. melanoblasts. This enzymatic protein is the only known early melanocyte-specific marker discovered to date, which can detect melanocyte precursor cells/melanoblasts. At present, there is no convincing data for the demonstration of proliferating melanocytes (Ki-67+/ MelanA+) in normal human skin.

2.5.2 Optimised immunofluorescent protocol

For immunofluorescent labelling of sections, both control and experimental sections were treated identically. Briefly, paraffin sections were dewaxed in xylene and passed through decreasing grades of alcohol to water. Due to formalin fixation of these tissues, epitope retrieval was necessary before immunostaining could commence. Heat-mediated antigen retrieval was performed in a 6- litre capacity domestic pressure cooker (Prestige® Smart Plus). Fifty ml of 10 mM citrate buffer, pH 6.0 (Appendix B.1.9) was added to each plastic Coplin jar, the lid was screwed on loosely, and it was placed into a special metal insert inside the pressure cooker. I was responsible for the design of the metal insert and commissioned our departmental workshop with its construction. The insert holds 4 plastic Coplin jars, preventing them from toppling over into the water (Fig.2.3 below). Tap water was added to the pressure cooker up to the level of the buffer in the plastic Coplin jar. The slides were held in antigen retrieval buffer at ~121ºC for 20 minutes. The Coplin jars were removed from the pressure cooker and the lids were loosened. The slides were kept in the buffer and allowed to cool down for 10 minutes. After 3 x 5 minutes each in phosphate buffered saline/ Tween 20 rinses (PBST) (see Appendix B.1.10), excess buffer was removed, and a “well” was created around each section. Care was taken not to dry out the

sections as drying of the sections at any stage of the protocol would cause non-specific background signal. The tissue sections were blocked for non-specific binding by treatment with 10% normal donkey serum in 1% BSA/PBS solution (Appendix B.1.11) for 1 hour at room temperature (RT). The serum block consists of non-immune serum from the animal host species of the secondary antibody.

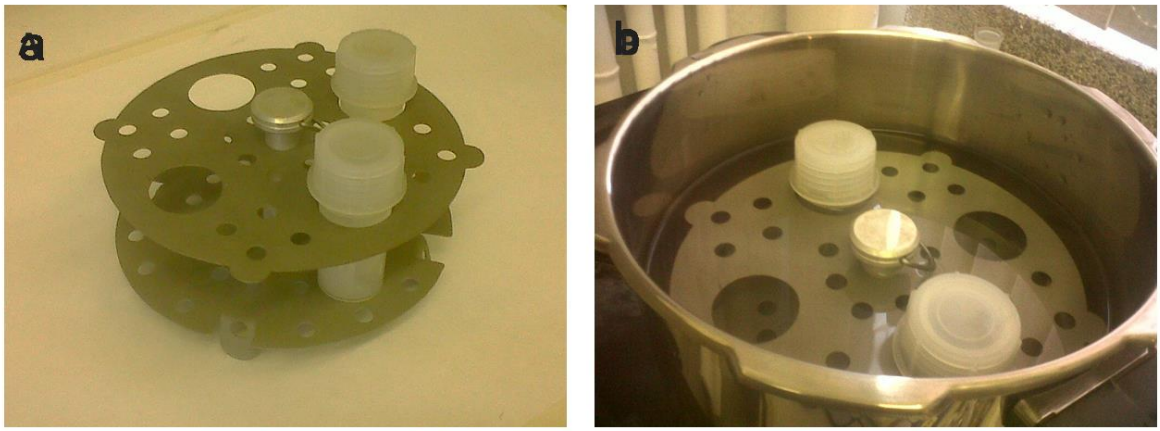

Figure 2.4 Digital images of specially designed metal rack.

The metal rack fits inside a 6-litre capacity domestic pressure cooker to keep plastic Coplin jars upright during antigen retrieval procedure. a) custom-designed metal rack holds 4 plastic Coplin jars; b) metal rack inside pressure cooker. The water level is just below the screw-on lid of the Coplin jar.

Blocking serum was removed from the sections by flicking off the excess. Sections were then incubated at RT for 60 minutes followed by incubation at 4ºC for 18 hours with primary antibody (see Table 2.1 below). 2% donkey serum in 1% BSA/PBS solution (Appendix B.1.12) replaced the primary antibody and served as a reagent control. Further procedural controls were included during optimisation, but were omitted once staining parameters were optimised (see Table 1.2 below). These were, however, performed periodically to ensure ongoing adequate technique. The primary and secondary antibodies were diluted in 2% donkey serum in 1% BSA/PBS solution at varied optimised concentrations (see Table 2.1 below). After overnight incubation, sections were washed thoroughly with PBST and incubated in the dark at RT for 2 hours with the host-appropriate fluorescent-conjugated secondary antibody. After rinsing thoroughly with PBST, the nuclei were stained with the light-sensitive nuclear dye, 4', 6-diamidino-2-phenylindole, dihydrochloride (DAPI) in the dark at RT for 20 minutes (see Appendix B.1.13). After one PBST rinse, sections were mounted under a coverslip with Mowiol coverslip mounting medium (Appendix B.1.14, placed in an aluminium foil-covered slide-holder to protect them from light, and refrigerated at 4ºC until viewing under the epifluorescent microscope.

It should be noted that immunostaining was first optimised in a single-labelling protocol to establish the reliability and sensitivity of the antibodies used in this study (see Chapter 3: Results, Part 1). Antigen retrieval method and primary and secondary antibody dilutions were optimised and the protocol was

repeated on several occasions before it was deemed to be robust and reproducible. All procedural controls (see Table 2.2 below) were carried out in initial experiments, and thereafter only the negative controls were included in each staining run. Dual immunolabelling was attempted once all the immunostaining parameters were established for each individual antibody. Please refer to Appendix A.4 for the detailed optimised double-immunofluorescence protocol.

Table 2.1 Optimised immunofluorescence parameters in FFPE skin samples

Primary antibodies	Concentration
BrdU (Roche, 11170376001; mouse monoclonal, clone BMC9318)	1:50
Ki67 (ab15580; rabbit polyclonal; Abcam, USA.)	1:200
Melan A/MART-1 (sc-20032, clone A103, mouse monoclonal; Santa Cruz Biotechnology, Inc., Santa Cruz, CA, USA)	1:25
Tyrosinase (NCL-TYROS, clone T311, mouse monoclonal, Novocastra, country.)	1:50
Tyrosinase C-19 (sc-7833, goat polyclonal; Santa Cruz Biotechnology, Inc., USA)	1:50
TRP-2 H-150 (sc-25544, rabbit polyclonal; Santa Cruz Biotechnology, Inc., USA)	1:50
Secondary antibodies	Concentration
Donkey anti-mouse (Cy3-conjugated, 715-166-150, Jackson ImmunoResearch Laboratories, Inc., PA, USA)	1:1000
Donkey anti-goat (Cy3-conjugated Cat: 705-166-147, Jackson ImmunoResearch Laboratories, Inc., PA, USA)	1:1000
Donkey anti-rabbit (Northern Lights™ Anti-rabbit IgG- NL493; R&D Systems, NL 006)	1:500

Table 2.2 Procedural controls used in the optimisation of FFPE skin samples

Controls		Method	Rationale
Tissue Controls	Internal positive control	Sections incubated with primary and secondary antibodies. Positive immunostaining resulting from expression of antigenic epitope present in basal melanocytes (MelanA, TYR, TRP-2), basal and	To exclude a **false negative** signal due to inadequate binding of either primary or secondary antibodies
	Internal negative controls	Sections incubated with primary and secondary antibodies. Negative immunostaining in cells not expressing antigenic epitope e.g. epidermal keratinocytes are MelanA-, TYR- and TRP-2-)	To exclude a **false positive** signal due to improper or non-specific binding of either primary or secondary antibodies
Reagent Controls	Negative primary antibody control	Control section incubated with primary antibody only	To exclude a **false positive** signal due to non-specific binding of primary antibody when secondary antibody is omitted
	Negative secondary antibody control	Control section incubated with fluorophore-conjugated secondary antibody only	To exclude a **false positive** signal due to non-specific binding of secondary antibody when primary antibody is omitted
Auto-fluorescence control		Omission of primary and secondary antibodies	To exclude a **false positive** signal due to autofluorescence or fixative-induced fluorescence following formalin fixation, processing and HIER

2.6 Data collection and analyses

2.6.1 Light microscopy and image acquisition

The H&E stained sections were examined by light microscopy on a Zeiss Axioskop microscope (Zeiss; Germany) and digital images were captured using the Zeiss Axiocam HRc camera and associated software (Axiovision version 4.7; Zeiss microscopy). Because of the availability of the technology, the H&E-stained slides were also digitally scanned using the Olympus VS120 digital slide scanning system. Further images were obtained by capturing screenshots of these digitally scanned slides. These digital images proved to be of a better quality and resolution than the images captured with the Zeiss Axiocam HRc camera and were subsequently used for histological assessment (Table 2.3).

Table 2.3 Number of stained sections examined over culture period

Time removed from culture	Number of skin samples	Number of sections per slide	Total number of sections examined
Day 0	1	4	4
Day 2	2	4	8
Day 5	2	4	8
Day 10	2	4	8
Day 12	2	4	8

Note: Data used for analysis excluded the sections where the wound was closed, therefore the data from all the sections might not have been used for certain investigations.

2.6.2 Fluorescent microscopy and image acquisition

For fluorescent microscopy, images were captured using a Zeiss Axiovert 200M fluorescence microscope (Carl Zeiss AG, Germany) with an HBO lamp. Detection of the Alexa 488-labelled antibodies bound to BrdU or Ki67 and Cy3-labelled secondary antibodies bound to Melan A/MART-1 in double-immunostained skin sections was possible using the dichroic filter set with excitation wavelength of 546nm and long-pass emission filter ranging from (590-700 nm). Images were captured with the Zeiss Axiocam HRm fitted to the microscope using AxioVision software, version 4.7 (Carl Zeiss Microscopy) and converted to either Joint Photographic Experimental Group (JPEG) format or Tagged

Image File Format (TIFF) format to facilitate image analyses. The sections were orientated with the epidermis above the dermis and several images were captured of the skin sections at 100x, 200x, and 400x magnification along the entire length of each section A 1000x magnification oil immersion lens was used occasionally to demonstrate increased cellular detail or when clarity was required.

2.7 Image Analysis

2.7.1 Qualitative analysis of H&E-stained sections

Qualitative analysis of tissue sections was performed by examining the H&E-stained sections and noting the tissue integrity, morphology and viability of the cultured samples (see Results, Part 2).

2.7.2 Quantitative analysis of immunostained sections

To determine the number of proliferating keratinocytes, all the Ki67-stained sections for each time point were analysed. The number of Ki67-positive (Ki67+) keratinocytes per unit length (1 mm) of basement membrane was determined by manually counting the number of Ki67+ cells in the epidermis as can be seen in Fig. 2.4 below (see Appendix D for data tables). Keratinocytes could be identified by *green nuclear staining* with the Alexa-488 fluorescent stain. Data were expressed as the average number of KI-67+ cells per mm of basement membrane.

To determine the number of melanocytes (non-dividing and dividing) present in the cultured skin samples, counting of MelanA-positive (MelanA+) along the basal layer cells was conducted as before for the keratinocytes. Melanocytes could be identified by *red cytoplasmic staining* with the fluorescent stain, Cy-3, and the *nucleus* stained *blue* with the DAPI nuclear counterstain. Data were expressed as the average number of MelanA+ cells per mm of basement membrane for the melanocyte counts when comparing the normal epidermis to the tongues. When encountered during screening, *dividing* melanocytes could be identified by the presence of red cytoplasmic staining (MelanA+) and a green/yellow nucleus (Ki-67+). The green/ yellow nuclear staining can be attributed to an overlap of the three fluorescent channels used, where the nucleus of a dividing melanocyte would stain mostly red with the Cy-3 fluorescent stain, the nucleus would stain green with the Alexa-488 fluorescent stain, and these two channels would overlap with the nuclear fluorescent counterstain, DAPI. Data were expressed as the average number of MelanA+ cells per mm of basement membrane for the melanocyte counts when comparing the normal epidermis to the tongues. When sections were screened for the presence of dividing melanocytes, the total number of melanocytes and the number of dividing melanocytes were recorded in the three zones examined. The three zones were: (i) the epidermis proximal to the wound edge, (ii) at the wound edge, and (iii) in the developing tongues. Note: that data

obtained from the sections that showed “closed” tongues, i.e. wounds that had fully re-epithelialised, were not included in these analyses.

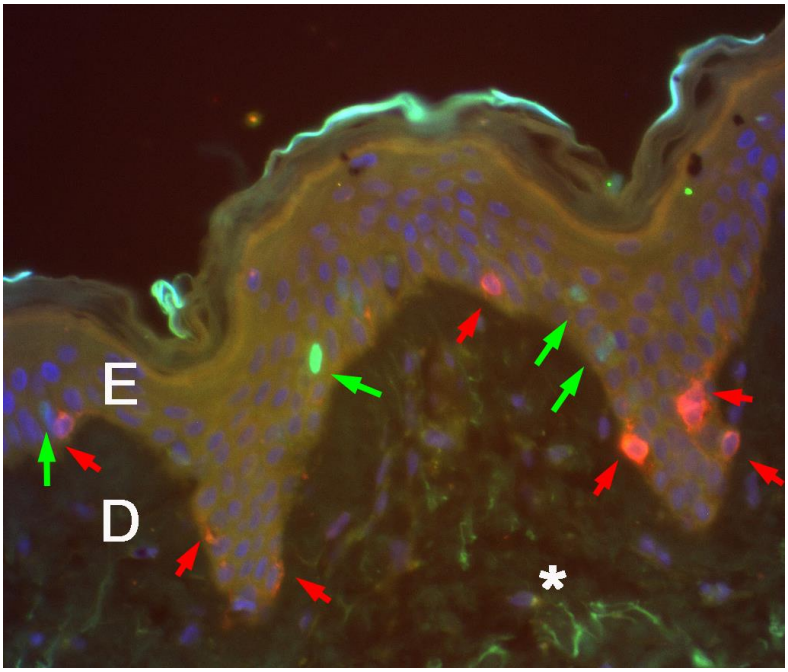

Figure 2.5 Representative image of double-immunostaining in normal skin.

Section showing double-immunostaining of skin using antibodies to Ki-67 and MelanA. The section is oriented in the longitudinal plane with the epidermis above the dermis. Melanocytes (red arrows) showing typical red cytoplasmic staining (MelanA+) are seen along the basement membrane. The green nuclei (green arrows) of proliferating keratinocytes (Ki67+) are seen in basal and suprabasal locations in the epidermis. Autofluorescence of upper corneal layer and collagen fibres in the dermis (asterisk) is seen. E = epidermis; D = dermis.

2.7.2.1 *ImageJ* software program

Image analysis was performed using NIH *ImageJ* (http://rsb.info.nih.gov/ij/). Briefly, a calibrated graticule was used to standardise measurements for each magnification of the image used at acquisition, namely, 100x, 200x and 400x (see Appendix B 6). Several tools available in the *ImageJ* software program are designed for image management and enable one to ‘draw” onto the image. To accurately measure the basement membrane length, a line was drawn along the basement membrane by following its natural curvature with the computer mouse. In *ImageJ*, a “macro” is a series of steps rolled into a single keystroke, which allows for a certain degree of automation. By invoking the appropriate “macro”, the length of the basement membrane was determined according to the calibrated parameters for images taken at different magnifications. The length of the basement membrane could

thus be accurately measured and the number of positively-labelled cells within the epidermis could be counted.

2.8 Statistics

All data are presented as an average ± standard error of mean (SEM). The raw data comprised measurements of the lengths of epidermis along the basement membrane and the cell counts of dividing keratinocytes in basal and suprabasal layers of the epidermis and non-dividing and dividing melanocytes along the basal layer. These data were averaged and tabulated (see Appendix D for all data tables). Differences were considered significant when * $p < 0.05$, ** $p < 0.01$, *** $p < 0.001$, **** $p < 0.0001$. Appropriate *post hoc* tests were performed in GraphPad Prism™ v6.0 (San Diego, CA, USA).

CHAPTER 3
RESULTS

3 Results

Melanocyte migration into healing wounds is essential for repigmentation of the neoepidermis to occur. It has been posited that melanocyte stem cell populations are present in the hair follicle and interfollicular epidermis, and that these melanocyte precursor cells become activated to differentiate and migrate to areas that require melanocyte replenishment. Since there is a paucity of literature regarding the activation of melanocyte migration into healing wounds during re-epithelialisation, this study sought to investigate the dynamics of melanocyte participation and proliferation during the re-epithelialisation phase of wound healing. In particular, it is not known whether melanocytes migrate passively along with the sheet of migrating keratinocytes into the wounded area, or whether they are capable of active migration from the wound edges. Furthermore, it is still unclear whether differentiated melanocytes present at the wound edge are able to de-differentiate and then divide, in order to migrate into the neoepidermis. This dissertation attempts to address the following questions:

(a) Whether differentiated melanocytes have proliferative potential;
(b) Whether dividing melanocytes can be found in the normal epidermis;
(c) Whether dividing melanocytes can be found in the neoepidermis;
(d) Do the melanocytes move into the developing tongues by an active process, or do they rely on being passively carried along by the migrating keratinocyte sheet?

3.1 Part 1: Antibody optimisation

3.1.1 Optimisation of immunofluorescence (IF) protocols

The first objective of this study was to optimise a single-labelling immunofluorescence (IF) protocol for selected markers of proliferation and for melanocyte-specific markers. Several variables were taken into account during optimisation procedures: a) the antigen retrieval method, b) the concentration of primary and secondary antibodies, and c) the choice of fluorescent-tagged secondary antibody. Each of these conditions will be dealt with separately in the results detailed below.

All samples were obtained after ethical approval (see Appendix C). Sections were obtained from normal skin as previously described in section 2.3.1, Chapter 2: Materials and Methods. Antibodies selected for analysis included: mouse monoclonal anti-BrdU, rabbit polyclonal anti-Ki-67, mouse monoclonal anti Ki-67, mouse monoclonal anti-MelanA/MART-1, rabbit polyclonal anti-TRP-2, and goat polyclonal anti-TYR. Optimised protocols are detailed in Table 2.1 of Materials and Methods section.

3.1.2 Optimisation of antigen retrieval protocol

Formalin fixation is known to form cross-linkages between proteins, which results in a “masking” effect on antigenic epitopes (Polak and Van Noorden, 1997). In order to recover antigenicity, it is necessary to perform an antigen retrieval procedure prior to immunostaining (Boenisch, 2006). After testing a variety of antigen retrieval methods, it was concluded that heat-induced antigen retrieval (HIER) produced the best means of unmasking and preserving the antigenic epitopes for all the primary antibodies selected. Both 0.1 mM sodium citrate buffer pH 6.0 and 10 mM EDTA buffer pH 8.0 were tested using the pressure cooker method, i.e. steam under pressure at a temperature of approximately 121°C. Citrate buffer pH 6.0 proved to be the most effective means of antigen retrieval for all antibodies tested and was used for all subsequent immunohistochemical staining.

3.1.3 Optimisation of primary antibody concentration

The primary antibodies used in this study were firstly optimised in a single-labelling protocol before dual immunolabelling was carried out. Detailed parameters for all primary antibodies are included in Table 2.1 of Materials and Methods section.

3.1.3.1 Optimisation of monoclonal BrdU antibody

Normal human skin samples were incubated with a 5 mM BrdU solution for 18-24 hours (i.e. overnight) to allow for BrdU incorporation into dividing cells (see section 2.1, Materials and Methods). After standard tissue processing and immunostaining with anti-BrdU and a species-matched Alexa-488 conjugated secondary antibody, sections were examined by epifluorescence. Initial image capture was performed using the monochrome channel only. BrdU-positive proliferating cells(BrdU+) were seen in the basal and suprabasal layers of the epidermis (Fig.1.2 a; red arrows). Non-specific staining was absent; intrinsic fluorescence of collagen fibres and erythrocytes in small blood vessels was observed in the dermis. No signal was seen in the negative control sections where the primary antibody was omitted (Fig.1.2 b).

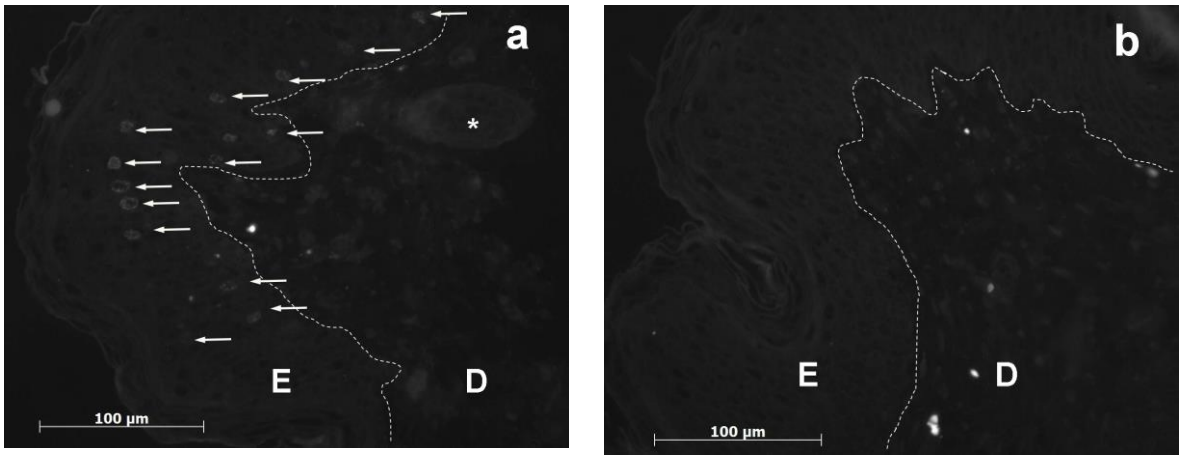

Figure 3.1 Representative monochrome digital images showing results of optimisation of anti-BrdU antibody.

(a) BrdU-positive keratinocyte nuclei (white arrows) were seen in basal and suprabasal layers of the epidermis using DARb-Cy-3 fluorescent secondary antibody. Pairs of dividing keratinocytes can be seen in basal and suprabasal positions (red arrows). (b) Negative control section shows no fluorescent signal, where primary antibody was omitted. Broken line depicts the dermo-epidermal junction. E = epidermis; D = dermis. Bar = 100 μm.

3.1.3.2 Optimisation of rabbit polyclonal Ki-67 antibody

In this investigation, it was not always possible to incubate the samples with BrdU solution prior to fixation, therefore immunostaining with anti-BrdU could not always be used. In these samples, the proliferation marker, Ki-67, was used to detect dividing cells within the epidermis of the skin samples provided. Of note, is that anti-Ki-67 differs from anti-BrdU staining, in that all dividing cells are labelled (i.e. not only cells in S-phase of the cell cycle, but proliferating cells in all phases of cell cycle, except G_0). Consequently, one would expect to find more Ki-67-positive (Ki-67+) cells per high power field in the epidermal layers (Fig. 3.3 a). Either a rabbit polyclonal or a mouse monoclonal anti-Ki-67 antibody was used where necessary with appropriate fluorescent secondary antibodies. No signal was detected in negative control sections without primary antibodies (Fig. 3.3 b).

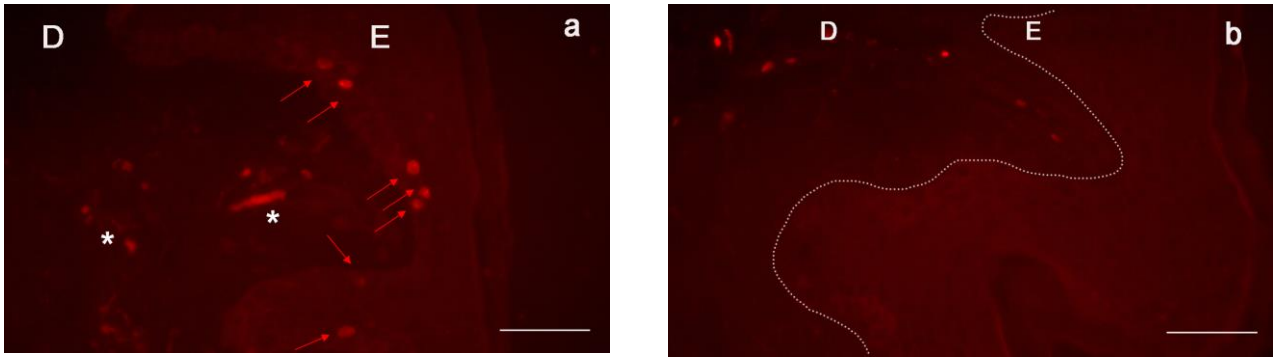

Figure 3.2 Representative images showing results of optimisation of anti-Ki-67 antibody.

(a) Proliferating keratinocytes showing red nuclear fluorescent staining (red arrows) were seen in basal and suprabasal layers of the epidermis; DARb-Cy-3 fluorescent secondary antibody was used. Some autofluorescence of erythrocyte nuclei was observed in the dermis(asterisks). (b) Negative control section shows no fluorescent signal, where primary antibody was omitted. Broken line depicts the dermo-epidermal junction (DEJ). E = epidermis; D = dermis. Scale = 50 μm.

3.1.3.3 Optimisation of mouse monoclonal MelanA/MART-1 antibody

MelanA/MART-1 is specific for melanocytes as it binds to the transmembrane protein on early melanosomes Coulie et al, 1994 Kawakami et al, 1994 Delevoye et al., 20011 . Note that MelanA/MART-1 antibody will be hereafter referred to as MelanA antibody. MelanA immunostaining in control skin biopsies showed positive labelling of the cytoplasm of melanocytes along the basal layer of the epidermis (Fig.3.4, red arrows). The melanocytes were evenly positioned along the basement membrane. Epidermal keratinocytes did not show a

positive signal for MelanA and no signal was observed in control samples where the primary antibody was omitted, confirming the specificity of anti-MelanA for melanocytes.

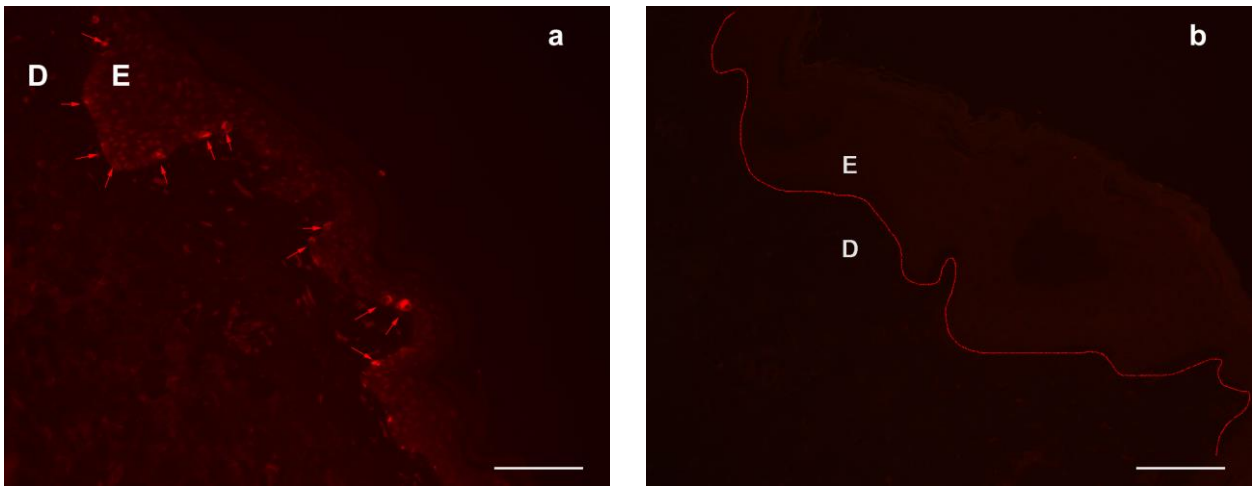

Figure 3.3 Representative images showing results of optimisation of anti-MelanA antibody.

(a) Melanocytes showing red cytoplasmic fluorescent staining with anti-MelanA were seen along basal layer of the epidermis (red arrows). (b) Negative control section shows no fluorescent signal, where primary antibody was omitted. Broken line depicts the DEJ. E = epidermis; D = dermis. Scale = 50 μm.

3.1.3.4 Optimisation of mouse monoclonal TYR antibody

The rate-limiting enzyme, tyrosinase, initiates the melanogenic pathway by catalysing the oxidation of tyrosine to DOPA and DOPA to DOPAchrome. Positive perinuclear cytoplasmic staining with anti-TYR antibody was observed in the cytoplasm of melanocytes along the basal layer of the epidermis (red arrows, Figure 3.5 a). As expected, the melanocyte dendrites were not stained as with anti-MelanA immunostaining, as TYR localises to the ER and perinuclear regions of the melanocyte (Jimbow et al., 2000b, Jimbow et al., 2000a, De Maziere et al., 2002). No other epidermal cells were immunopositive for TYR antibody and immunoreactivity was not observed in control samples where the primary antibody was omitted (Fig.3.5 b). The alternative rabbit polyclonal anti-TYR antibody showed similar immunostaining results (image not shown).

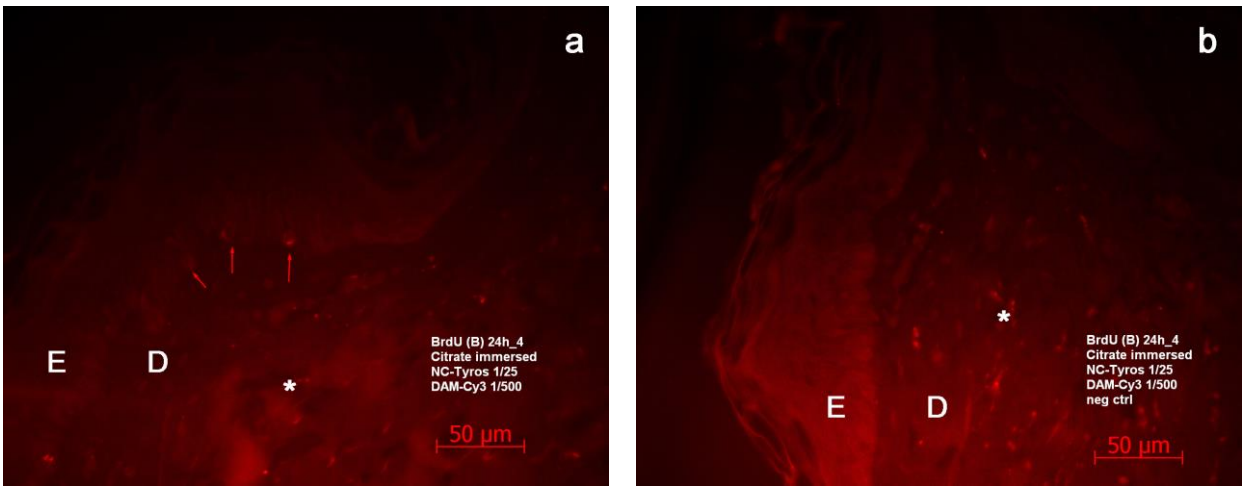

Figure 3.4 Representative images showing results of optimisation of monoclonal anti-TYR antibody.

(a) Melanocytes showing red cytoplasmic fluorescent staining (TYR+; red arrows) were seen in basal layer of the epidermis; DARb-Cy-3 fluorescent secondary antibody was used. (b) Negative control section shows no fluorescent signal, where primary antibody was omitted. Autofluorescence of collagen fibres and erythrocyte nuclei were seen in the dermis (asterisk). E = epidermis; D = dermis. Scale = 50 µm.

3.1.3.5 Optimisation of rabbit polyclonal TRP-2 antibody

Tyrosinase-related protein-2 or TRP-2 is one of the tyrosinase-related proteins and functions as a DOPAchrome tautomerase in the melanin synthetic pathway (Aroca et al., 1992). Importantly, TRP-2 is the first of the melanogenic proteins that is expressed in the early migratory pathway of neural crest-derived melanocytes, and is thus considered an early melanoblast marker. Anti-TRP-2 immunostaining showed cytoplasmic staining in positively-labelled melanocytes (TRP-2+) along the basal layer of the epidermis (Figure 3.6; red arrows). As with TYR-positivity, typical cytoplasmic staining was evident with TRP-2 immunostaining (Fig. 3.6). Similarly, no other epidermal cells stained positively with TRP-2 antibody and no signal was observed in sections where the primary antibody was omitted (image not shown).

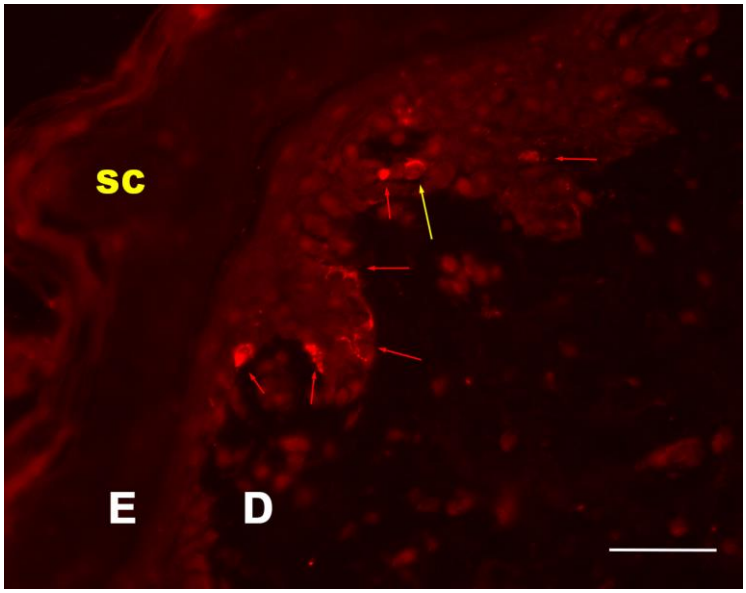

Figure 3.5 Representative image showing results of optimisation of anti-TRP-2 antibody.

TRP-2-positive melanocytes showing red cytoplasmic fluorescence (red arrows) were seen in basal layer of the epidermis. Negative control section (no primary antibody) showed no fluorescent signal (image not shown). sc = stratum corneum; E = epidermis; D = dermis. Bar = 50 μm.

3.1.4 Optimisation of fluorescent secondary antibodies

To determine which fluorescent secondary antibody would best suit the primary antibodies used in this study, various primary and secondary antibody combinations were investigated. Species-specific Alexa-488 and Cy-3 conjugated secondary antibodies were matched to the primary antibodies (see Table 2.1, Materials and Methods for details of antibodies used). It was found that for the proliferation marker, anti-BrdU, the Alexa 488-conjugated secondary antibody was the best option because it gave the least amount of background signal (see Figure 3.7 below). The same choice of secondary antibody was used for the anti-Ki-67 antibody. The Cy-3 conjugated secondary antibody, which emits in the red channel, exhibited the best fluorescent signal for all of the melanocyte-specific primary antibodies used in this study. Furthermore, by using the Cy-3 secondary with the melanocyte antigenic markers, good contrast was achieved against the green Alexa-488 fluorescent signal of the proliferation markers (Fig. 3.7). These staining parameters were maintained for all subsequent immunostaining.

Of note, when using the secondary antibodies as described, the least amount of intrinsic fluorescence was observed (i.e. autofluorescence of collagen fibres and erythrocytes in small blood vessels in the dermis). All images were captured in all three channels, viz. Alexa-488 (green), Cy3 (red) and DAPI (blue) channels, regardless of the secondary antibody selected. Composite or merged images were found to better define the skin architecture since the dermo-epidermal junction was clearly visible. Furthermore, DAPI images were only shown when it enhanced the visualisation of the results of immunohistochemical staining. Finally, only those

cells showing both Ki-67- (nuclear staining) and MelanA- (cytoplasmic staining) immunopositivity were regarded as proliferating melanocytes.

3.1.5 Double-labelling immunofluorescence protocol

In line with the aims and objectives of this study, and to implement our double-labelling strategy to detect dividing melanocytes in human skin, a highly effective, robust, double-labelling technique was developed and optimised (see Aims and Objectives in Chapter 1). By using the staining parameters determined in the single-labelling protocols, a double-labelling protocol for FFPE skin was subsequently optimised to demonstrate both dividing epidermal cells i.e. keratinocytes, differentiated melanocytes and dividing melanocytes within the epidermal compartment (Petersen et al., 2012). Of note, when both the primary antibodies used were monoclonal in origin, a sequential application of species-matched primary and secondary antibodies was used (see Appendix A4 for detailed protocol). On the other hand, when one of the primary antibodies was monoclonal and the other polyclonal in origin, then a simultaneous application in the form of a cocktail of antibodies was applied (refer to Table 2.1 for details of these optimised protocols).

3.1.5.1 Optimisation of double-immunolabelling with anti-BrdU and anti-MelanA/MART-1.

Double-labelling with anti-BrdU and anti-MelanA was performed on control samples of normal human skin according to an optimised protocol. Simultaneous incubation of primary antibodies could not be implemented in this instance, since both anti-BrdU and anti-Melan-A were monoclonal in origin. Sequential application of both the primary and secondary antibodies was necessary in this instance. Proliferating cells (BrdU+ keratinocytes) were seen in both basal and suprabasal locations in the epidermis (Fig.3.7 below). The melanosomal protein, MelanA was detected in the cytoplasm of melanocytes located at regular intervals along the basal epidermal layer. No staining was seen where the primary antibody was omitted (not shown).

3.1.5.2 Optimisation of double-labelling with anti-Ki-67 and anti-MelanA/MART-1.

Anti-Ki-67 was used as the molecular marker of proliferation for the samples that were not incubated with BrdU solution. In this instance, a cocktail application of species-matched primary and secondary antibodies was used in a double-labelling technique on control samples of normal human skin. Ki-67 immunoreactivity was observed in the nuclei of dividing keratinocytes (Ki-67+) within the basal and suprabasal layers of the epidermis (Fig.3.8 a below; green arrows). Cytoplasmic localisation of the melanocyte-specific marker, anti-MelanA, was observed in melanocytes along the basal layer (Fig.3.8 a; red arrows). Optimisation included using the fluorescent secondary antibodies interchangeably, i.e. using Donkey-Anti-mouse (DAM) -Alexa for the nuclear proliferation marker and DAM-Cy-3 for the melanocyte-specific cytoplasmic marker, when both primary antibodies were monoclonal (Fig.3.8 b). Further, by using Donkey-anti-rabbit (DARb) -Cy-3 with the polyclonal proliferation marker, Ki-67, and DAM-Alexa with the monoclonal MelanA, the optimal combination

of secondary antibodies was found (Fig.3.9 below). No staining was seen in the control samples where the primary antibody was omitted (not shown).

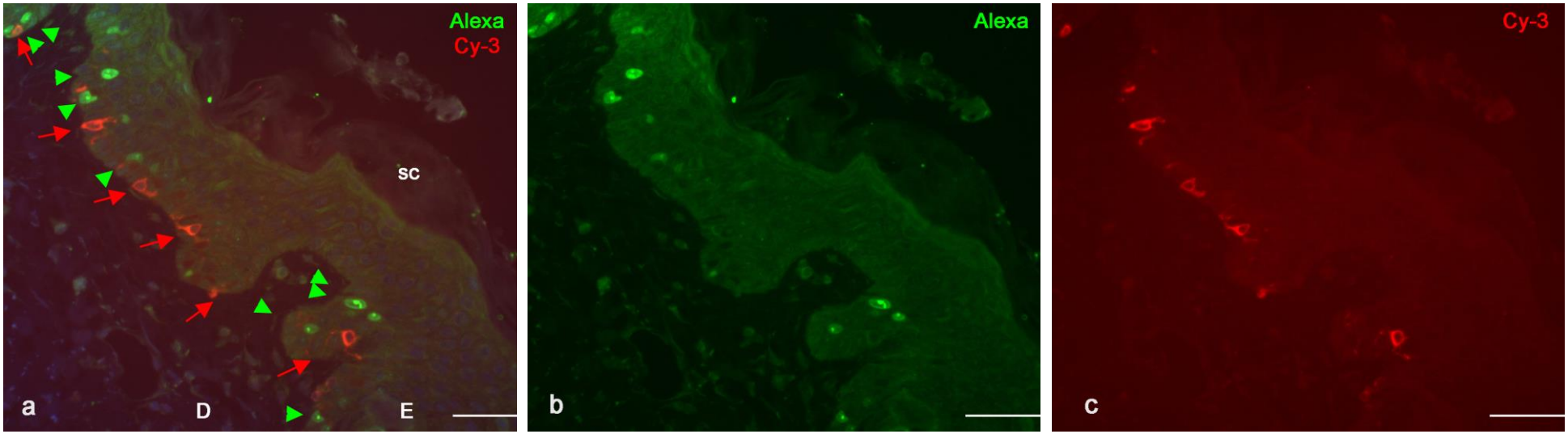

Figure 3.6 Representative images showing results of optimisation of anti-BrdU and anti-MelanA dual immunostaining.

(a) Merged image showing proliferating keratinocytes with green fluorescent labelling seen in basal and suprabasal layers of the epidermis (green arrowheads) and melanocytes showing red fluorescence seen along basal layer (red arrows). (b) BrdU+ proliferating keratinocytes were seen in basal and suprabasal locations; green channel only shown here (c) MelanA+ melanocytes were seen along the basal layer; red channel only shown here. E = epidermis; D = dermis; sc = stratum corneum. Bar = 50 um.

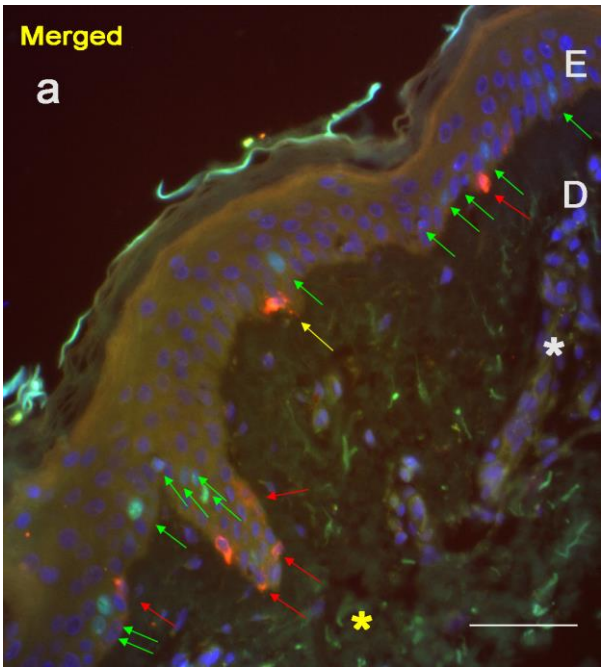
Merged
a
E
D
*
*

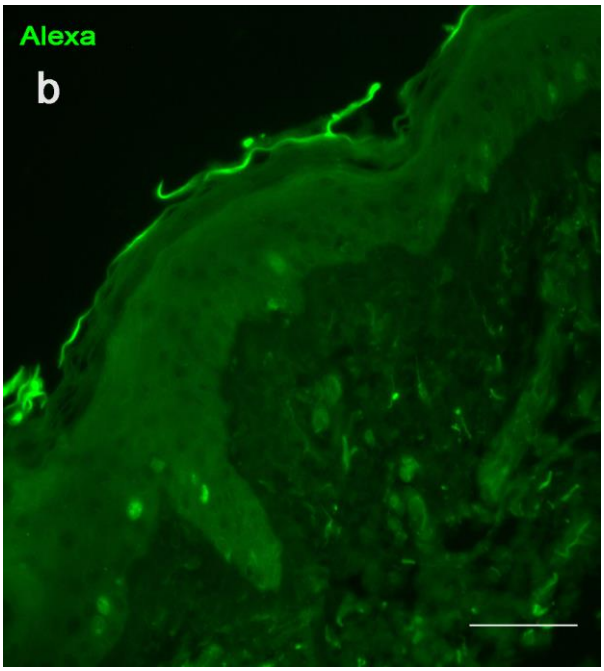
Alexa
b

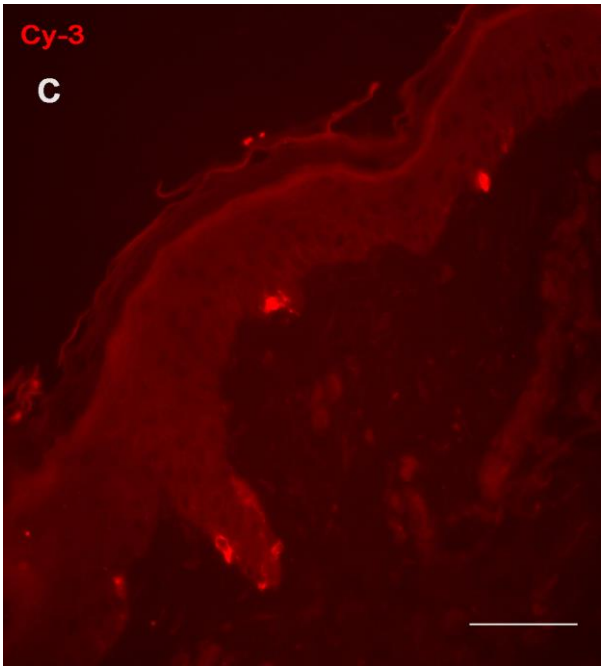
Cy-3
c

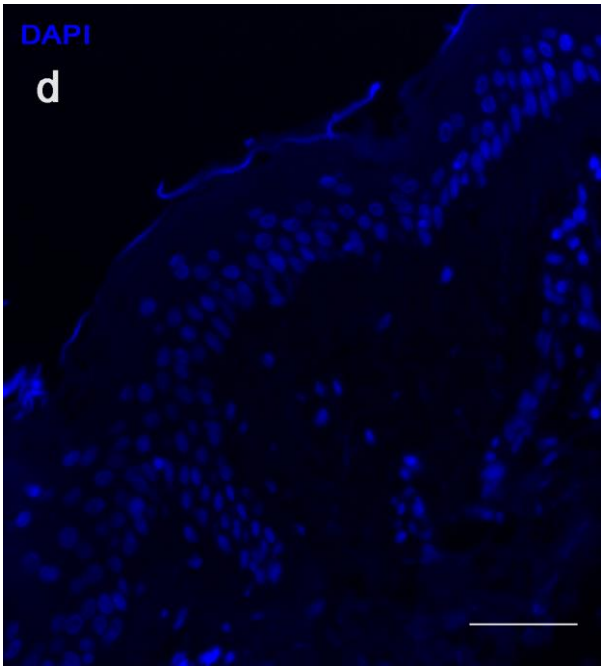
DAPI
d

Figure 3.7 Representative images showing results of optimisation of dual immunostaining with anti-Ki-67 and anti-MelanA.

(a – d) Digital images of dual immunostaining using anti-Ki-67 and anti-MelanA antibodies and DARb-Alexa and DAM-Cy-3 secondary antibodies respectively. (a) Ki-67-positive keratinocytes showing green immunofluorescent staining of nuclei were seen in basal and suprabasal layers of the epidermis (green arrows). Melanocytes were located by positive red cytoplasmic staining with anti-MelanA (red arrows). A single double-labelled melanocyte is seen in the basal layer (yellow arrow). A remnant of a sweat gland is visible in this section (white asterisk). Green autofluorescence of collagen fibres is seen in the dermis (yellow asterisk). (b to d) Digital images of Alexa staining only, Cy-3 staining only and DAPI staining only respectively. E = epidermis; D = dermis. Scale = 50 μm.

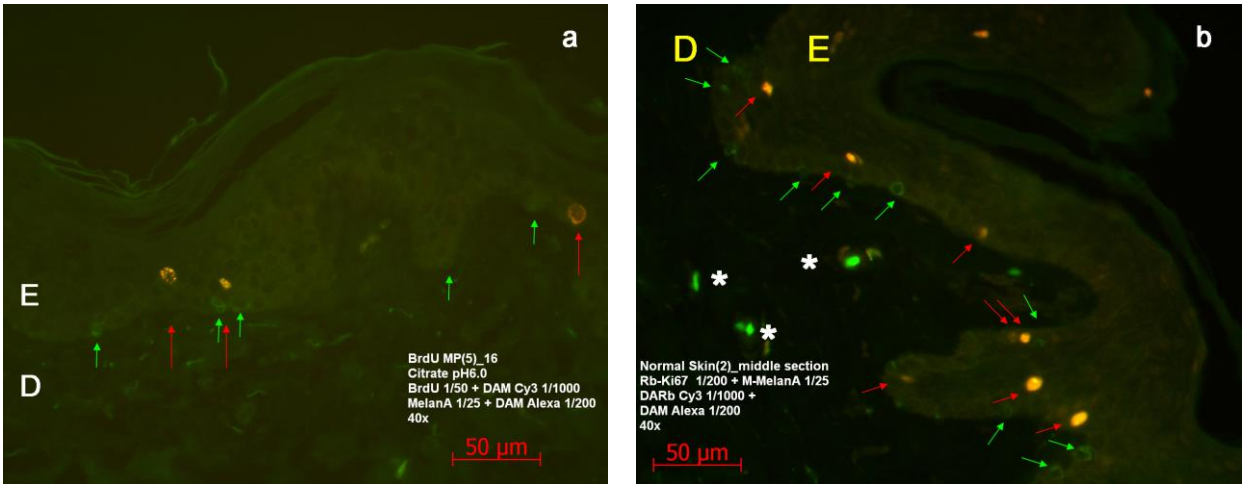

Figure 3.8 Representative images showing results of optimisation of fluorescent secondary antibody combinations

a) BrdU-positive keratinocytes showing red/orange immunofluorescence were seen in basal and suprabasal layers of the epidermis (red arrows). Optimisation using primary monoclonal anti-BrdU antibody (1:50 dilution) and monoclonal MelanA antibody (1:25 dilution) with DAM-Alexa (1:500) and DARb-Cy-3 fluorescent secondary antibodies (1:1000) respectively. b) Ki-67-positive keratinocytes showing red/orange immunofluorescence were seen in basal and suprabasal layers of the epidermis (red arrows). Optimisation using rabbit polyclonal Ki-67 antibody (1:200 dilution) and monoclonal MelanA (1:25 dilution) primary antibodies with DARb-Cy-3 (1:1000 dilution) and DAM-Alexa (1:500 dilution) fluorescent secondary antibodies respectively. E = epidermis; D = dermis. Scale = 50 μm.

3.2 Part 2: Organ culture model

The wound healing experiments were aimed at investigating whether melanocytes migrate and /or proliferate during wound healing. While many studies have uncovered the intricacies of keratinocyte migration and proliferation during wound healing, it remains unclear whether melanocytes: 1) are capable of active division during wound healing, 2) move in concert with migrating and/ or dividing keratinocytes, 3) migrate after or prior to keratinocytes and remain quiescent until complete re-epithelialisation has occurred. The following results are an analysis of melanocyte–keratinocyte spatial relationships in healing wounds following *in vitro* culture.

3.2.1 Histological analysis of organ-cultured skin samples

To gain a deeper understanding of the spatial relationship between melanocytes and keratinocytes and the participation of melanocytes during the re-epithelialisation process, a robust organ culture model of wound healing was employed. This experimental model was used to recapitulate as close as possible the physiology of the healing wound at it is *in vivo*. As described in Materials and Methods, organ culture was carried out by collaborators at A*Star Institute (Singapore). In brief, large (8mm) biopsies were taken from normal skin obtained from elective abdominoplasty, and an excisional wound of about 4-6 mm in length and 2 mm in width at the centre (refer to section 2.3.2 in Materials and Methods), was made in the centre of the biopsies by cutting with scissors. Such cuts resulted in the removal of the epidermis plus the papillary layer of the dermis to simulate a partial-thickness wound (see Figure 3.10 below). The samples were cultured at the air-liquid interface on a platform in a serum-containing medium as detailed in Materials and Methods. Migration and proliferation of epidermal cells (re-epithelialisation) occurred from the margins of the wound and was monitored as follows: Samples were obtained from the pre- and post-wounded samples on day 0, thereafter samples were removed from culture at day 1, day 2, day 5, day 10 and day 12 post-wounding, formalin-fixed and processed to wax. Sections from each time point were cut for investigation and analysis (see Chapter 2, Materials and Methods). The H&E stained sections were scanned with an Olympus VS120 digital slide scanner and used for histological assessment. Please refer to Table 2.x for number of sections examined at each time point

3.2.2 Topographical markers in the wound area

To facilitate examination of the wound area in finer detail, five topographical markers were defined for the purpose of qualitative histological assessment and semi-quantitative analysis of cellular migration and proliferation (Fig.3.10 below):

- Zone 1 is the unwounded epidermis adjacent to the wound edge. Note: when referring to zone 1 in the context of the healing wounds, this zone is the epidermis immediately adjacent to the wound edge in one field of focus; with regards to the unwounded epidermis, zone 1 is the entire normal epidermis from the wound edge to the lateral margins on both sides.
- Zone 2 is from the wound edge to the tip of the extending epidermal tongue, also referred to as the neoepidermis. Note: when the two tongues from each side of the wound meet, zone 2 is the complete neoepithelium.
- The line separating the normal epidermis from the neoepithelium (hereafter referred to as the wound edge) represents the junction between zones 1 and 2.
- Zone 3 is the wound gap, which is the region of the wound not covered by neoepithelium.
- Zone 4 is the lateral wound margins of the tissue block (i.e. original punch biopsy) where epithelial outgrowths were seen to be growing.

Representative image of zones 1 - 3 is shown in Fig. 3.10 a and zone 4 (epithelial outgrowths) is shown in Fig.3.10 b.

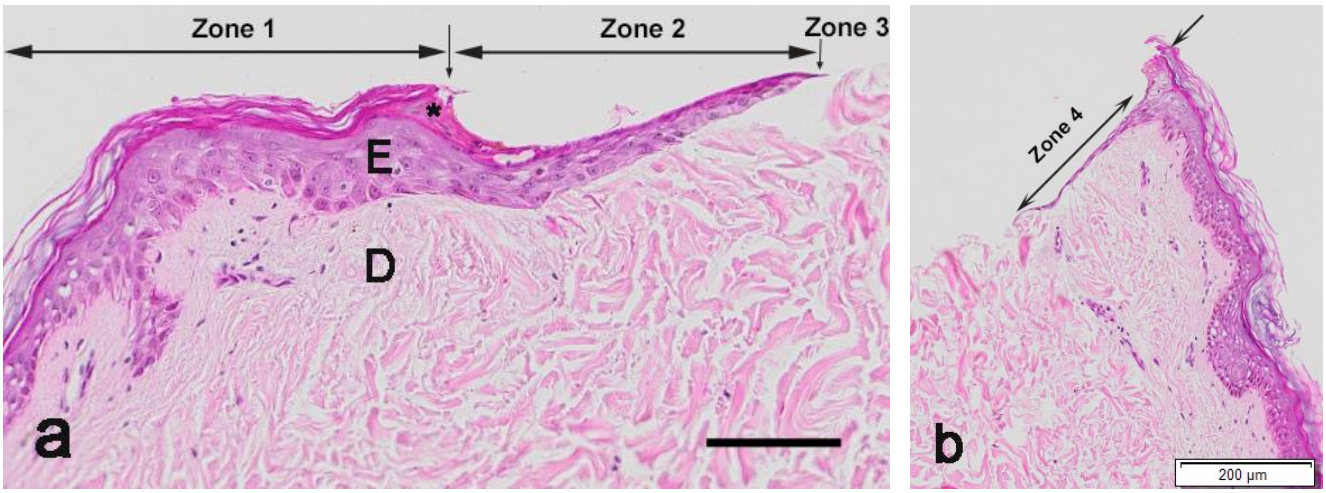

Figure 3.9 Topographical markers identified in the wound area to aid histological assessment.

(a) Digital image of representative section of the epidermis and dermis from a healing wound removed after 48 hours (day 2) in culture. Three distinct zones were defined for the wound area. From left to right, zone 1 is the epidermis adjacent to the wound; zone 2 comprises the neoepidermis extending from the wound edge to the tip of the migrating tongue; zone 3 represents the wound gap (yellow dotted line). The wound edge is indicated by the long black arrow. The tip of the healing tongue is seen extending into the gap (short black arrow). An area of hyperparakeratosis is visible in the stratum corneum at the wound edge (asterisk). (b) Zone 4 comprises the epithelial outgrowth (double-ended arrow) originating from the lateral margins of the original punch biopsy (short arrow). E = epidermis; D = dermis. Bar = 100 μm.

3.2.3 Histological assessment of tissue viability in cultured skin samples

The first step of this study was to establish whether the organ-cultured skin remained viable during the entire culture period of 12 days, using the culture method as described in Materials and Methods. To do this, histological assessment of wounded skin sections after in vitro culture was performed and tissues were scrutinised to check for viability and structural integrity of the epidermis and dermis and to establish whether the wounds underwent the typical wound healing response. Two sections from each time point were first examined at low magnification to obtain an overall picture of the cultured skin samples, and again at a higher magnification to scrutinize the normal epidermis of the wounded skin cultures to determine the growth of the tongues, and the nature of cells that populate the neoepidermis during wound healing. A histological overview of the wound healing process is shown in Fig.3.11 below. The wound edges created by partial-thickness excisional wounds are evident in all of the samples. Zone 2 has a fully re-epithelialised epidermis indicating complete wound closure as seen in skin samples from day 2 (Fig.3.11 c) to day 12 (Fig.3.11 f) post-wounding. In some of the sections examined, separation of the upper keratinised layers of the epidermis was seen (Fig.3.11 e). This is a typical tissue-processing artifact commonly seen in histological sections of skin. The lateral wound margins (from original biopsies) are seen (asterisk), and epithelial outgrowths were observed growing from these margins, sometimes extending all the way around the dermal aspect of the biopsies. These outgrowths did not appear to be stratified and consisted of about 2-3 layers and will be more fully described below (see Fig. 3.20 below).

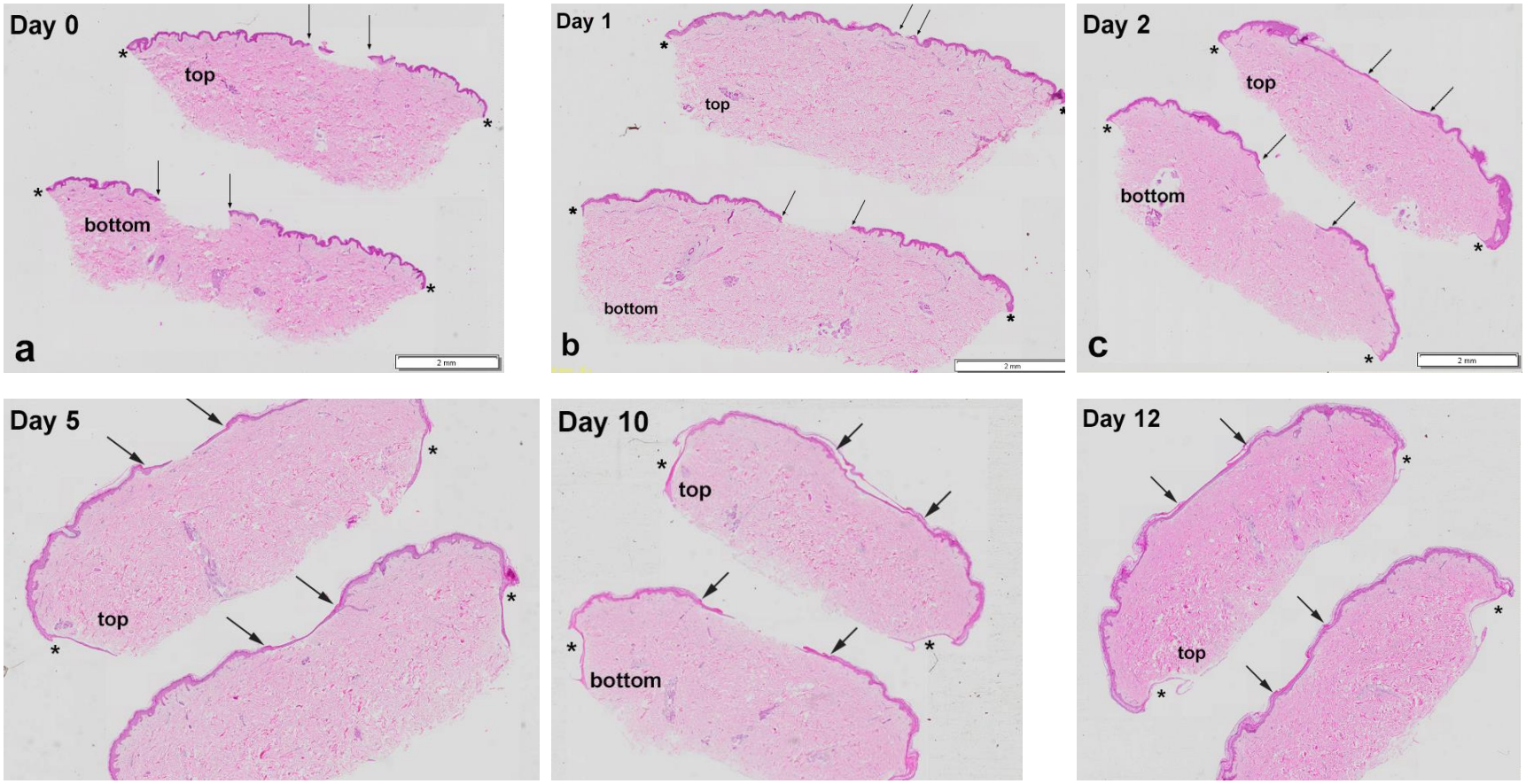

Figure 3.10 Histological overview of the healing wounds in culture.

Representative H&E-stained sections of the wounded skin samples from day 0 to day 12, cultured at ALI (a-f respectively). Two sections from each time point are shown. The wound edges (created by partial-thickness excisional wounds) are marked by arrows on both sides of the wound gap (when visible). Complete closure is seen in skin samples from day 5 (Fig. 3.9 d) to day 12 (Fig. 3.9 f) post-wounding. The lateral wound margins (zone 4) are marked with an asterisk. Epidermal outgrowths are seen growing from these lateral margins around the dermal aspect of the biopsy. Bar = 2 mm.

The normal epidermis of the wounded skin cultures was then examined to see whether any cellular abnormalities/disturbances were present (Fig.3.12 below). Approximately 6 to 8 cell layers were present in the unwounded epidermis across all the time points analysed (Fig.3.1.2 a-f). Stratification of the unwounded epidermis appeared normal since all epidermal layers were identifiable from stratum basale to stratum corneum. Rete pegs were still visible up to day 12 of culture in the normal epidermis. Hyperparakeratosis was seen in days 10 and 12 samples with accompanying stratum corneum thickening. Several retained nuclei within mildly vacuolated cells were seen in the lower stratum corneum layers (arrows). The staining intensity of the epidermis also appeared to be reduced from day 2 through to day 12 of culture.

Upon further examination, epidermal perturbances typical of prolonged tissue culture were detected in the sections from day 5 to day 12 post-wounding. A mild degree of vacuolation, which is an indicator of apoptosis and cellular degradation, was seen in sections from day 5 through day 12 (Fig.3.12 d-f; asterisks). Nuclear condensation, as suggested by the presence of vacuolated cells was also observed, although pyknotic cells were not evident in any of the epidermal layers. A mild degree of acantholysis within the upper strata was observed. Detachment of epidermis from dermis (epidermolysis) was not observed. The dermis was histologically unremarkable. In sum, in this wound healing assay, skin was cultured up to 12 days with evidence of neoepidermis formation and little apparent evidence of deleterious effects due to organ culture.

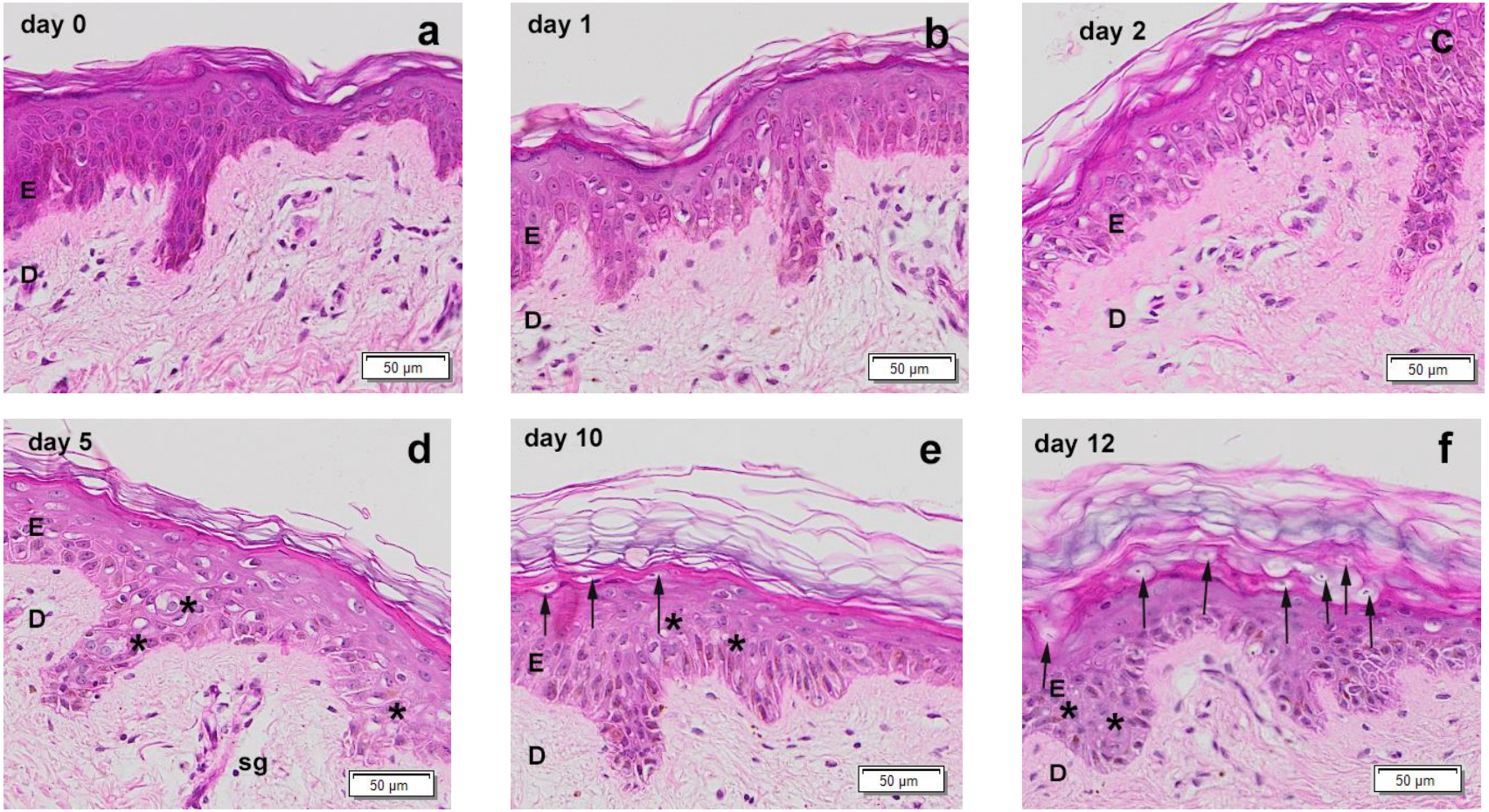
day 0
a
E
D
50 µm
day 1
b
E
D
50 µm
day 2
c
E
D
50 µm
day 5
d
E
D
sg
50 µm
day 10
e
E
D
50 µm
day 12
f
E
D
50 µm

Figure 3.11 Histological appearance of normal unwounded epidermis.

Representative sections of unwounded skin samples that were cultured at ALI across all time points. The epidermis appeared normal and the stratified layers were clearly seen. The epidermis however, appeared progressively less cellular (generally paler staining) from day 5 to day 12 compared to day 0 and day 1 of culture. Mild vacuolation of the epidermis was seen from day 5 to day 12 (asterisks). The stratum corneum appeared hyperparakeratotic from day 10 to day 12 and several retained nuclei were seen in the lower corneal layers (arrows). Rete pegs and dermal papillae are still visible up to day 12 of culture in the unwounded epidermis. No visible cellular abnormalities were observed. Bar = 50um.

3.3 Growth of the epithelial tongues (neoepidermis) during culture

To determine the length and extension of the tongues post-wounding, the tongue lengths (zone 2) were measured along the basement membrane using *ImageJ* (see Appendix D 2 for data table). Only the data for tongues showing incomplete closure of the wound gap were used for statistical analysis to preclude skewing of data due to cessation of growth that can arise as a result of confluence due to meeting of tongues. The data were analysed using Graphpad Prism 6 software (see Fig.3.13 below). Statistical analysis was performed using one -way analysis of variance (ANOVA) and a Dunnett's post hoc test. One-way Anova was used to compare the cultured samples against a control, in this instance, the day 1 samples. For one way-ANOVA, the criterion for statistical significance used was $p < 0.0001$, and for the Dunnett's Multiple Comparison Test, $p < 0.05$. Please see text below for further analysis and comment.

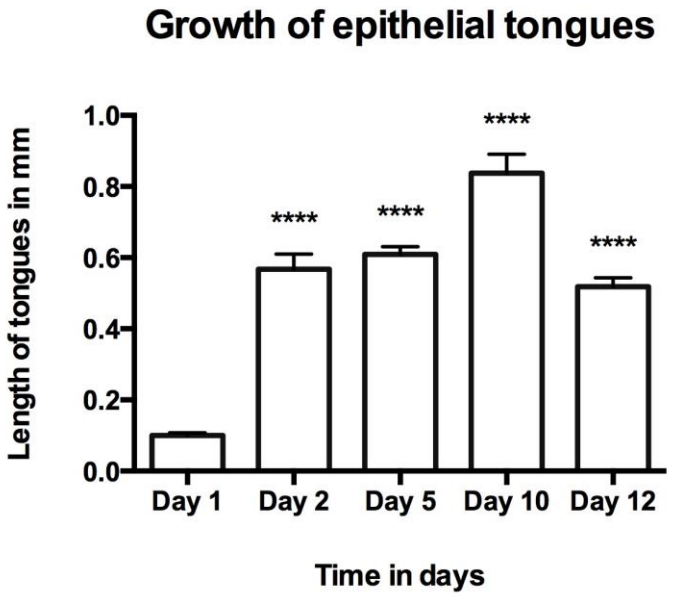

Figure 3.12 Graphic representation of the growth of epithelial tongues in healing wounds from day 1 to day 12 of ALI culture.

The epithelial tongue lengths are represented in mm as measured along the basal layer of the epidermis. Results are displayed as mean ± SEM (n = x). Significance was determined using one-way ANOVA with Dunnett's post-hoc test. **** = p<0.0001.

Next, an in-depth examination was carried out to assess the healing wounds for tongue/ neoepidermis formation. The following evidence of successful wound healing in vitro was noted: At time zero (wounded skin samples), the

cut edges and adjacent epidermis of the full-thickness wounded sections (zone 1) and the wound gap (zone 3) were clearly discernible (Fig.3.14). Since these samples were fixed immediately after wounding, epithelial tongue growth was not monitored in these sections.

Re-epithelialisation of the wounded area was observed in all of the sections examined from day 1 to day 12 (Fig. 3.15 to Fig. 3.19 below). After one day in culture, epiboly (rolling over of epidermal cells) occurred at the wound margins (Fig.3.15 below). A short `' lip`' of cells was observed at the wound edge consisting of up to 4 cells across (Fig.3.15 a & b). Taking both sides of the wound into account, the average length of the epibolic cells was 0.1 mm (± 0.008 SEM). The formation of a hyperparakeratotic layer (stained darker pink) can be seen at the wound edges just above the migrating cells (Fig.3.15 a & b; asterisks). The wound gap (zone 3) was clearly visible. The dermis was unremarkable.

Samples cultured for 2 days showed growth of the tongues from both edges towards the centre of the wound. The resultant formation of zone 2 (neoepithelium) extending from the wound edge into zone 3 (wound gap) is seen in Fig.3.16 a & d. Epithelial tongues were inconsistent in length on opposing sides of the wound as seen in day 1 samples. The average combined tongue length at day 2 was 0,568 mm (± 0.043 SEM) along the basement membrane (see Appendix D.2). The wound margins are still visible on either side (arrows). High power view images taken from the left and right sides of the wound are shown in Fig.3.16 b & c. An area of hyperparakeratosis is visible at the wound margins in Fig.3.15 a & b, as shown by an asterisk. The confluent retained nuclei in the stratum corneum form a dark purple band between the granulosum layer and the eosinophilic corneal layer in b & c. The neoepidermis is thinner (3-4 cells thick) than the normal epidermis in zone 1 which is several cell layers thick. The neoepidermis was 4-5 cells thick at the wound edge and tapered to one cell at the tip. The basement membrane was regular (straight) and neither dermal papillae nor rete pegs were evident.

The uppermost layer of the neoepidermis in day 2 samples stained a darker pink compared to the lower epidermal layers and was continuous with the stratum corneum of the adjacent epidermis (also see Fig.3.17 below). Usui et al. (2013) examined archival human skin sections and observed that the parakeratotic keratinocytes (corneocytes) found in the stratum lucidum played an active role in wound healing. Firstly, by expansion, most likely via loss of terminal differentiation into anucleate horny layer cells, and second, by migration as a result of cellular displacement (due to confluence), these corneoocytes provided a temporary buffer zone between the scab and the neoepidermis by migrating around and under the scab. On closer examination, the migrating tongues that were observed in day 2 samples were comprised of two components: an upper dark pink-stained component (Fig 3.16 b & c; asterisk) and

a cellular component beneath. It is highly likely that the former is analogous to the parakeratotic corneocyte layer as described by Usui et al. (2013) and the latter is the proliferating and migrating neoepidermis.

By day 5 the average length of the neoepidermis was 0,61mm, (± 0.021 SEM) indicating that there had been further outward growth of the neoepidermis between days 2 and 5 (Fig.3.17). The neoepidermis was on average 6-8 cells thick at its widest and tapered off to 3-4 cells at the tip. Although the layers were stratified, the epithelial layers were not discernible since all the cells looked the same and all the cells were lying in the horizontal plane (i.e. parallel to the basement membrane). The first portion of the tongue closest to the wound edge showed the same darker pink staining (hyperparakeratosis; asterisk) in the uppermost layer as previously described for the day 2 sections (see Fig.3.15). The leading edges (tips) of the tongues, however, were not covered by the parakeratotic layer (Fig.3.17). Flattened nuclei were visible underneath this layer and appeared to be oriented perpendicular to the basement membrane at the wound edge and parallel to the basement membrane across the length of the tongue (Figure 3.17 b & c).

At day 10, the average length of the neopidermis measured 0,84 mm (± 0.053 SEM) (Fig.3.18). There was inconsistent growth in the day 10 samples examined. One of the samples examined showed complete neoepidermis formation and gap closure (Figure 3.18 a), whereas the second sample showed incomplete re-epithelialisation with the wound gap (zone 3) still evident (Figure 3.18 b). In the section that showed complete closure, the neoepidermis (zone 2) was thinner than the normal epidermis (zone 1). The sample that was not fully re-epithelialised revealed an uppermost eosinophilic layer with retained nuclei, which appeared as a distinct layer above the migrating epithelial tongue beneath, as described before for day 2 skin explant culture; this layer did not extend across the full upper surface of the developing tongue. Similarly, this darker pink upper layer was also seen in the sample that showed complete wound closure, but it extended across the entire neoepidermis in this sample (Figure 3.18 a). The upper corneal layers have become detached from the lower layers in (a). This is a commonly seen histological artifact and does not detract from the analysis.

At day 12, there appeared to be an apparent decrease in average tongue length; actual average measurement was 0,52 mm (± 0.025 SEM). Bearing in mind that the skin samples have been in culture for almost two weeks, this is not an unexpected result. This decrease in the average lengths of neoepidermis can most likely be attributed to firstly, cessation of growth in these late culture skin samples; secondly, possibly due to contact inhibition because of the tongues meeting; or thirdly, most likely due to prolonged organ culture. Complete re-epithelialisation representing wound closure was seen in all but one of the day 12 sections examined (Fig. 3.19). The day 12 neoepidermis was up to four cells thick in the middle portion.

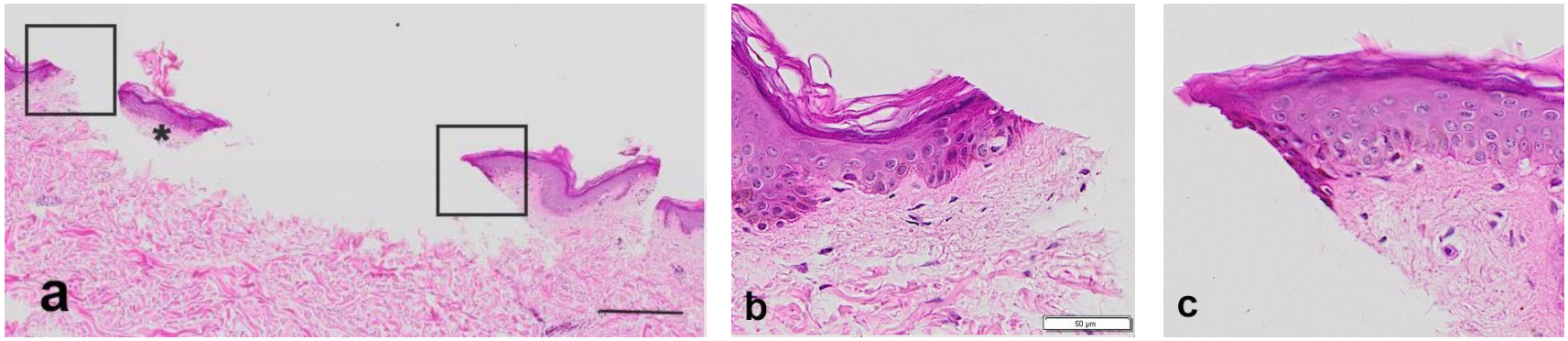

Figure 3.13 Re-epithelialisation during wound healing (day 0)

(a) Representative digital images taken from H&E-stained sections of day 0 (day of explant) samples. Section shows the wound margins (boxed areas) and the wound gap between. Epidermal tongue growth was not monitored in these samples. A retained portion of cut epidermis is still present in this image (asterisk). (b & c) High power view images of boxed areas in (a) showing the left and right wound margins. Bar = 500 µm for (a); 50 µm for (b) & (c).

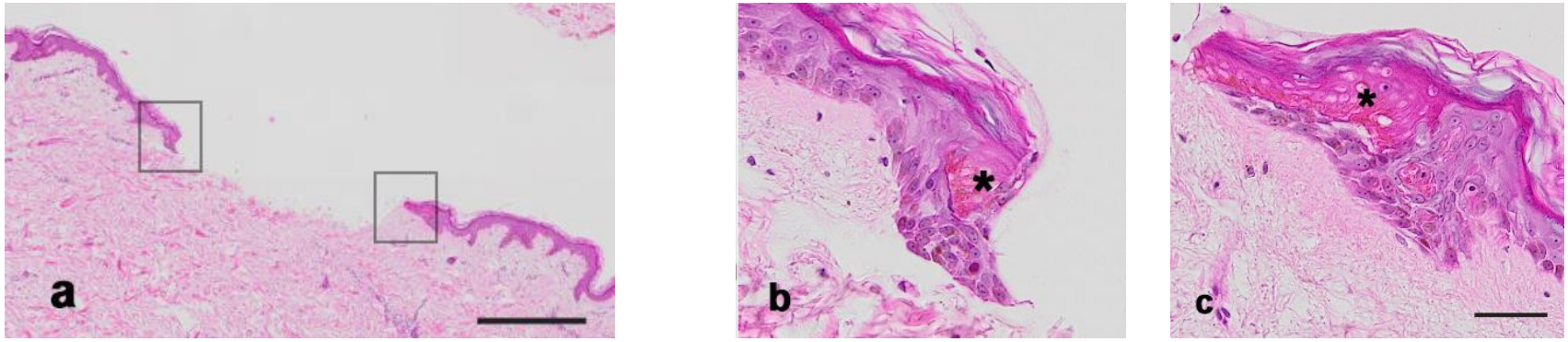

Figure 3.14 Re-epithelialisation during wound healing (day 1)

(a) Representative digital images taken from H&E-stained sections of day 1 post-wounding samples. The wound gap is still visible. (b & c) High power view images of boxed areas in (a) showing the left and right wound margins respectively. Sections show the rolling over of epidermal cells (epiboly) occurring at the wound edges. Formation of hyperparakeratotic layer can be seen (asterisk). Bar = 500 µm for (a); 50 µm for (b) & (c).

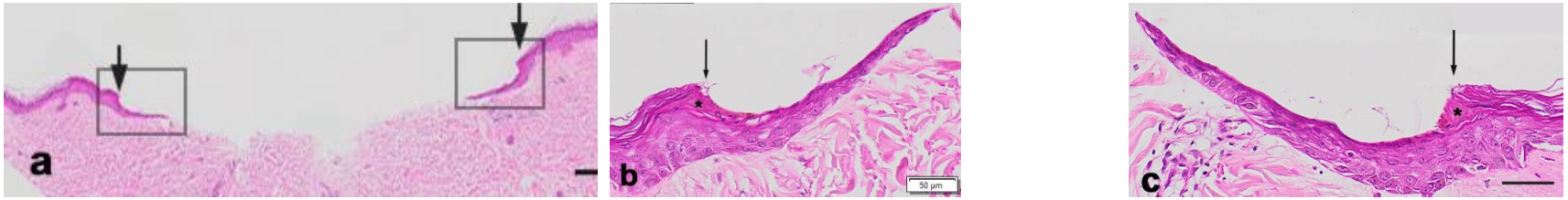

Figure 3.15 Re-epithelialisation during wound healing (day 2).

(a) Representative digital images taken from H&E-stained sections of day 2 post-wounding samples. Section show the wound margins (arrows) and the wound gap between. Epithelial tongues are seen growing towards each other. (b & c) High power view images of boxed areas in (a) showing the left and right wound margins respectively. The neoepidermis (zone 2) is thinner than the normal epidermis (zone 1). Areas of hyperparakeratosis are seen above the developing tongues (asterisk). Bar = 500 µm for (a); 50 µm for (b) & (c).

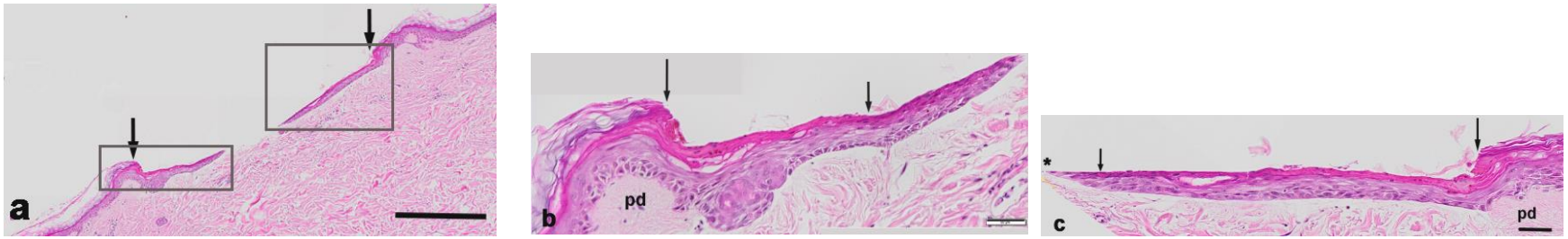

Figure 3.16 Re-epithelialisation during wound healing (day 5).

(a) Representative digital images taken from H&E-stained sections of day 5 post-wounding samples. The neoepidermis does not extend fully across the gap (zone 3) in (a); High power view images of boxed areas showing the left and right wound margins as seen in (b & c) respectively. The neoepidermis is thinner than the normal epidermis and appears to be 3-4 cells thick. The normal epidermis consists of up to 6 cell layers. The parakeratotic layer extends from the wound margin (longer arrow) to the distal third of the tongue (shorter arrow). The leading edge of the tongue is not covered by this parakeratotic layer (asterisk) in (c). The papillary dermis is evident in these high-power images. Pd = papillary dermis. Bar = 500 µm for (a); 50 µm for (b) & (c).

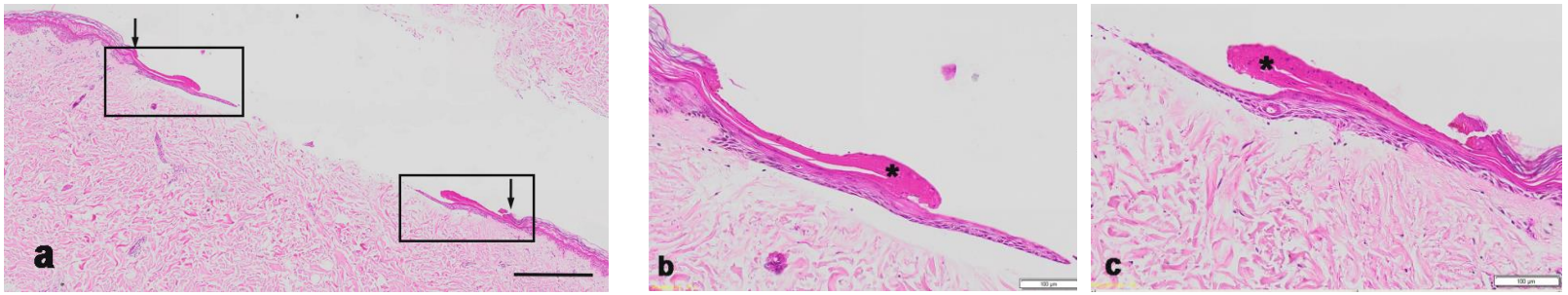

Figure 3.17 Re-epithelialisation during wound healing (day 10).

(a) Representative digital images taken from H&E-stained sections of day 10 post-wounding samples. High power view images of boxed areas taken from the left and right wound margins as seen in (b & c) respectively. The parakeratotic layer (asterisk) appears to be more prominent and does not extend across the full surface of the developing tongue. Bar = 500 µm for (a); 100 µm for (b) & (c).

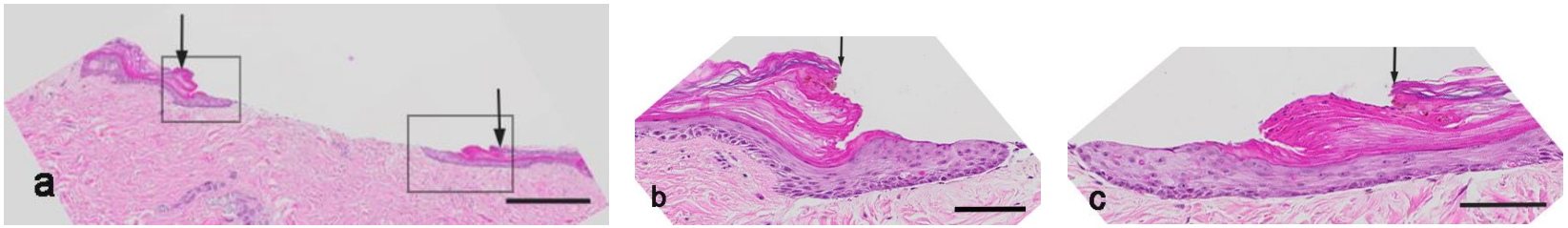

Figure 3.18 Re-epithelialisation during wound healing (day 12).

a) Representative digital images taken from H&E-stained sections of day 12 post-wounding samples. The epithelial tongues are seen growing towards each other; wound edges are marked by arrows. The wound gap is still visible in this day 12 section. (b &c) High power view images taken from the left and right wound margins are shown in (b) & (c) respectively. Bar = 500 µm for (a); 50 µm for (b) & (c).

3.1 Epithelial outgrowth formation at the lateral biopsy edges

In all the skin explant cultures from day 1 onwards it was evident that there were epithelial outgrowths at the outer free lateral aspects of the biopsies in submerged culture (zone 4). The lengths of these lateral outgrowths were measured in a similar fashion to that of the epithelial tongues, using ImageJ software. Data were analysed using GraphPad Prism 6 software. The outgrowths continued around to the inner aspect of the dermis and grew towards each other in a similar fashion to that seen in the healing tongues (Fig.3.20). However, in contrast to the healing tongues, these epithelial outgrowths appeared to grow faster, since these outgrowths were longer in length than the neoepidermal tongues (Fig.3.20; see Appendix D.3 and D.4 for data tables). The average lengths for the epithelial outgrowths at days 5, 10 and 12 were greater than that of the epithelial tongues for the same time points. Moreover, epidermal stratification and formation of corneal layer were not evident in these outgrowths, as they were only 2-3 cells thick at the widest part. This suggests that elongation/growth of these tongues occurred faster than stratification or differentiation of the cell layers. A further interesting observation was a supply of cells from a nearby hair follicle and associated sebaceous gland to the epithelial outgrowths was seen in one of the day 12 samples (Fig.3.21a & b). Several cell nuclei appeared to be undergoing linear organisation along the anterior aspect of the dermis close to the migrating epithelial outgrowth (Fig.3.21 b; arrows). Augmentation of wound repair by hair follicles and sebaceous glands during wound healing has been previously described (Levy et al., 2007a).

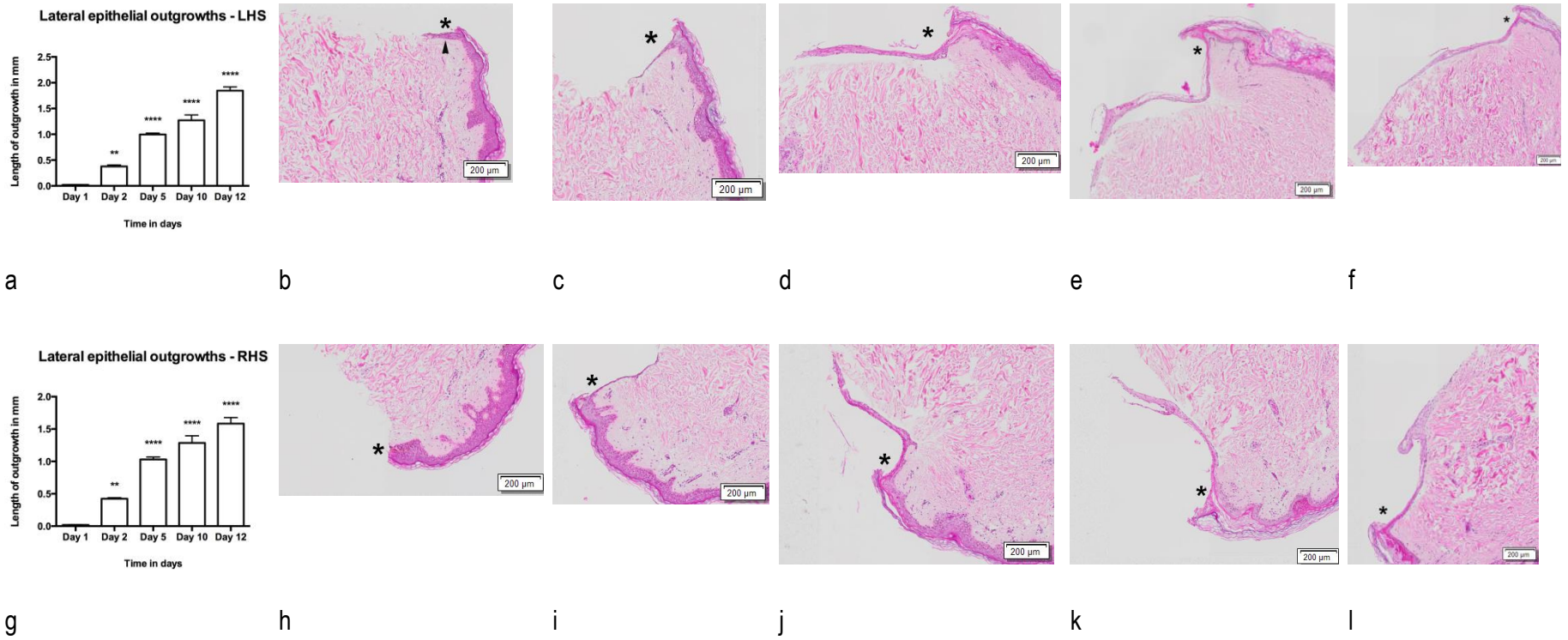

Figure 3.19 Epithelial outgrowths in skin explant cultures under submerged conditions.

(a) and (g) Graph of epithelial outgrowth lengths (zone 4) from day 1 to day 12, showing left and right side of biopsies respectively. (b-f) Representative digital images of days 1 to 12 cultured skin samples showing submerged epithelial outgrowths on left hand side extending along the lateral aspect of the dermis (asterisk denotes start of outgrowth). On the left biopsy edge in (b) what appears to be epithelial growth, is in fact part of a rete peg (arrowhead), since no growth was evident on day 1. (h-l) Representative digital images of days 1 to 12 cultured skin samples showing submerged epithelial outgrowths on right hand side extending along the lateral aspect of the dermis (asterisk denotes start of outgrowth). The lengths of the epithelial outgrowths on both sides were proportional to the number of days spent in culture. Results are displayed as mean ± SEM (n = 4, 8, 8,6, & 11 for day 1, 2, 5, 10 & 12 respectively). Significance was determined using one-way ANOVA with Dunnett's post-hoc test. ** = $p<0.01$; *** = $p<0.001$. Bar = 200 µm.

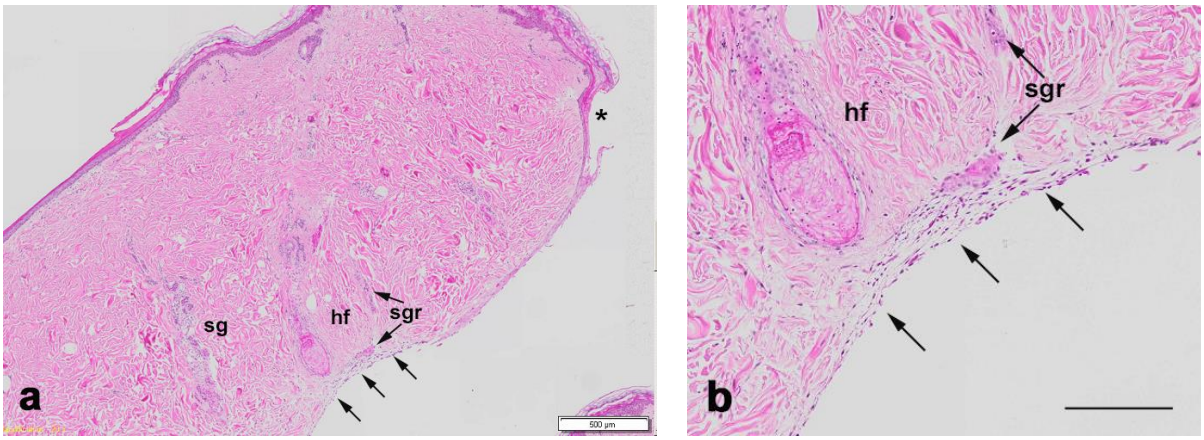

Figure 3.20 Growth augmentation of the epithelial outgrowth on dermal aspect of day 12 cultured skin sample.

Representative digital image of growth augmentation by a nearby hair follicle and fragment of sweat gland in a day 12 cultured skin sample (submerged culture conditions). (a) Arrows show linear organisation of cells in continuity with the epithelial outgrowth along the dermal aspect of the cultured skin sample. A hair follicle (hf) and sweat gland (sg) are seen proximal to the dermal outgrowth. The lateral epithelial outgrowth starts at the right hand side edge of the biopsy (asterisk) and continues along the dermis until the two dermal outgrowths almost meet. (b) Digital image of the same area described in (a) at a greater magnification. The same hair follicle (hf) and remnants of a sweat gland (sgr) are seen close to the dermal outgrowth. Scale = 500 µm and 200 µm for (a) and (b) respectively.

To provide further evidence to support the previous finding of diminished stratification and/ or cellular differentiation in the lateral outgrowths, the average thickness of both the tongues and the epithelial outgrowths was determined using ImageJ software as before. Measurements were captured in triplicate at the following sites in day 10 and 12 cultured skin samples: i) just beyond the wound edge (first third of tongue), ii) approximately midway along the tongue (middle third of tongue), and iii) towards the end of the epithelial tongues (last third of tongue). Similar measurements were taken along the lateral outgrowths of the same skin samples. Data were analysed as before using Graph Pad Prism 6 (see Appendix D.5 for data table). Results show that the average epithelial tongue thickness was greater than the thickness of the lateral outgrowths in the day 10 and day 12 samples analysed (Fig.3.22 below). A statistical significance was reported for the differences between the means, ($p < 0.05$) using Sidak's multiple comparisons post-hoc test. Moreover, by performing a visual estimation of the number of cell layers in these two epithelial compartments, it was evident that the epithelial tongues were up to 4 – 5 cells thick and up to 5 – 6 cells thick at day 10 and 12 respectively, compared to the lateral outgrowths, which were 2-3 cells thick and 3-4 cells thick at days 10 and 12 respectively.

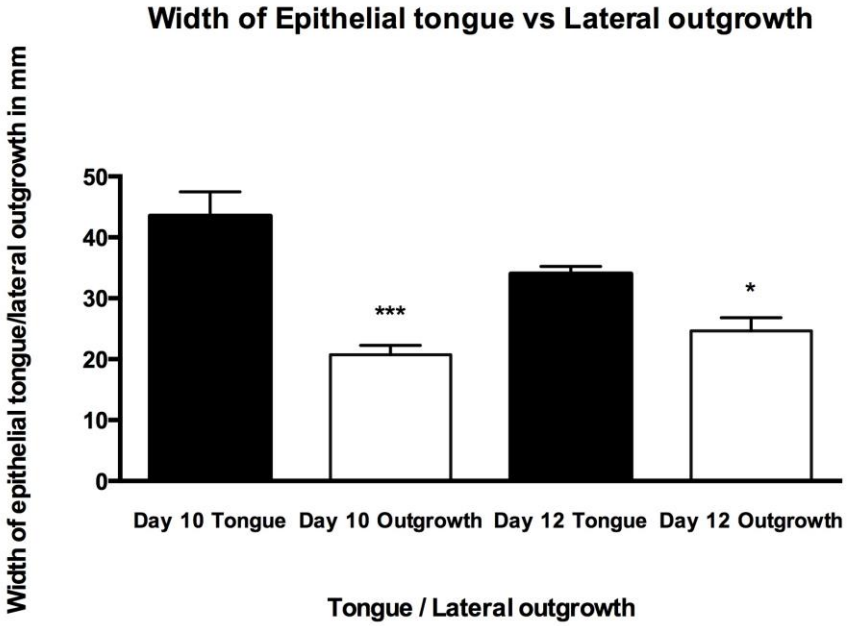

Figure 3.21 Comparison of thicknesses between epithelial tongues and submerged lateral outgrowths.

Graph showing comparison of thickness of tongues and lateral outgrowths for days 10 and 12 samples. The thickness of the epithelial tongues was compared to the lateral outgrowths in day 10 and 12 samples, both time points analysed showed a statistical significance for the differences between the means ($p < 0.05$). Significance was determined using one-way ANOVA with Sidak's multiple comparisons post-hoc test. *$p < 0.05$; ***$p < 0.001$.

Together these results show that tongue growth and extension contributed to wound closure, providing evidence that re-epithelialisation occurred in the cultured wounded skin samples in this experimental setup. A complete neoepidermis was observed in some of the day 2, 5, 10 and 12 cultured skin samples. Furthermore, the results showed that after an initial increase in average measurement of the tongue lengths between days 1 and 2, the tongues showed little growth between days 5 and 10. At day 12, an apparent decrease in tongue length was observed. This suggests that either growth of the tongues had ceased, or that the tongues were shrinking. Minimal hyperparakeratosis was seen in the corneal layer of the healing wounds.

Epithelial outgrowths were seen at the cut edges of the submerged skin biopsies as early as day 2, and extended all the way around the dermal aspect of the biopsies by day 12. These outgrowths wrapped around the dermis, almost meeting in the middle in one of the sections examined (Fig.3.20 above). These lateral epithelial outgrowths were thinner than the neoepithelial tongues and the normal epidermis and were on average 2 -3 cell layers thick.

Based on the above observations one can conclude that the organ culture model of wound healing used in this study was adequate to recapitulate the re-epithelialisation phase of the wound healing process and confirms what others have found during in vitro studies of wound healing in human skin.

3.4 Part 3: Cell proliferation dynamics during re-epithelialisation

3.4.1 Keratinocyte proliferation during re-epithelialisation

Following the wounding of skin, keratinocytes are mobilised and activated in order to close the wound and to restore essential barrier function. To assess keratinocyte proliferation during re-epithelialisation in this *in vitro* model of wound repair, cultured skin samples were fixed, processed, sectioned and subjected to immunofluorescent staining using the nuclear antigen Ki-67, which is a marker of all cycling cells (except cells in G_0 phase) as described above. Cell proliferation was analysed within the normal epidermis on both sides distal to the wound edge, and in the epithelial tongues from and including the wound edge to the tip of the tongues. Data were analysed using GraphPad Prism 6.0 and results were expressed as the average number of dividing keratinocytes (± SEM) per mm along the basement membrane.

3.4.2 Analysis of keratinocytes in normal epidermis

Dividing keratinocytes (Ki-67+), showing red fluorescence, were seen mainly in the basal layer and immediate suprabasal layer in the normal epidermis of cultured skin samples (Figure 3.23 a-d). The dividing keratinocytes occurred close together in clusters (Fig 3.23 a; long green arrow), but more often occurred singly (Fig. 3.23 a; short yellow arrow) or as dividing pairs (Fig, 3.23 a; short green arrows & c; green arrows; insert). Sometimes one of a pair of dividing or recently-divided keratinocytes appeared to be located just above its mate, thus appearing to be migrating upwards, with the second of the two keratinocytes remaining in a basal position (Fig. 3.23 b; long green arrow). In all of the sections examined, autofluorescence of collagen fibres was observed, as seen by green fluorescence in the dermal compartment (Fig.3.23 b). Remnants of sweat glands were sometimes visible in the dermis, with their nuclei counterstained with the DAPI nuclear counterstain (white asterisks).

.

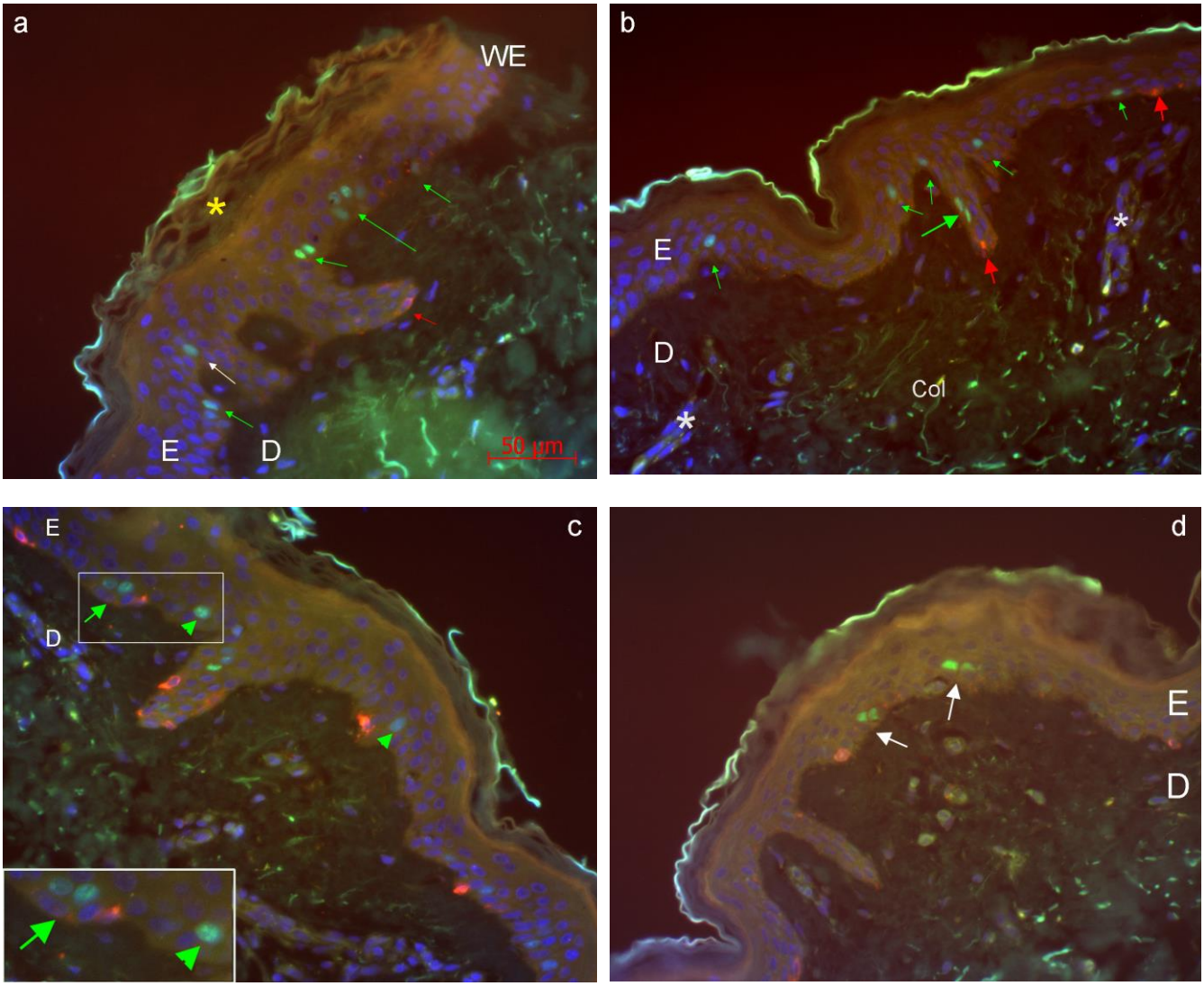
a
WE
E
D
50 µm
b
E
D
Col
c
E
D
d
E
D

Figure 3.22 Representative images of skin in longitudinal section showing the normal epidermis immunostained with anti-Ki-67 and anti-MelanA.

(a - d) Dividing keratinocytes showing typical nuclear staining for anti-Ki-67 antibody were seen in both basal and suprabasal locations in the epidermis (green arrows),. (a) Keratinocytes occurred either singly (short green arrows), in pairs (green arrows) or sometimes in clusters (long green arrow). The outer keratin layer is visible and also exhibits autofluorescence (yellow asterisk). (b) Dividing keratinocytes were seen in the epidermis, one situated above the other as if the former were migrating upwards. Collagen fibres, seen in the dermis, exhibit green autofluorescence with the Alexa fluorescent tag. Remnants of sweat glands are visible in the dermis (white asterisks). (c) Occasionally dividing keratinocytes were seen just proximal to the basal layer, sometimes in pairs and sometimes singly. Insert shows a high-power view of the boxed area. (d) Pairs of dividing keratinocytes were seen in basal and suprabasal layers (white arrows). (a & b) Melanocytes showing cytoplasmic staining for anti-MelanA antibody (red arrowheads) are seen along the basal layer in these dual stained sections. The nuclei of non-dividing keratinocytes in epidermis and fibroblasts in dermis are stained blue with DAPI fluorescent counterstain. E = epidermis; D = dermis; WE = wound edge; Col = collagen fibres. Bar = 50 μm.

3.4.3 Quantitative analysis of dividing keratinocytes in normal epidermis

To ascertain the viability of this culture model, the number of proliferating keratinocytes was determined over the 12-day culture period. As can be seen from the graph (Figure 3.24 below) and data table (Appendix D.6), the average numbers of dividing keratinocytes in the normal epidermis (dark green bars) remained more or less constant over the culture period. There appeared to be a drop between day 0 (day of explant) and day 1. This can probably be explained as a drop in the overall metabolism as the skin adjusts to the new culture environment. Because the average number of dividing keratinocytes did not decrease, one can deduce that the skin remained viable during this period.

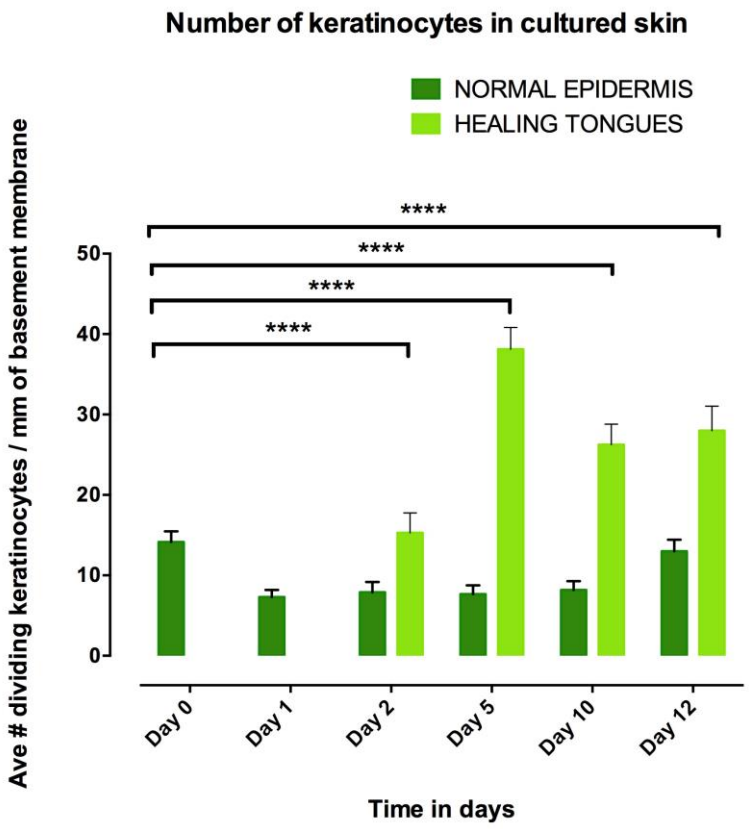

Figure 3.23 Graph representing keratinocyte proliferation in cultured skin.

Dividing keratinocytes (Ki-67+) were counted in normal epidermis and in healing tongues from day 0 to day 12. Data are expressed as the average number of dividing keratinocytes per mm of basement membrane at each time point. **** = $p<0.0001$ using Tukey's multiple comparisons test.

Next, the number of proliferating keratinocytes in the wound/ tongue zone was determined. In Day 0 samples (prior to culture), there was obviously no tongue and at day 1, the tongue had not yet begun to grow. From day 2 onwards, proliferating keratinocytes were seen in basal and suprabasal locations at the wound edge and in the tongues. On day 2, there were approximately 15 dividing cells per mm, with a further increase that peaked at day 5, Thereafter there was a slight drop in the numbers of dividing keratinocytes, but the number remained constant over the last seven days of the culture period.

Quantitative data analysis of day 2 samples as shown in the graph (Figure 3.24 above), showed an average of 15.28 (± 2.49 SEM) dividing keratinocytes (light green bars) present in the migrating tongues/wound edge area. On day 5, growth of the developing tongues showed a peak with a mean value of 38.13 (± 2.69 SEM) dividing keratinocytes, indicating an increase in dividing keratinocytes on day 5 when compared to day 2. The majority of these dividing keratinocytes were observed just proximal to the wound edge (Fig.3.25 a below; green arrows) and were usually observed in the first proximal third of the migrating tongues (Fig. 3.25 a & b). In the last two distal

thirds of the tongues, dividing keratinocytes occurred in less frequent numbers (Fig. 3.25 a & b; green arrow). Importantly, none were seen at the very tip of the migrating tongues (Fig. 3.25 a & b; blue arrow).

Similarly, in day 10 samples, proliferating keratinocytes were seen mainly proximal to the wound edge and in first proximal portion of the tongue (Fig. 3.26 a and Fig. 3.26 b below). As before, dividing keratinocytes were not seen at the extreme tips of the migrating tongues (blue arrow). Numerous dividing keratinocytes (Ki-67+; green arrowheads) were seen along the entire length of neoepidermis in both basal and suprabasal positions. Sometimes, dividing keratinocytes could be seen in close contact with melanocytes in the basal layer (Fig. 3.26 b; red arrowhead). As before, proliferating keratinocytes (Ki-67+) were seen at the leading edge of the migrating tongues (green arrowheads). There were no proliferating keratinocytes seen at the tip of the tongues (Fig. 3.26 a & b; blue arrow). The average number of dividing keratinocytes in the tongues was 26.24 (± 2.55 SEM) for day 10 samples.

In the day 12 sections numerous dividing keratinocytes (Ki-67+; green arrowheads) were seen along the entire length of neoepidermis in both basal and suprabasal positions. The white arrow denotes the wound edge. The tongues measured on average 505 μm and 489 μm for (a) and (b) respectively, when measured from the wound edge to the tip of the tongue. No proliferating keratinocytes were seen at the tips of the tongues (Fig.3.27 below; blue arrow). The average number of dividing keratinocytes in the tongues was 27.99 (± 3.03 SEM) for day 12.

In conclusion, these results demonstrate that (1) the tissue remains viable over the period of 12 days in culture (as evidenced by continued proliferation), and (2) there is a surge in the number of dividing keratinocytes after day 2, and these cells together with non-dividing cells migrate and form the regenerating tongue or neoepidermis. No dividing keratinocytes were seen at the extreme tips.

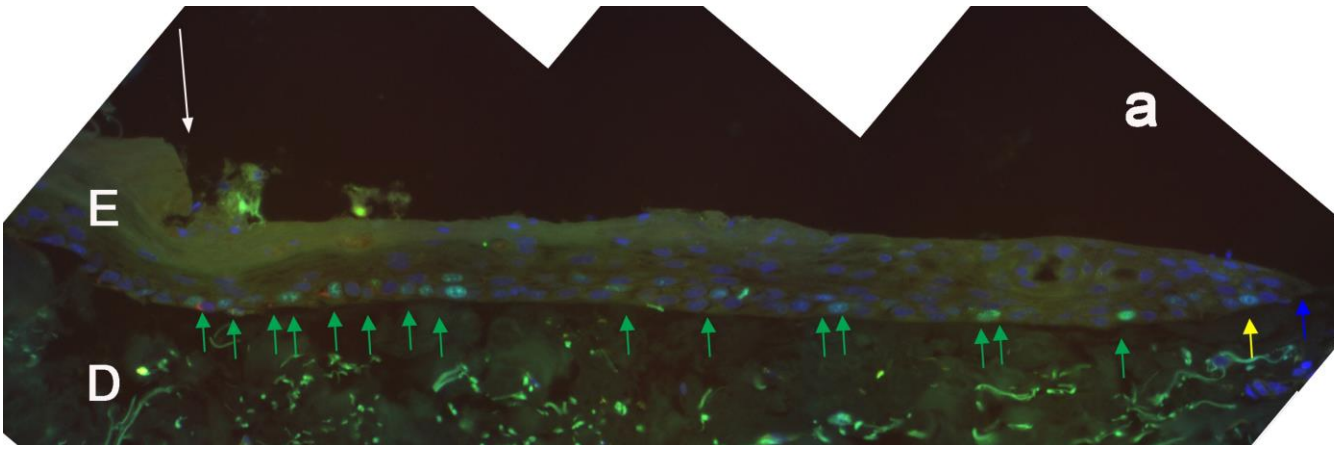

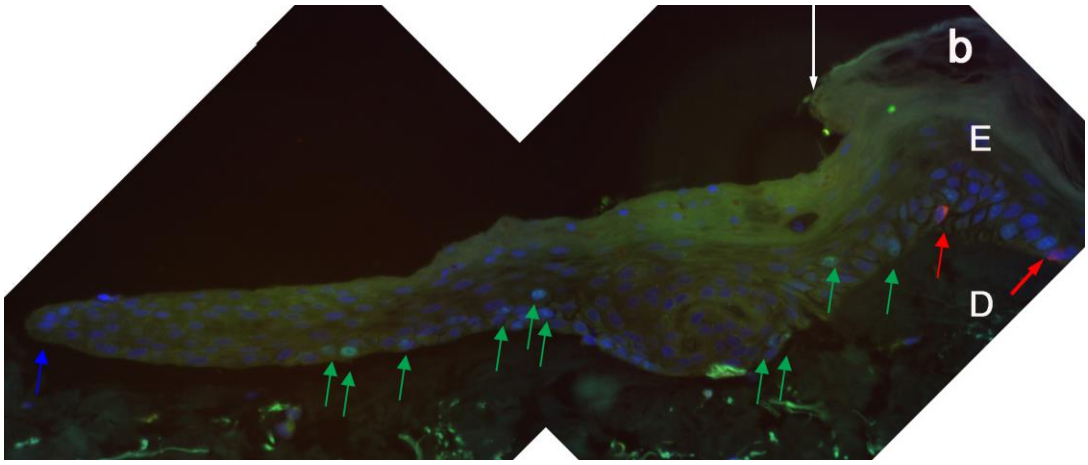

Representative digital images of immunostained sections of epithelial tongues at day 5.

(a) Shows left side of neoepidermal tongue at day 5, and (b) shows the right side of tongue. Numerous dividing keratinocytes (Ki-67+; green) were seen along the entire length of neoepidermis in both basal and suprabasal positions. The white arrow denotes the wound edge. Dividing keratinocytes were seen at the wound edge (green arrows). Two melanocytes are seen in the basal layer just proximal to the wound edge in the normal epidermis (MelanA+ cytoplasmic staining; red arrows). Proliferating keratinocytes were seen at the leading edge of the developing tongues in (a) (yellow arrow). No proliferating keratinocytes were seen at the tips of the tongues (blue arrow). E = epidermis; D = dermis. Bar = 50 µm.

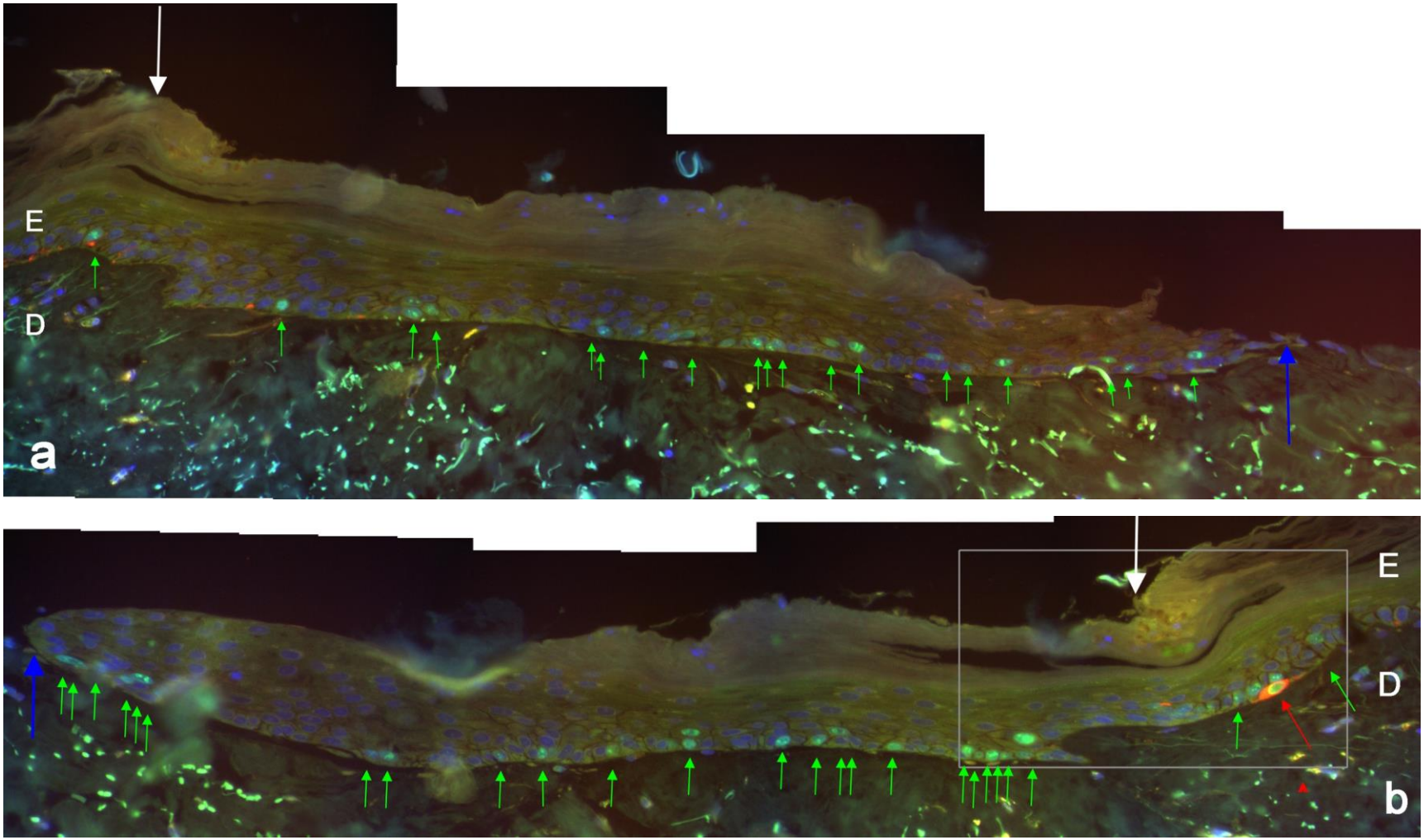
E
D
a
E
D
b

Figure 3.25 Representative digital images of immunostained sections of epithelial tongues at day 10.

(a) Shows composite image of left side of neoepidermal tongue at day 10 and (b) shows the right side of tongue. Numerous dividing keratinocytes (Ki-67+; green) were seen along the entire length of neoepidermis in both basal and suprabasal positions. The white arrow denotes the wound edge. Proliferating keratinocytes (Ki-67+) were seen at the leading edge of the migrating tongues (green arrowheads). There were no proliferating keratinocytes seen at the extreme tip of the tongues (blue arrow). A single proliferating melanocyte (red arrow) with green-stained nucleus (Ki-67+) and red cytoplasmic staining (MelanA+) is seen just proximal to the wound edge (white arrow). See Fig. 3.31 below for more details on boxed area shown in (b). E = epidermis; D = dermis. Bar = 50µm.

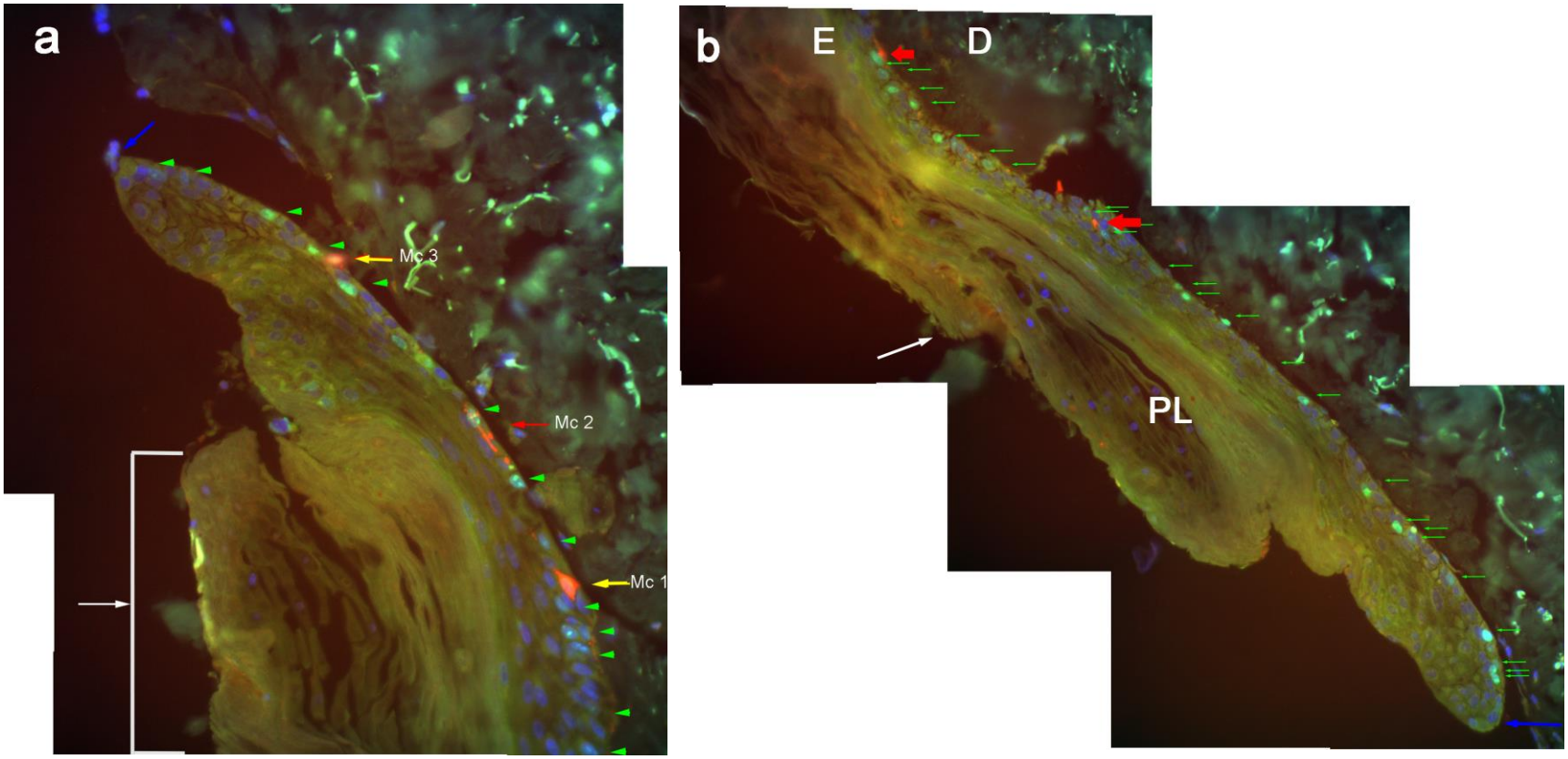
a
Mc 3
Mc 2
Mc 1
b
E
D
PL

Figure 3.26 Representative digital images of immunostained sections of epithelial tongues for day 12.

(a) Shows the left side of the neoepidermal tongue at day 12 and (b) shows the right side of tongue. Numerous dividing keratinocytes (Ki-67+) stained green, were seen along the entire length of neoepidermis in both basal and suprabasal positions. The white arrow denotes the wound edge. The tongues measured 505 µm and 489 µm for (a) and (b) respectively, when measured from the wound edge to the tip of the tongue. (a) One non-dividing melanocyte (MelanA+) (red arrow) and two dividing melanocytes (Ki-67+/ MelanA+) (yellow arrows) were seen in the basal layer of the neoepidermal tongues in the left-hand side developing tongue. b) One non-dividing melanocyte was seen at the wound edge (larger red arrow) and one melanocyte was seen in the epidermis proximal to the wound edge (smaller red arrow). No proliferating keratinocytes were seen at the tips of the tongues (blue arrow) in (a) or (b). E = epidermis; D = dermis; PL = Parakeratotic Layer. Bar = 50 µm.

3.5 Melanocyte location and proliferation during re-epithelialisation

Much is known about the mechanism of keratinocyte mobilisation and migration during the re-epithelialisation phase of wound healing. However, very little is known about the role of melanocytes during the re-epithelialisation process. In order to investigate melanocyte proliferation during the re-epithelialisation process in this *in vitro* model, sections were subjected to immunofluorescent staining using the melanocyte-specific marker, MelanA, as described in Results, Part 1. Melanocyte location and proliferation were analysed within the normal epidermis on both sides distal to the wound edge, and in the epithelial tongues from and including the wound edge to the tip of the tongues. Melanocytes were positively identified using three criteria: their location along the basal layer, the presence of dendrites, and MelanA immunopositivity (see Chapter 2, Materials and Methods). Data were analysed using GraphPad Prism 6.0 and the results were expressed as the average number of melanocytes (± SEM) per mm along the basement membrane.

3.5.1 Identification and location of melanocytes in normal epidermis

In the normal epidermis, melanocytes were seen along the basal layer at regular intervals and occurred at a frequency of approximately 1 in 10 basal cells (Fig. 3.28 a – f below). Melanocyte cell bodies were mostly rounded, with some having multiple dendrites that extended towards the upper epidermal strata (Fig.3.28 a and c). The nuclei of some melanocytes were often oriented perpendicular to the basement membrane, while some melanocyte nuclei were oriented parallel to the basement membrane with their dendrites extended along the basement membrane (Fig. 3.28 e; boxed inserts). Interestingly, a few melanocytes seemed to be “hanging by pendulous threads” from the basement membrane, but were still enclosed by it (Fig. 3.28 a). Melanocyte density was very often increased along the rete pegs (Fig. 3.28 e & f). A rare instance of a basal melanocyte with its dendrites extending down into the dermis was observed in the normal epidermis (Fig. 3.28 f).

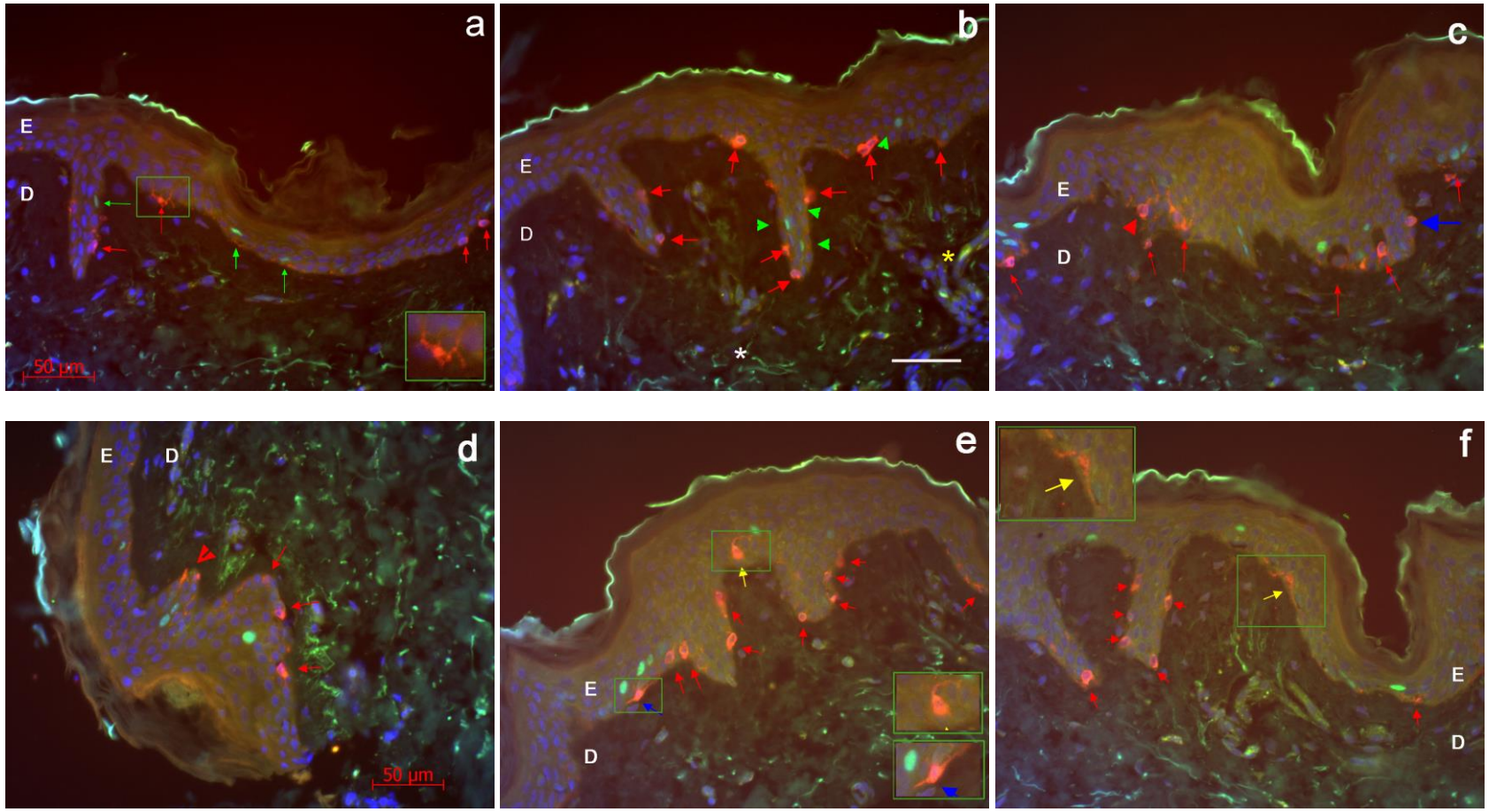

Figure 3.27 Representative images of skin in longitudinal section immunostained with anti-Ki-67 and anti-MelanA.

a –f) Nuclei of proliferating keratinocytes (Ki-67+) showed a green signal and MelanA+ melanocytes showed red cytoplasmic staining. The blue nuclei in the epidermal layers represent non-dividing keratinocytes and are counterstained with DAPI. Collagen fibres (asterisk) are seen in the dermis and exhibit green autofluorescence as seen in (b). (a - c) Melanocytes were seen along the basal layer of the epidermis (red arrows). A pendulous melanocyte can be seen in (a) with its cell body protruding into the dermis (red arrow; boxed insert = magnified image). (e) A

melanocyte is seen with its dendrites extending upwards into the stratum spinosum layer (upper boxed insert = magnified image). A dividing melanocyte Ki-67+/MelanA+) is seen with its dendrites extended along the basal layer (lower boxed insert = magnified image). (f) Melanocytes were sometimes positioned more frequently along the rete pegs. A rare basal melanocyte with its dendrites extending down into the dermis can be seen in this image (yellow arrow; boxed insert = magnified image). Green autofluorescence of collagen fibres can be seen in the dermis in all sections. E = epidermis; D = dermis. Bar = 50μm.

3.5.2 Average melanocyte counts in normal epidermis

To ascertain the average number of melanocytes within the normal epidermis, all melanocytes with a whole or partial cell body located along the basement membrane were counted and the average number of melanocytes per mm of basement membrane across the 12-day time course was plotted. As can be seen from the graph (Fig. 3.29 below), and data table (Appendix D.6), the average number of melanocytes in the normal epidermis (red bars) remained constant across all time points for the duration of the culture period. There were approximately 10 melanocytes per mm of basement membrane. This demonstrates that for this culture period, the melanocytes remained viable and phenotypically normal, and expressed the MelanA differentiation marker.

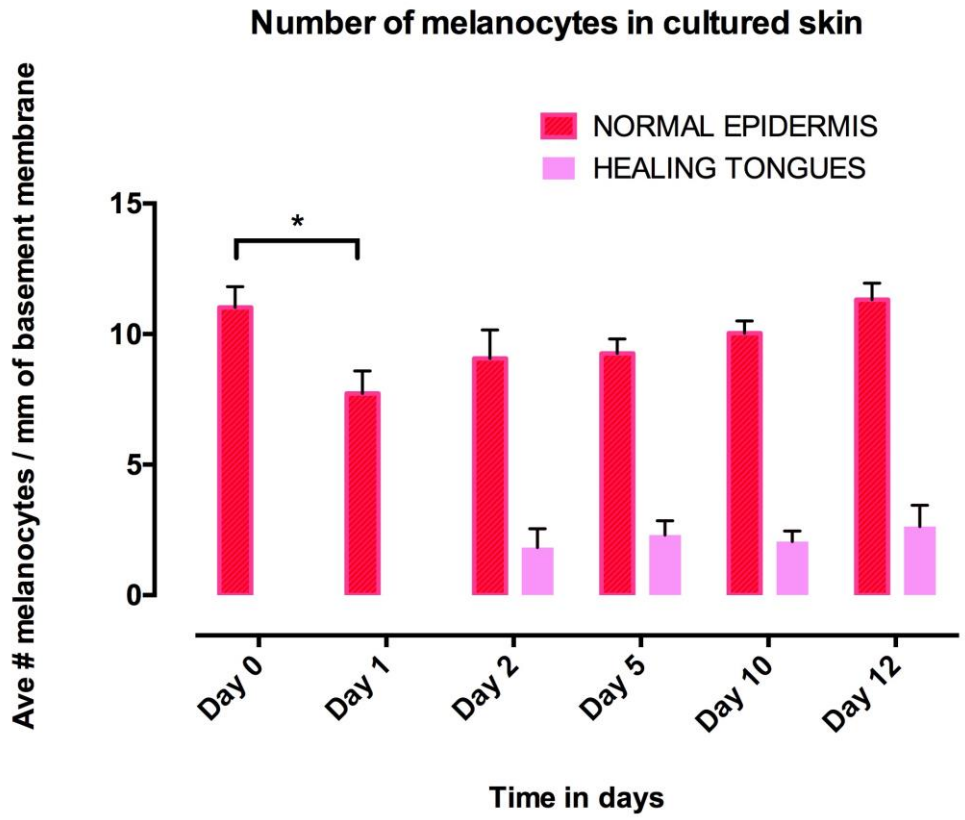

Figure 3.28 Graph showing the number of melanocytes present in normal epidermis and healing tongues from days 0 to 12.

Melanocytes were counted in the normal epidermis and in the migrating tongues from day 0 to day 12. The data represent the average number of melanocytes (± SEM) per mm of basement membrane counted along the full length of basal layer of normal epidermis and along the basal layer of healing epithelial tongues for each time point examined. * = $p < 0.05$.

3.5.4 Average number of melanocytes in healing tongues/neoepidermis

To determine the number of melanocytes that were involved in the re-epithelialisation process, basal melanocytes were counted at the wound edge and along the migrating epithelial tongues (pink bars) (see Fig. 3.29 above). Because there was negligible growth of the tongues, no melanocytes were seen beyond the wound edge on day 1. On day 2, an average of 1.8 (± 0.72 SEM) melanocytes were visible in the migrating tongues, and by day 5, an average of 2.36 (± 0.19 SEM) melanocytes were seen in the neoepidermis. The average number of melanocytes present in the migrating tongues remained constant from day 5 to day 12, again confirming the viability of the culture model. This also suggests that melanocytes do participate in the wound healing process.

3.5.5 Location of melanocytes in wound area and developing tongues

To determine in greater detail how melanocytes enter the healing wound over the culture period, the wound area of samples with open tongues were examined for the presence of both non-dividing and dividing melanocytes. Samples with "closed" tongues were not included (see Chapter 2, Materials and Methods). This was quite evident in some cases as can be seen in Fig. 3.30 below, where a very clearly dividing melanocyte can be seen showing a green/ yellow nucleus and a red cytoplasm (refer to boxed area in Fig. 3.25 above). In other cases, dividing melanocytes were not as easy to detect, but the strict search criteria were that the nucleus had to be stained green/ yellow with red cytoplasmic staining in order to definitively record the cell as a dividing melanocyte. A clear example of a dividing or recently-divided melanocyte (Ki-67+/ MelanA+) can be seen in the merged fluorescent channel image shown in Fig.3.31 d below. This high resolution confocal image (see Fig. 3.30 below) was acquired to provide further clarity and to unequivocally prove that the nuclear staining was "real". As can be seen in Fig.3.31 a, the nucleus shows the typical green staining pattern and the cytoplasm of the melanocyte cell body and dendrites shows red fluorescent staining (Fig. 3.31 b). Similarly stained melanocytes were recorded as either "dividing" or "recently divided".

The basal melanocytes and dividing melanocytes were counted in the wound area and developing tongues, and scored as being "in epidermis proximal to the wound edge", "at the wound edge", or "in the tongue" (refer Table 3.1 below). As shown in Table 3.1, melanocytes were seen in all three zones from day 2 to day 12. In day 2 samples, there were thirteen basal melanocytes proximal to the wound edge, two melanocytes at the wound edge, and four melanocytes were seen in the tongues. No *dividing* melanocytes were seen in the sections at day 2.

Similarly, day five sections showed four basal melanocytes in total in the epidermis proximal to the wound edge, seven melanocytes were seen at the wound edge, and one melanocyte was seen in the tongues. No *dividing* melanocytes were seen in the sections at day 5.

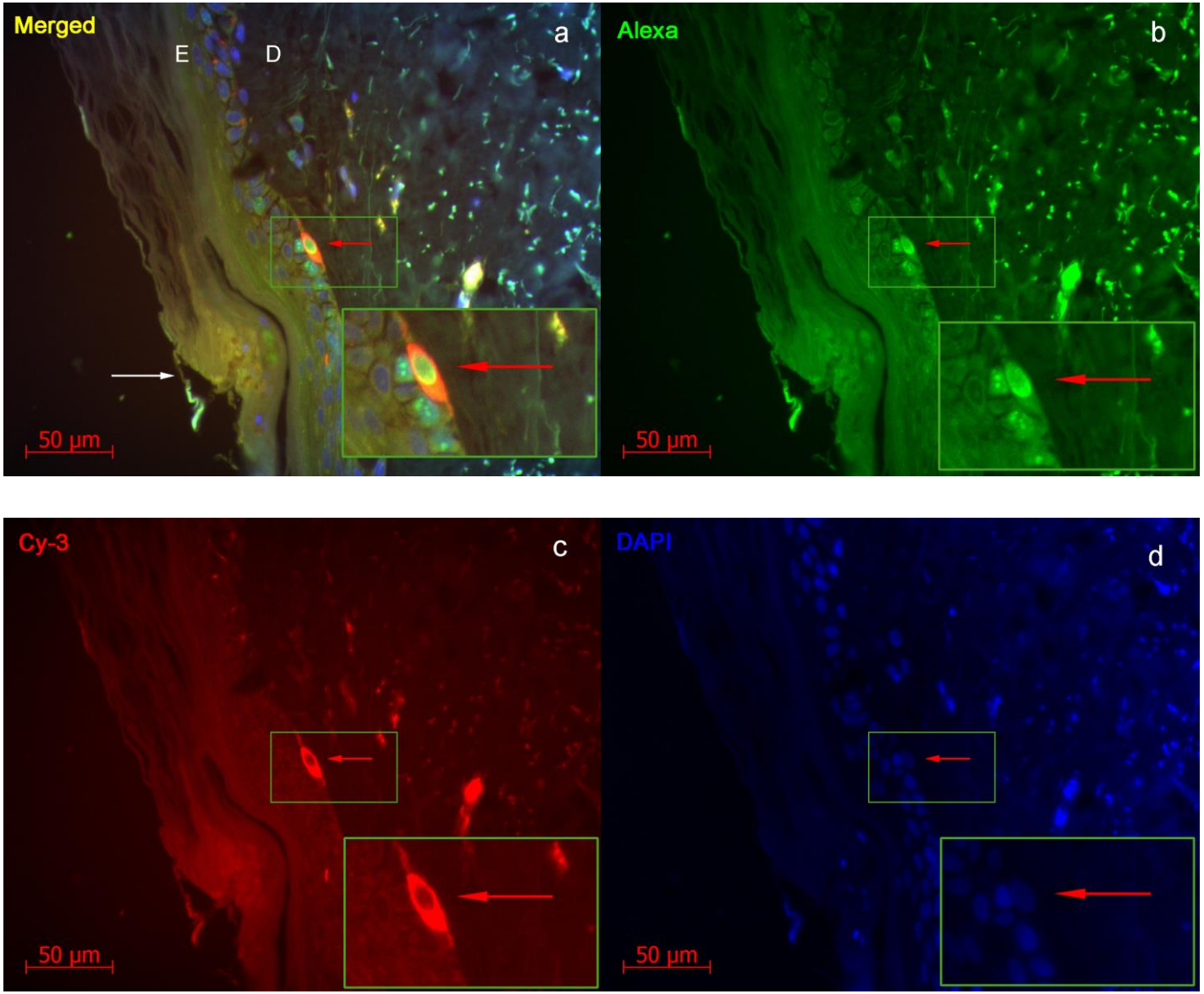
Merged
E
D
a
50 µm
Alexa
b
50 µm
Cy-3
c
50 µm
DAPI
d
50 µm

Figure 3.29 Magnified digital images of boxed area in Fig.3.26 above.

(a) Digital image of day 10 sample showing a single proliferating melanocyte (Ki-67+ nucleus; green and MelanA+ cytoplasmic staining; red) seen just proximal to the wound edge (white arrow) on the right side of neoepidermal tongue at day 10. The boxed area shows the same dividing melanocyte at a higher magnification. (b to d) Image of dividing melanocyte in the Alexa-488 (green) channel, Cy-3 channel (red) and DAPI (blue) channel respectively. E = epidermis; D = dermis. Bar = 50μm.

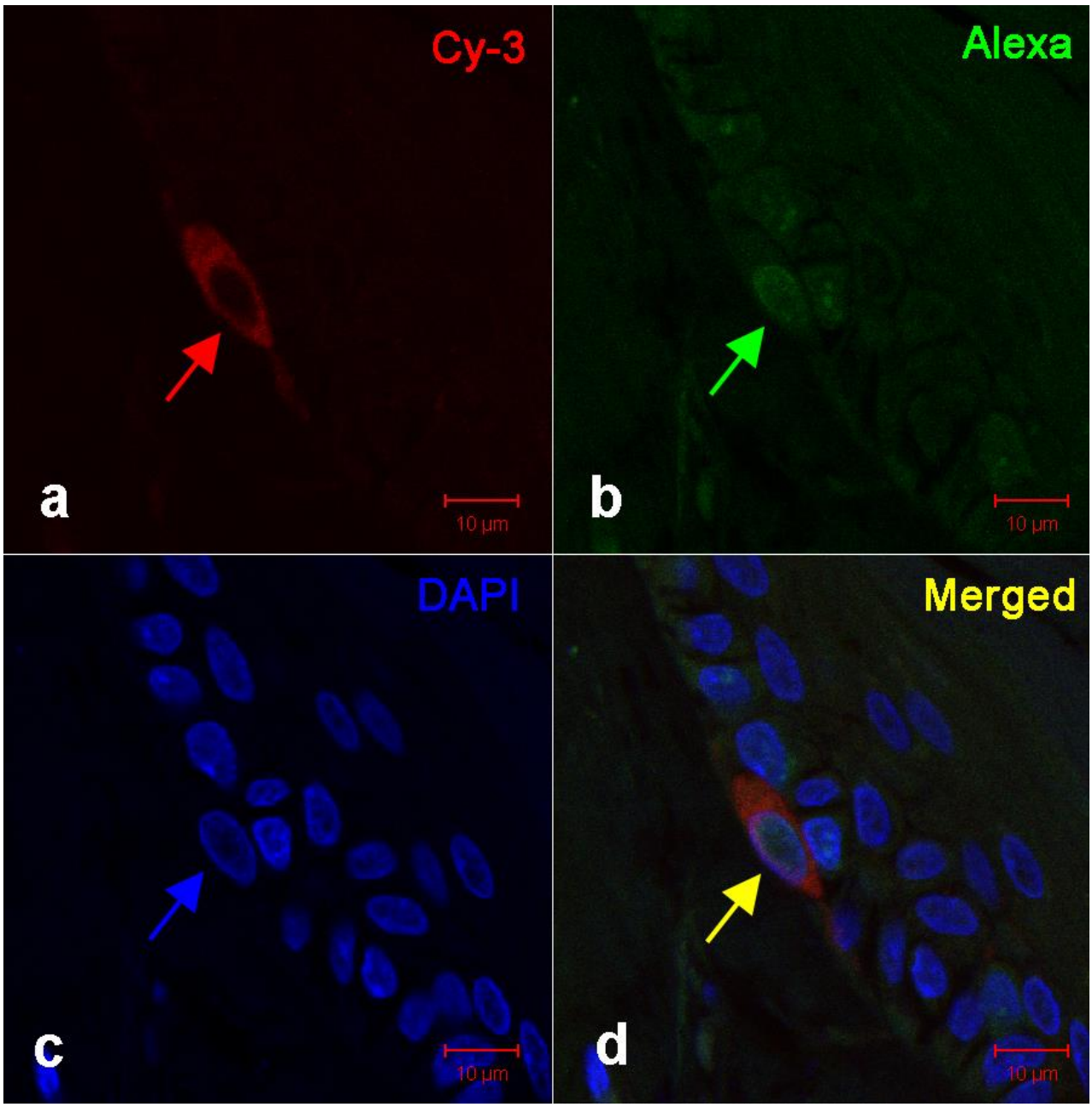

Figure 3.30 High resolution confocal images of fluorescent –labelled sections showing the boxed area in Fig.3.30 above in greater detail.

(a - d) Confocal images of dual immunostained sections show a single proliferating melanocyte (Ki-67+ nucleus; green and MelanA+ cytoplasmic staining; red) located proximal to the wound edge at day 10. The Cy-3 channel (red) , the Alexa-488 (green) channel, and DAPI (blue) channel respectively are shown in (a to c). (a) The melanocyte cell body (red arrow) seen in this image exhibits red cytoplasmic staining (MelanA+) which extends into the dendrites. (b) The nucleus (green arrow) of dividing cells stain green (Ki-67+). (c) DAPI stains the nuclei of all non-dividing cells blue. A merged channel image is seen in (d) showing the dual stained dividing melanocyte (yellow arrow). Bar = 10µm.

On day 10 a different picture emerged, where eighteen basal melanocytes in total were seen in the epidermis proximal to the wound edge, twelve at the wound edge, and eleven in the developing tongues. **Five** out of the eighteen melanocytes seen in the proximal epidermis were **dividing**. At the wound edge only **one dividing melanocyte** was found. **Two dividing melanocytes** were seen in the tongue. A specific example of dividing melanocytes in the proximal epidermis can be seen in Figure 3.32 below. **Two dividing** (or recently divided) melanocytes were seen just proximal to the right-hand side wound edge. These melanocytes had 'green/yellow'-coloured nuclei and red cytoplasmic staining. The melanocytes appeared to be facing in opposite directions, because their cell bodies were apart. Their dendrites were touching and they were seen to have a fusiform rather than a round shape, suggesting that these melanocytes had recently divided and were migrating in opposite directions. A parakeratotic layer (PL) extends above the neoepithlium (NE) from the wound edge (white arrow), but does not extend to the tip of the tongue (blue arrow).

Examination of two consecutive sections from a second day 10 sample revealed a serendipitous finding of a dividing melanocyte in the proximal epidermis and in the tongue (see Fig. 3.33 a & b below). As can be seen in Fig.3.33 a below, two melanocytes were seen in the developing tongue along basal layer (red arrows), none at the wound edge (white arrow) and two melanocytes were seen in the epidermis just proximal to the wound edge (red block arrows). These were deemed to be non-dividing melanocytes because only red cytoplasmic staining (MelanA+) was detected. However, in the consecutive section (Fig.3.33 b below), two melanocytes were detected in the developing tongue: **one was a dividing melanocyte** (yellow arrow) and the other was a non-dividing melanocyte (red arrow). This dividing melanocyte was located 445 µm from the wound edge, i.e. approximately halfway in tongue, of which the total length from wound edge to tip was 850 µm. A third melanocyte was situated proximal to the wound edge in adjacent epidermis (yellow arrow), and was seen to be **dividing**. This set of observations highlight the fact that sometimes dividing melanocytes can be missed during screening.

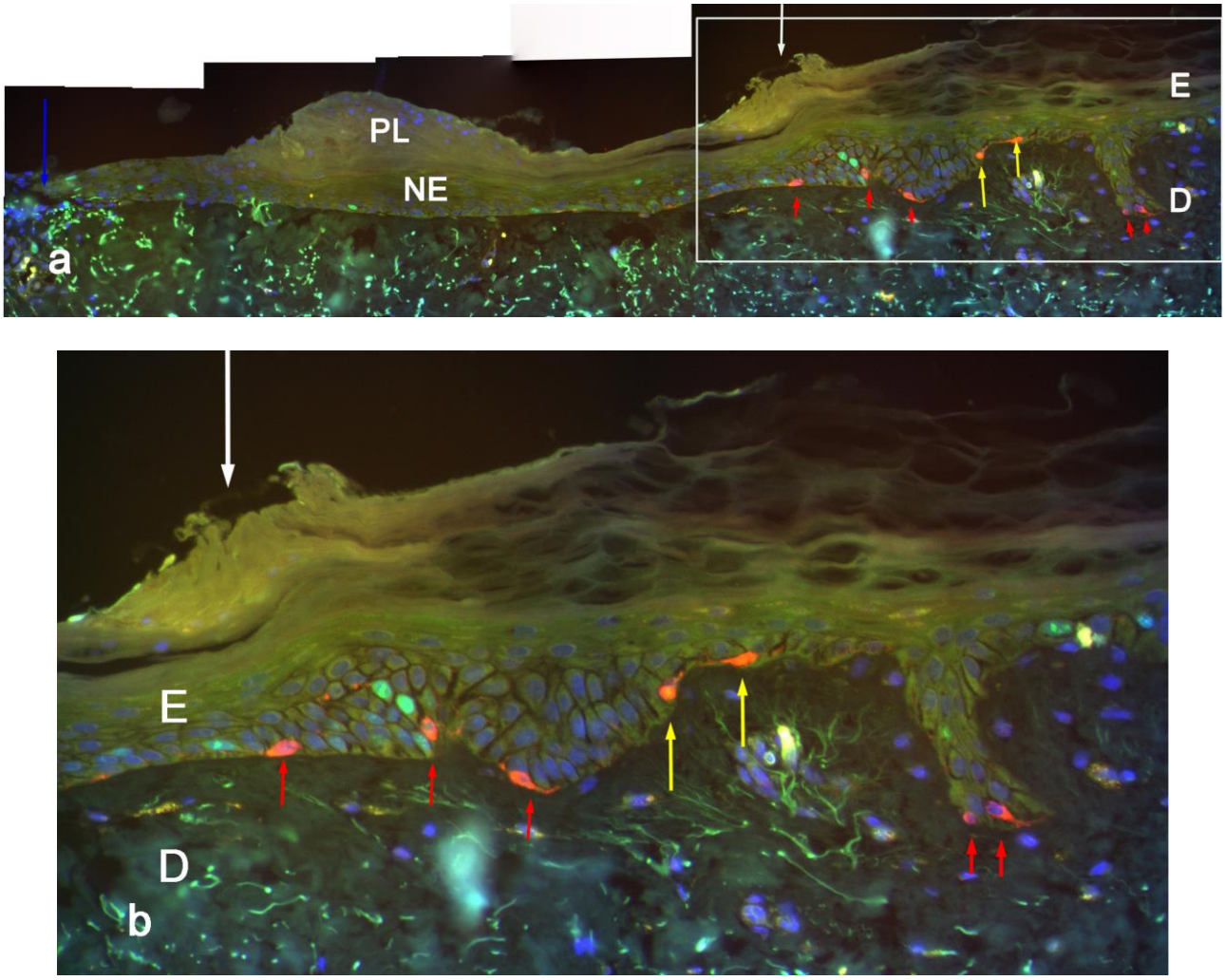

Figure 3.31 Figure 3.32 Digital images of cultured skin at day 10 immunostained with Ki-67 and MelanA antibodies.

(a) Section shows an overview of the wound area on the right-hand side, including the epidermis proximal to the wound edge, the wound edge (white arrow), and the developing tongue in a day 10 sample. A parakeratotic layer (PL) extends above the neoepithlium (NE) from the wound edge (white arrow), but does not extend to the tip of the tongue (blue arrow). (b) Boxed insert of image shown in (a) shows a magnified view of the wound edge and proximal epidermis, showing two dividing melanocytes (yellow arrows) that are located in the epidermis proximal to the wound edge (long white arrow). Non-dividing melanocytes (red arrows) are seen at wound edge and in basal epidermis proximal to the wound edge, two were seen ahead of the two dividing melanocytes, and two more basal melanocytes were seen immediately proximal to the dividing melanocytes (yellow arrows). These melanocytes had a fusiform appearance with long extended dendrites that followed the curvature of the basement membrane. E = epidermis; D = dermis; PL = parakeratotic layer; NE = neoepithelium.

Studies on wound healing have revealed the presence of a parakeratotic layer that formed above the developing tongue (Usui et al., 2013). In this *in vitro* study, the development of a parakeratotic layer (PL) which traversed about two-thirds across the upper part of the neoepidermis was evident from day five through to culture-day 12 (see Chapter 4, Discussion). Interestingly, dividing melanocytes were not seen beyond this layer in the healing tongues, further supporting the idea that the parakeratotic layer protects the neoepidermis much like a scab does during *in vivo* wound healing. Further, dividing melanocytes were also not seen at any point in front of the leading edge of the developing neoepithelium.

On day 12, a total of ten melanocytes were seen in the basal layer of the epidermis proximal to the wound edge. A further seven melanocytes were found in the wound area, i.e. in the epidermis proximal to the wound edge and at the wound edge, and three melanocytes were seen in the developing tongues. Of the ten melanocytes seen in the proximal epidermis, **three were dividing**, whereas **two** of the seven melanocytes seen at the wound edge were **dividing**. Only **one dividing melanocyte** was seen in the tongues out of three melanocytes seen in total in the day 12 sections examined.

In sum, there were **fourteen dividing melanocytes in total** seen in all the sections examined from day 2 to day 12: **eight dividing** melanocytes were located in the epidermis proximal to the wound edge, **three dividing** melanocytes were seen at the wound edge, and **a total of three dividing melanocytes** were seen in the developing tongues (see Table 3.1 below). Taken together, the results show that melanocytes do participate in the re-epithelialisation process and they appear to migrate and some divide.

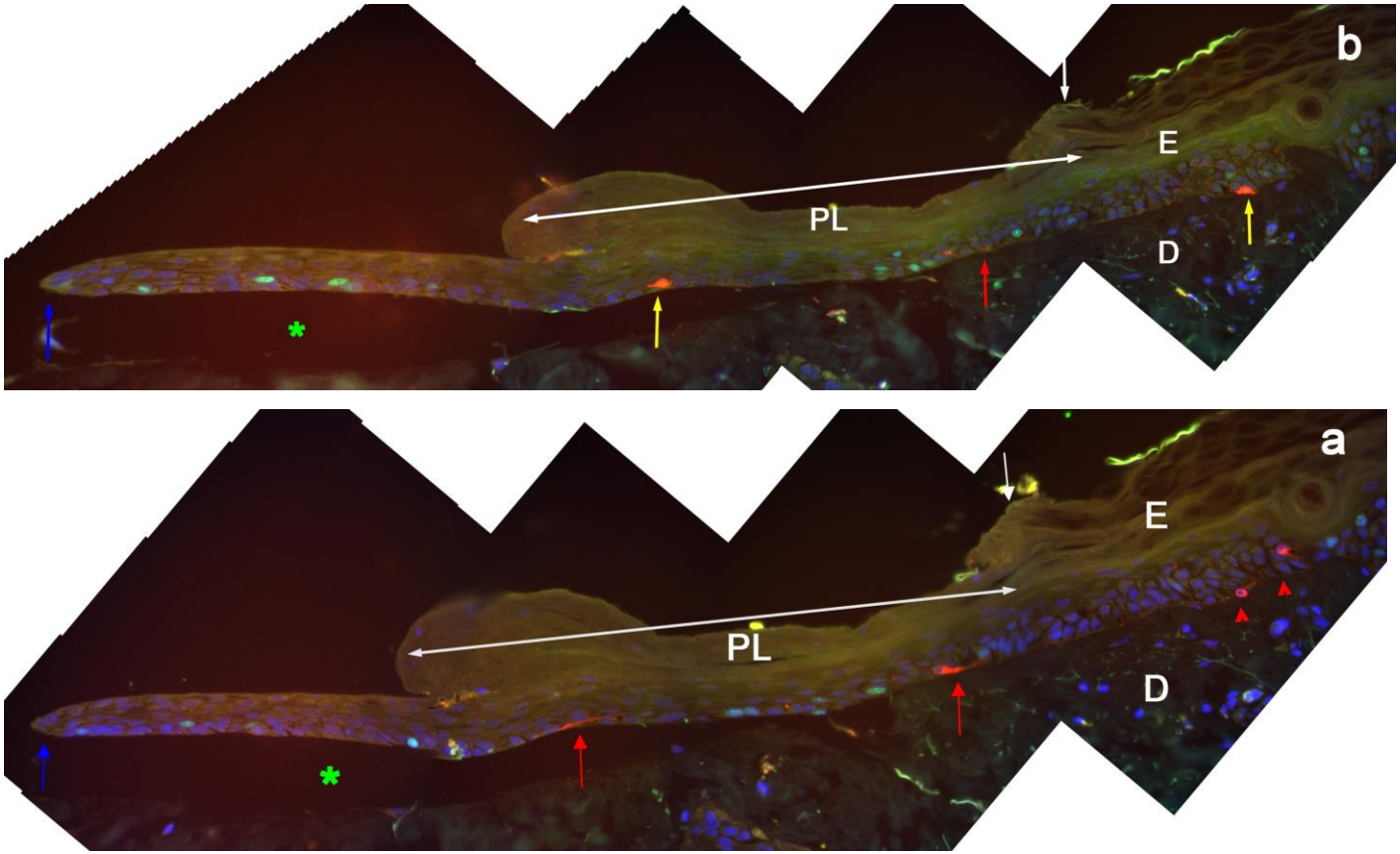

Figure 3.32 Dual immunostained sections of cultured skin samples at day 10 using anti-Ki-67 and anti-MelanA.

(a) and (b) represent digital images taken from two consecutive sections of the right-hand side wound area at day 10. In (a) four melanocytes were seen: two melanocytes were seen in the developing tongue (red arrows), none at the wound edge (white arrow) and two melanocytes were seen in the epidermis proximal to the wound edge (red block arrows). (b) In this consecutive section, three melanocytes were detected. One dividing melanocyte (yellow arrow) and one non-dividing melanocyte (red arrow) can be seen in the tongue. The third melanocyte was a dividing melanocyte (yellow arrow) and was situated proximal to the wound edge (white arrow). A parakeratotic layer (PL) traverses about two-thirds across the upper part of the neoepidermis and can be seen in both sections (white double pointed arrow). The neopidermis appears to have separated from the dermis leaving an artefactual gap (green asterisk). PL = parakeratotic layer; E= epidermis; D = dermis.

Table 3.1 Total number of basal melanocytes and dividing melanocytes in wound area and healing tongues.

	Section #	Proximal to Wound edge		Wound edge		Tongue	
		Total #MCs	Total # DivMCs	Total # MCs	Total # DivMCs	Total #MCs	Total # DivMCs
Day 2	Section1	1	0	1	0	2	0
	Section2	4	0	0	0	0	0
	Section3	3	0	0	0	2	0
	Section4	5	0	1	0	0	0
	Totals	**13**	**0**	**2**	**0**	**4**	**0**
Day 5	Section1	1	0	2	0	0	0
	Section2	1	0	2	0	0	0
	Section3	2	0	2	0	1	0
	Section4	1	0	1	0	0	0
	Totals	**4**	**0**	**7**	**0**	**1**	**0**
Day10	Section1	2	0	2	0	1	0
	Section2	2	1	2	0	1	0
	Section3	7	3	5	0	2	0
	Section4	1	0	2	1	0	0
	Section5	3	0	1	0	2	0
	Section6	3	1	0	0	3	2
	Totals	**18**	**5**	**12**	**1**	**11**	**2**
Day12	Section1	2	2	0	0	0	0
	Section2	2	1	2	1	1	1
	Section3	4	0	2	1	1	0

	Section4	2	0	3	0	1	0
	Totals	**10**	**3**	**7**	**2**	**3**	**1**

MC = melanocytes; DivMcs = dividing melanocytes; # = number of

3.5.6 Observation of melanocytes in submerged epithelial outgrowths

Although it was not an original aim of this dissertation, it was noted that there were several melanocytes present in the epithelial outgrowths along the inferior dermal aspect of the biopsies submerged in culture, further supporting the hypothesis that melanocytes are present in the submerged regenerating neoepidermis. The number of melanocytes in the epithelial outgrowths could not be quantified, because not all the outgrowths were photographed. Nevertheless, although the entire length of the outgrowth cannot be seen at this magnification, several basal melanocytes were seen in these outgrowths proximal to the cut edge of the biopsy (Figure 3.34 a and b below; white asterisk). **Two dividing melanocytes in total** were seen close to the lateral biopsy margin in the few sections examined of day 10 and day 12 samples (Figure 3.34 c and d respectively; red arrows). (d) Two melanocytes were seen along the basal layer (red arrows) showing mostly parts of dendrites seen on the left, and on the right, a dividing or recently divided melanocyte nucleus (stained yellow), with a fusiform melanocyte body with elongated dendrites that lay flat along the basement membrane. Several dividing keratinocytes were also seen in the epithelial outgrowths in basal and suprabasal positions (white arrows in Fig.3.34 a and green arrows in Fig. 3.34 b, c & d).

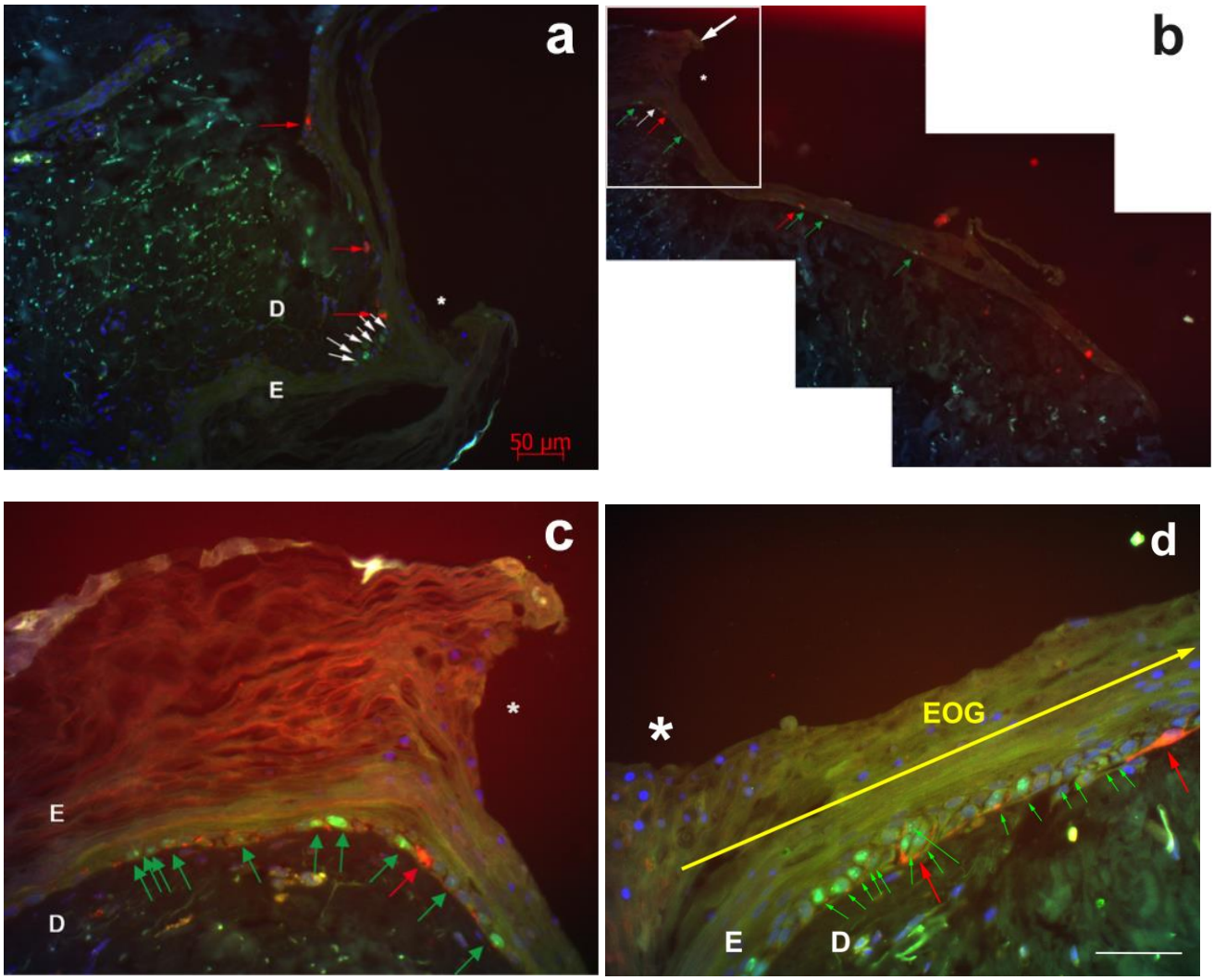

Figure 3.33 Representative immunostained images showing submerged epithelial outgrowths.

(a) and (b) Sections immunostained with anti-Ki-67 and anti-MelanA in day 10 and 12 samples respectively. (c) A magnified image of boxed insert in Fig. 3.34 b showing a dividing melanocyte at the cut edge of the biopsy (red arrow). (a – d) Several basal melanocytes (red arrows) can be seen in the epithelial outgrowths that emerged from the lateral edges (white asterisk) and extended around the inferior dermal aspect of the submerged culture biopsies. Dividing keratinocytes were also seen in the epithelial outgrowths (white arrows in (a) and green arrows in (b, c & d) in basal and suprabasal positions. (d) shows the lateral biopsy edge from a day 12 submerged culture sample. Several dividing keratinocytes can be seen in the basal epidermal layer. Two melanocytes were seen along the basal layer (red arrows); mostly parts of dendrites were seen in the melanocyte on the left, and on the right, a dividing or recently divided melanocyte with a fusiform melanocyte body and elongated dendrites that lay flat along the basement membrane can be seen. The white asterisk shows the lateral aspect of the biopsy at the cut edge in all images. EOG = epithelial outgrowth; E = epidermis; D = dermis. Bar = 50 µm.

CHAPTER 4
DISCUSSION

4 Discussion

When the skin is wounded, the epithelial covering needs to be restored as soon as possible to maintain the integrity of the moisture barrier. Healing of wounded skin results in a scar, and repigmentation of the skin occurs to varying degrees. While normal skin pigmentation is well documented (Lin and Fisher, 2007), the mechanisms underlying hypo- and hyperpigmented scar formation are not clearly understood (Velangi and Rees, 2001). In some cases, skin repigmentation may occur soon after re-epithelialisation has occurred, while in others repigmentation may be delayed or even incomplete (Velangi and Rees, 2001, Chadwick et al., 2012). In contrast, there is also significant evidence in the literature that in humans, susceptible individuals may develop benign hyperproliferative or keloid scars (Aarabi et al., 2007, Gao et al., 2013), which may then also develop into hyperpigmented scars (Chadwick et al., 2012, Gauglitz, 2013).

The involvement of melanocytes in the re-epithelialisation process, and the mechanisms of repigmentation are still poorly understood. In part, this is because one cannot study human skin *in vivo*. Therefore, it is necessary to optimise an *ex vivo* culture method that adequately mimics normal wound healing *in vivo* (Lebonvallet et al., 2010). This study attempted to answer the question of when melanocytes enter the wound during re-epithelialisation in an organ culture model of wound healing.

4.1 Does the in vitro model of wound healing used in this study adequately reflect normal wound healing?

In this study, skin samples were “wounded” with an elliptical cut, then cultured for varying lengths of time. The course of re-epithelialisation was studied over a period of twelve days. Extension and growth of the neoepidermis was monitored by indirect fluorescence and then analysed using histomorphometric methods. To test the adequacy of this culture model, several parameters including tissue quality and integrity, different culture conditions, (air-liquid interface versus submerged culture), keratinocyte proliferation and tongue growth and extension were investigated.

It was found that the epidermis retained a “normal” appearance over the culture period, with few obvious cellular changes observed. Towards the end of the culture period (on days 10 and 12), some typical features of cellular degradation were observed in the superficial layers, including acantholysis and mild vacuolation. This was accompanied by nuclear pyknosis in the suprabasal layers.

Histological analysis of the skin samples showed that in the first stages of regeneration of the wound (on day 1), epiboly was seen at the wound edges. This is in agreement with many studies that have shown, both *in vivo* and *in vitro,* that epiboly or active cell migration is the initial epithelial response to wounding of skin as first described by Marks & Nishikawa (1973). An interesting point of discussion relates to the word “epiboly” itself.

The etymological roots of the word “epiboly” is Greek from the word “epibolé, meaning “addition”. There are numerous definitions available which, taken together, describe epiboly as “the rolling movement and spreading out of cells into sheets of tissue that overlie or surround other groups of cells, especially during gastrulation”. This type of movement allows for the physical reorganisation and restructuring of embryonic cells and tissues during development (Panousopoulou et al., 2016). The Merriam Webster medical dictionary definition aptly describes epiboly in the context of gastrulation as “the growing of one part about another”. However, in the wound healing context, epiboly is recognised as the process of closing of a wound surface by active movement of cells from the wound edge without proliferation (Luo et al., 2011).

Marks and Nishikawa (1973) described the initial migration of cells and tongue formation in skin healing as a “rolling” or “leap-frog” mechanism. Using autoradiographic methods with tritiated thymidine as a marker of cell proliferation, they showed that cell proliferation did not occur at this stage. Similarly, the results of this study showed that after an initial lag period, cell proliferation occurred at the wound edges resulting in growth of the tongues only from day 2 onwards, up to a maximum tongue length of approximately 700 μm at day 5. A possible reason for the initial delay could be that the skin samples had to firstly acclimatise to the new culture environment. Similarly, by using Ki-67 as a proliferation marker in human skin wounds from day 0 to as long as seven months, Betz et al. was able to estimate the age of skin wounds (Betz et al., 1993). They observed an absence of Ki67 immunostaining in the skin samples before one and a half days’ post wounding. In this context, one could speculate that either the Ki-67 protein was not detected before day 2 in this study, or that no proliferation had occurred before day 2. This result suggests that at least for the first twenty-four hours of re-epithelialisation, the normal sequence of events seen during *in vivo* wound healing is recapitulated in this study.

From day two onwards, epithelial regeneration occurred from the wound edges towards the centre of the wound gap, with some of the sections showing complete closure of the wound. Similarly, Xu et al. (2012) showed that keratinocyte migration occurred from day 2 onwards in a human *ex vivo* skin culture model, with complete closure seen at day 6 post-wounding. However, it should be noted that these wounds were just surface incisions made in the epidermal surface without removal of the epidermis and dermis. The stratum corneum formation in the neoepidermis differed from the surrounding “normal” epidermis, since hyperparakeratosis was observed across part of the upper layer of the neoepithelium. This phenomenon was also more recently demonstrated by Usui et al (2013), who showed that these parakeratotic corneocytes acted as a buffer between the migrating epidermis and the wounded epidermis, thereby forming a protective layer over the migrating neoepidermis, and also providing a tension substrate for the migrating epithelial tongue. This suggests that the formation of this buffer layer consisting of parakeratotic keratinocytes is a protective measure (likened to scab formation *in vivo*) to ensure that effective wound healing has occurred.

Histologically, the cells present in the neoepidermis did not typically resemble normal stratified epidermis. These keratinocytes were more flattened, rather than cuboidal in shape, especially along the basal layer. Such elongated cells resemble the migrating keratinocyte phenotype, as described before by Jansson, Kratz & Haegerstrand (1996) and Patel et al. in 2006, and confirmed by Mendoza-Garcia (2015). This result is also in keeping with the extending sliding mechanism proposed by Safferling et al.(2013), whereby the basal cells maintained migratory phenotypic flexibility while the suprabasal cells expanded into a multi-layered epidermis that moved in tandem as a sheet of cells. Although the neoepidermis was a stratified epithelium, it never reached the same height (number of layers) as the normal unwounded epidermis in this study. Furthermore, the epidermal-dermal interface of both the epithelial tongues and the submerged outgrowths lacked the undulations present in normal skin. Since basal undulations are formed under the direct influence of dermal cues and mechanical stress *in vivo* (Xiong et al., 2013), one can deduce that the dermal signals which are present in this model are sufficient only to activate tongue growth, but insufficient for basal undulation formation.

For the remaining three days of culture, i.e. from days 10 to 12, growth of the tongues slowed down. There are several possible explanations for this, the most plausible one being that the maximum time spent in *in vitro* culture was reached and the cells were no longer metabolically active due to the prolonged culture period. This result is in keeping with the abnormal histological changes that were observed including vacuolation and pyknosis of the superficial layers. These observations are in agreement with Kleszczynski & Fisher (2012) who also showed that similar structural disturbances correlated to the duration of culture. Similarly, Tammi, Jansen & Santti (1979) showed in their model that skin can be safely cultured for up to 5 days, where after cells are thought to die off. In contrast, Mendoza-Garcia et al. (2015) showed that cell death occurred only after culture day 14 in their study. Vollmar et al. (2002) confirmed previous reports made by Desmoulière et al. (1995) that the decrease of cellular proliferation during final wound maturation may be controlled by a p53-regulated increase in apoptosis. Further, Vollmar et al. (2002) also found that a temporary decrease in apoptosis occurred because of p53 inhibition and this was indeed a self-regulatory mechanism during early wound healing.

While epithelial regeneration does not usually occur at a liquid interface, the present study provided some interesting observations regarding epithelial tongue growth under submerged conditions. Since the biopsies were placed on rafts with the epidermal surface exposed to air and floated in the culture medium, the lower part of the biopsies, i.e. the dermal aspect, remained submerged in the culture medium throughout the culture period. It was noted that in addition to the wound healing on the air-liquid interface, epithelial outgrowths formed around the inferior lateral biopsy edges at the liquid- liquid interface. Furthermore, an increased rate of growth, compared to the developing tongues grown at the air- liquid interface, was noted. These lateral submerged outgrowths were thinner than the equivalent healing tongues at each respective time point examined. This is in keeping with Le Poole et al. (1994) who investigated melanocyte migration in an organotypic culture model of wound healing, and found that epidermal growth occurred from the outer rims of the biopsies and completely

encircled the dermal aspect of the biopsies within their culture period of seven days. This is most likely because of direct access to nutrients in the culture medium in addition to chemotactic factors produced by the local environment. Furthermore, since these were the cut edges of the original punch biopsy, they could therefore be regarded as full thickness wounds. Using various wound types and sizes during the optimisation of their wound healing organ culture model, Mendoza-Garcia et al. (2015) observed that re-epithelialisation of partial thickness wounds occurred faster (within 14 days) than full thickness wounds (>1 mm wide) that failed to fully re-epithelialise. Similarly, they also observed advancing re-epithelialisation tongue formation at both wound edges in these full thickness wounds. These advancing tongues in the Mendoza-Garcia study also did not appear fully differentiated, which is comparable to the lateral epithelial outgrowths described in this study. Keratinocyte differentiation and maturation can only occur at the air-liquid interface during *in vitro* culture. Consequently, the epithelial tongues at the air-liquid interface in this study showed the presence of several epidermal layers, while this was not true for the submerged tongues. To investigate factors influencing re-epithelialisation, Harrison et al. (2006), developed an in vitro tissue-engineered human skin model to study keratinocyte migration and found that the lack of a basement membrane favoured keratinocyte migration. Similarly, in this study, the growth of tongues under submerged conditions suggests that keratinocyte migration and proliferation with subsequent tongue extension and the absence of layer formation occurs as a direct consequence of the lack of a basal keratinocyte layer and no exposure to air, the latter two factors being essential for normal tongue growth and stratification of the neoepidermis (Rittie, 2016).

4.2 The presence and proliferation of melanocytes during wound healing.

This study investigated the question of whether melanocytes form part of the growing neoepidermis, or whether they enter the newly formed epidermis only after complete re-epithelialisation has occurred. Other investigators have also identified this as a key question and further asked what the role of the depth of injury was in wounded skin (Chadwick et al., 2012). This study has addressed the specific question of whether melanocyte proliferation occurs in the wound area, and if so, in which region of the wound: in the epidermis proximal to the wound edge, and/ or at the wound edge, and/ or in the developing tongues? By mapping melanocyte location within the above zones at different time periods, a model of melanocyte involvement is put forward (see Fig.4.1 below).

4.2.1 Localisation of melanocytes in healing wounds

This study clearly demonstrates that melanocytes are indeed found in the healing wound during re-epithelialisation. In particular, the time course studies here reveal that melanocytes can be seen proximal to the wound edge, at the wound edge and in the developing tongue as early as day 2 after wounding. Thereafter the number rises so that by day 10 and 12, there are significantly more melanocytes present. In the Snell (1963) study mentioned before (see Chapter 1: Introduction and Literature Review, section 1.4.1), melanocytes were

seen within the neoepithelium, as soon as the developing tongues started to migrate, which was shown to be on the fourth day. In contrast, Heath et al. (2009) reported that in their human *in vivo* study of wound healing, melanocytes were absent in the migrating epithelial tongue. They however, showed that melanocytes were present in the "surrounding neoepithelium in various stages of maturation". This is not made entirely clear, but can be taken to mean that, although the melanocytes were not seen in the tongue, they were seen in the wound area/ wound edge. Further, in their study, they concluded that the "melanocytes lag behind the advancing epithelium". This statement can be interpreted as: (i) either the melanocytes were present in the neoepithelium, but were closer to the wound edge than to the leading edge of the tongue, or (ii) the melanocytes were present at the wound edge and/or proximal to the wound edge, but not in the tongue. Since they did not use a proliferation marker in their study, they did not confirm the presence (or absence) of *dividing* melanocytes. The result of the present study concurs with studies done by Hirobe (1988), who detected precursor melanocytes (TRP-2+) in wounded mouse skin, located mainly adjacent to the wound edge. The key question that then arises, is whether these melanocytes are passively carried along by the wave of migrating keratinocytes i.e. as part of the epibolisation process, or whether they are independently migrating within the keratinocyte layer (or both). The present study cannot distinguish between these two hypotheses and would be a difficult question to address. Perhaps a live imaging study using fluorescent GFP-labelled melanocytes in a co-culture experiment with keratinocytes might be of use to address this hypothesis (Keswell et al., 2012). Keswell et al. (2012) examined melanocyte migration in a three-dimensional skin construct and found that melanocytes can migrate and push in between keratinocytes along the basal layer. However, it should be noted that these experiments were carried out *in vitro* in a dish and not *in vivo* and therefore might not necessarily be the ideal tool to explore the temporal and spatial mechanisms of melanocyte migration. of proliferating and migrating keratinocytes.

The present study shows that the furthermost melanocyte from the wound edge, i.e. the melanocyte located within the tongue furthest from the wound edge, was not found ahead of the leading edge of the developing tongue (see Results, Fig.3.33). This concurs with observations made by Snell (1963) who investigated melanocyte repigmentation in deep healing wounds in guinea-pig skin. Snell also found that within the wound, the furthermost melanocyte was situated a short distance behind the advancing epithelium and no melanocytes were seen in front of the leading edge of the neoepithelium. This result suggests that melanocyte-keratinocyte interaction is finely orchestrated during re-epithelialisation and that melanocyte proliferation, migration and relocation in the basal epidermis is dependent on keratinocyte-derived cues and/ or dermal cues.

The literature provides some useful information on how, at a cellular level, melanocyte migration occurs. It should be noted however that most of the work on melanocyte migration is focused on early developmental stages and melanoma migration ((Petit and Larue, 2016). Melanocytes are attached to keratinocytes by cadherins and to the basement membrane by integrins. To initiate migration or proliferation, cadherins (Tang et al., 1994, Li et al., 2001) must be down-regulated, and attachment to the basement membrane must also be

down-regulated (Keswell et al., 2015). Desmoglein is a protein normally associated with desmosomes and is a co-receptor for E-cadherin. Although melanocytes do not have desmosomes, they do express desmoglein. (Li et al., 2001) have shown that during melanogenesis, desmoglein is down-regulated, and one might speculate that during wound healing, desmoglein in melanocytes is also down-regulated to facilitate proliferation and/ or migration.

Attempts to uncover the mechanisms of melanocyte migration in adult skin during wound healing, have shown that the nuclei of melanocytes display a certain degree of “malleability” and “fluidity” whilst migrating through keratinocyte layers during *in vitro* culture experiments (Keswell et al., 2012, Keswell et al., 2015). Similarly, this nuclear “plasticity” was previously demonstrated in human embryonic stem cells using micromanipulation methods (Pajerowski et al., 2007). Pajerowski (2007) showed that human embryonic stem cells exhibit a high degree of malleability but stiffen irreversibly during terminal differentiation. Thus, it would seem that melanocytes are capable of migration through spaces that have a much smaller diameter than their cell bodies, and that less differentiated melanocytes e.g. recently divided melanocytes, would also possess similar contortionist properties.

In normal skin, the melanocyte nucleus is normally round with numerous dendrites that extend to touch neighbouring keratinocytes to maintain the epidermal melanin unit (Fig.4.1 a). For melanocytes to divide, dendrites are withdrawn (Fig.4.1 b) and the cell undergoes mitosis while being located on the basement membrane (see Fig.4.1 c). The results of the present study show that after mitosis of the melanocyte, the dendrites of the recently-divided melanocytes were always flattened against the basement membrane and the cell bodies were less round (more elongated) and appeared to be migrating away from each other (see Fig. 3.30 and Fig.4.1 d for a typical example). The same phenotype was seen in at the biopsy edges of the submerged culture samples (see Fig. 3.34). This might suggest that these fusiform melanocytes are indeed the cells that have recently divided. (Of note, in culture, melanocytes also take on a bipolar, dendritic and elongated appearance). While recently-divided melanocytes are seen to be migrating in the developing tongues in this study (Fig.4.1 e), they were not seen with dendrites extended into the upper epidermal layers to re-establish contact with neighbouring keratinocytes. This is most likely because the culture period in this study was too short to observe this part of the process of melanocyte relocation along the basement membrane, i.e. the re-establishment of the epidermal-melanin unit (EMU) after migration (Fig.4.1 g).

This study supports the hypothesis that melanocytes enter the wound during the re-epithelialisation process. So broadly, one can conclude that re-epithelialisation and repigmentation occur as follows:

after wounding, the keratinocytes respond to signals coming from the wound bed, and they migrate in the direction of an electric field to cover the wound (Tai et al., 2009, Zhao, 2009). The melanocytes, in contrast, require additional signals emanating from basal keratinocytes, in order to migrate.

4.2.2 Melanocyte proliferation in healing wounds

The next point to consider is whether there are also dividing melanocytes in the tongues and whether melanocyte proliferation contributes to tongue extension? Using a double immunostaining protocol for the presence of double-labelled melanocytes (Ki-67+/ MelanA+) (see Fig. 3.1 and a typical result can be seen in Fig. 3.28, in Chapter 3, Results). There were no dividing melanocytes seen in the epidermis proximal to the wound edge, at the wound edge or in the tongues, before day 10 of the culture period. Dividing melanocytes were first detected at the wound edge at day 10.

A total of fourteen dividing melanocytes were seen in the three zones of the wound area across approximately 64 sections with a total number of approximately 1600 images examined. A single dividing melanocyte was found approximately in the middle part of the epidermal tongue in one day 10 section (Fig. 3.33). Since the data in this study has shown that keratinocyte proliferation decreased from days 10 to 12 (see Fig. 3.23), since dividing melanocytes were seen at the wound edge on day 10, and melanocytes were seen in the tongue on day 12, it is plausible that melanocyte migration into the tongue may have occurred. However, it should be noted that studies to determine whether migration of melanocytes has occurred is yet to be undertaken. This result confirms that melanocyte proliferation is a rare occurrence during cutaneous wound healing and that once divided, melanocytes can and do enter the sheet of proliferating and migrating keratinocytes, i.e. the neoepithelium.

The finding of dividing melanocytes (Ki-67+/ MelanA+) in normal human epidermis suggests that differentiated melanocytes are capable of cell division. It is therefore completely plausible that differentiated melanocytes contribute to normal skin homeostasis by dividing and thus also contribute towards re-epithelialisation of wounded skin. By investigating MiTF expression in zebrafish to explore differentiated melanocyte division, Taylor et al. (2011) showed that when there was a decrease in the number of melanocytes, MiTF expression decreased, with a resultant increase in proliferation of differentiated melanocytes. This result thereby shows that MiTF expression controls melanocyte differentiation and withdrawal from the cell cycle (senescence). Similarly, although very few melanocytes were seen in the normal epidermis and in the developing tongues, the data in the present study, although greatly limited, provide evidence for the notion that differentiated melanocytes retain the ability to re-enter the cell cycle when micro-environmental conditions become favourable. In the present study, the melanocyte-specific marker, MelanA was used to detect melanocytes in the normal epidermis and in the healing wounds. MelanA localises to pre-melanosomes, trans-Golgi network, nuclear envelope and plasma membrane and its expression in melanocytes decreases with melanosomal maturation (De Maziere et al., 2002, Hoashi et al., 2005). This makes MelanA an ideal marker for less differentiated melanocytes. However, additional melanocyte precursor markers, such as MiTF and TRP-2/ DCT, could have improved phenotypic characterisation of melanoblasts in the healing wounds.

Another interesting point to consider when analysing the repopulation or regeneration of healing wounds, is whether there is a dermal component that contributes to wound regeneration. Studies have shown that the sebaceous glands associated with hair follicles in the dermis, can contribute to re-epithelialisation in hair-bearing skin (Levy et al., 2007b). Questions that arise from this study are: (i) whether dermal melanocytes are present, and (ii) whether they too contribute to the repopulation of the neoepidermis. Although the presence of a putative stem cell niche for melanocyte stem cells in humans and mice has been established (Nishimura et al., 2002; Yu et al., 2006), there is ongoing research into a possible reservoir for human melanocyte stem cells in glabrous skin and the possible existence of a dermal melanocyte precursor population. Using a three-dimensional skin reconstruct model, Li et al. (2009) have shown the presence of multipotent dermis-derived stem cells, with the potential of developing into melanocytes. Further, these dermal stem cells could migrate from the dermis to the epidermis, suggesting that a reserve population of dermal melanocyte precursor cells could be found in this sub-epidermal layer of the skin. In another study by Zabierowski et al. (2011) it was shown that dermal-derived melanocyte precursors exist and that they can migrate to the epidermis through the basement membrane and differentiate into functional basal melanocytes. In the present study, a few dermal melanocytes were detected, although not in the wound area, as can be seen by the specific example in Figure 4.2 below. Two melanocytes with red cytoplasmic staining (Fig.4.2; red arrowheads) were seen in the dermis in a day zero sample (not subjected to culture). Two basal melanocytes with red cytoplasmic staining (Fig.4.2; red arrows) were also seen along the basement membrane in the section examined.

In sum, this study sought to investigate the participation of melanocytes during the re-epithelialisation phase of wound healing, by using an in vitro human skin organ culture model over a culture period of twelve days. This skin culture model was shown to be a reliable and robust model to investigate melanocyte proliferation and participation during wound healing, then by using an optimised double-labelling technique to search for non-dividing and dividing melanocytes in the wound area of cultured skin, the results show that melanocytes are indeed present in healing wounds, more specifically, in the epidermis proximal to the wound edge, at the wound edge up to day 5. In addition, dividing melanocytes were seen in the proximal epidermis, at the wound edge and in the developing tongues at days 10 and 12 post-wounding.

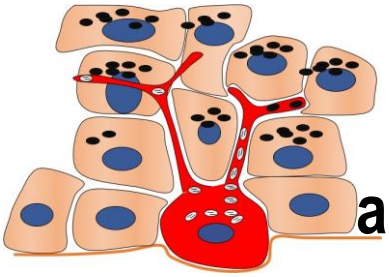

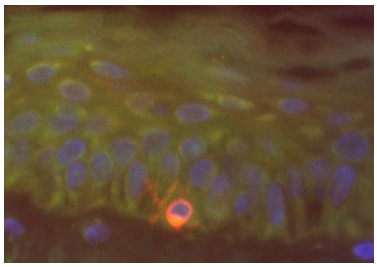

Basal melanocyte with a rounded cell body and dendrites arborising up into the suprabasal layers to contact maintain contact with keratinocytes

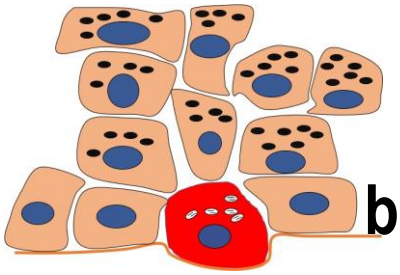

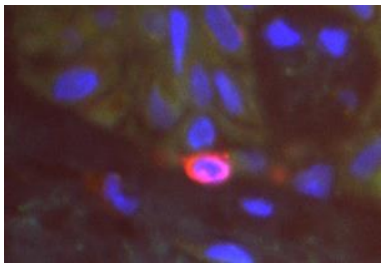

Retraction of dendrites to facilitate mitosis

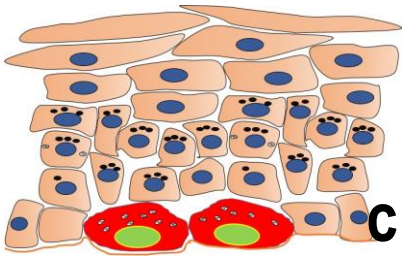

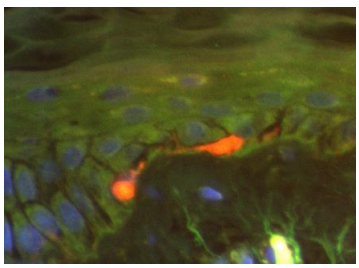

Melanocyte cell division by mitosis

(refer to Fig.3.32)

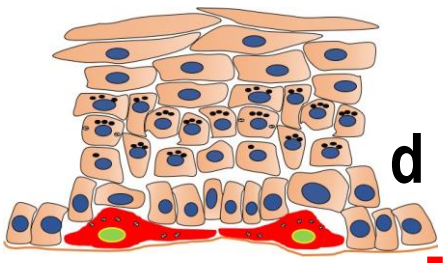

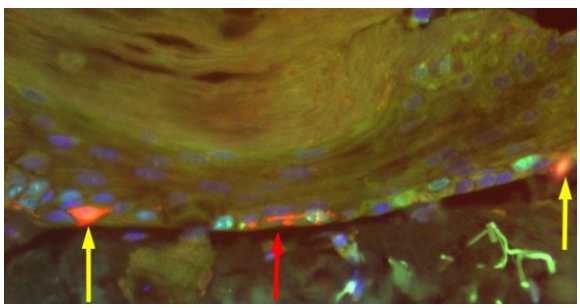

Recently-divided melanocytes in tongue migrating away from each other

(refer to Fig.3.27)

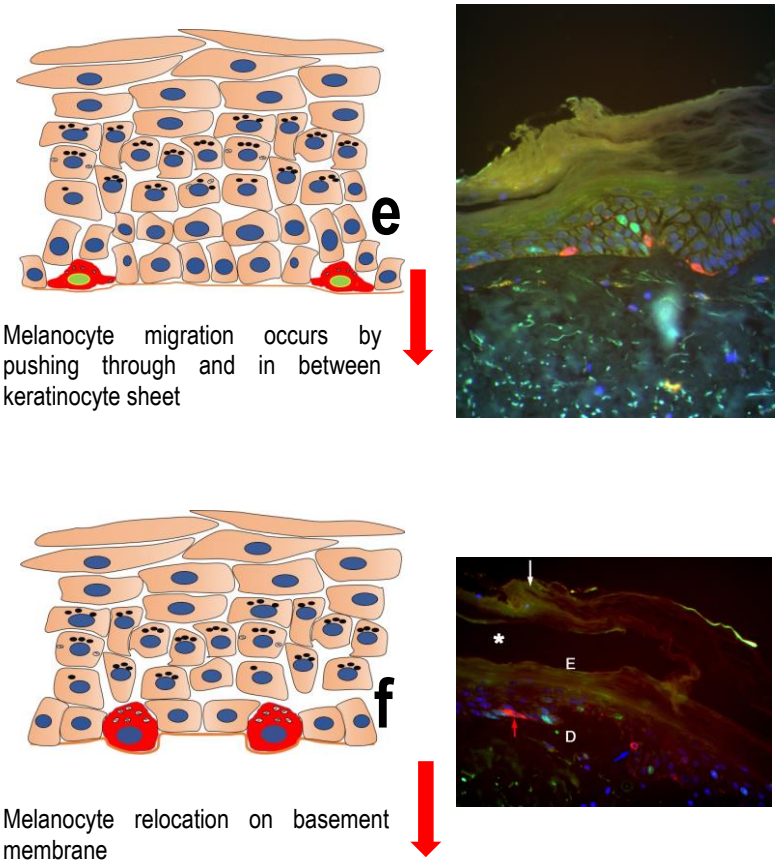

Figure 4.1 Proposed model for the role of melanocytes in wound healing

(a – g) Left column shows schematic diagrams of a step-by-step account of the possible mode of proliferation and migration of melanocytes in healing tongues of cultured skin. Right column shows (where possible) an image taken from double-immunostained sections of healing tongues. Fig.4.1 (a) shows a quiescent melanocyte in basal layer with dendrites making contact with adjacent keratinocytes (b) shows melanocyte with retracted dendrites in basal layer (c) shows a melanocyte that has undergone cell division by mitosis, still located on basal layer (d) shows two recently-divided, flattened melanocytes that are facing in opposite directions melanocytes and are migrating away from each other (e) shows recently-divided melanocytes with fusiform shape that are navigating between basal keratinocytes (f) shows melanocyte relocation along basement membrane after proliferation and migration where the cell body becomes more rounded (g) shows melanocyte dendrites become extend up into suprabasal layers to make contact with neighbouring keratinocytes to re-establish the EMU; a corresponding image for (g) could not be found (see text for explanation).

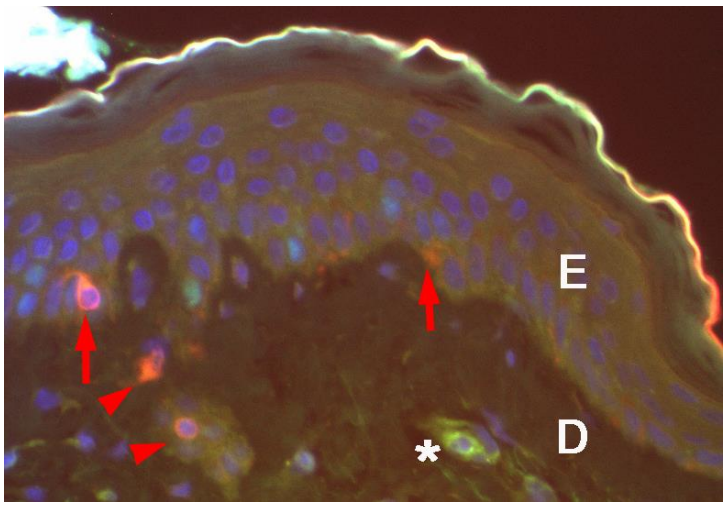

Figure 4.2 Digital image of cultured skin immunostained with anti-MelanA showing an example of a dermal melanocyte.

This image shows two rare dermal melanocytes with red cytoplasmic staining and blue nuclei (red arrowheads) present in the dermis of cultured skin at day 0. Two melanocytes can also be seen in the basal epidermis (red arrows). A fragment of sweat gland can be seen in the dermis (asterisk). E= epidermis; D = dermis.

4.3 Technical aspects and limitations of study

This study provides strong evidence for the presence of proliferating melanocytes within human skin during wound healing. The proliferation potential of melanocytes within the wound environment can reasonably be used to explain how melanocytes enter the wound during the re-epithelialisation phase of wound healing. However, this study provides only a glimpse into a very small cohort of skin samples and further similar investigations and quantitative analyses are necessary to obtain more convincing data. In addition, because there were two- or three- day gaps between sampling, the temporal development of the healing tongues cannot be precisely determined. It is entirely possible that the proliferating melanocytes result from de-differentiation of basal melanocytes as described before. Further studies examining the temporal development of healing tongues by investigation with markers for less differentiated melanocytes e.g. PAX3 and Hairy enhanced split-1 or HES-1 which is present in the less differentiated melanocytic phenotype (Medic and Ziman, 2010), or indeed melanocyte precursor cells (melanoblasts) are needed to fully unpack melanocyte dynamics within healing wounds. In addition, further studies examining the possible molecular phenotype of melanocytes *in vivo* and *in vitro*, and the location of putative cutaneous stem cell niches, are necessary. Furthermore, melanocytes express the protein desmoglein (Dsg1), the co-receptor for E-cadherin (Li et al., 2001). Investigations into expression of Dsg1 by melanocytes during re-epithelialisation will provide better evidence for the hypothesis that differentiated melanocytes actively migrate following de-differentiation and subsequent proliferation.

4.4 Future directions and conclusions

The finding of the epidermal outgrowths under submerged conditions lends itself to more rigorous investigations to study the melanocytes and dividing melanocytes along these submerged epidermal outgrowths. Expression of keratins by epidermal keratinocytes in the latter time points was not investigated in this study because the focus was limited to the role of melanocytes during re-epithelialisation. Keratin expression using immunohistochemical means may assist with the characterisation of epidermal differentiation during air-liquid culture and during submerged culture in this culture model (Luo et al., 2011).

microRNAs (miRNAs) are small, noncoding double-stranded RNAs that are present in all types of tissue and regulate a wide variety of processes at the cellular level including proliferation, differentiation, and apoptosis (Banerjee and Sen, 2015). miRNAs downregulate the expression of genes post-transcriptionally and have been shown to be involved in all three phases of wound healing including inflammation, proliferation, and remodelling (Shilo et al., 2007, Yang et al., 2011, Viticchie et al., 2012, Fahs et al., 2015). In a recent pilot study by Banerjee and Sen (2015), the expression of microRNAs (miRNAs) was examined in scar and normal skin samples from patients who suffered acute skin injuries. Several differentially expressed miRNAs were identified, whose target genes participated in biological functions, such as cell signalling and communication and/ or cellular metabolism. These miRNAs were also involved in various pathways such as mitogen-activated protein kinase, Wnt signalling, and focal adhesion pathways, which are all pathways involved with melanocyte proliferation, differentiation and migration. By focusing on the miRNAs which are differentially expressed during the re-epithelialisation phase of wound healing, one could establish to what extent they are implicated in the modulation of melanocyte proliferation and repopulation of the neoepidermis during acute wound healing.

The use of a standardised *in vitro* skin culture model facilitates the study of the complex events that lead to re-epithelialisation following wounding of skin. Such *in vitro* models obviate the variability brought about by paracrine and autocrine signalling, providing a regulated means to recapitulate the healing processes seen in partial thickness wounds *in vivo*. The present study demonstrates that skin can be cultured for up to 12 days with few deleterious effects. Secondly, this data supports the validity of the wound-healing model to examine melanocyte proliferation and migration during re-epithelialisation. Thirdly, this study convincingly demonstrates the presence of dividing and non-dividing melanocytes in the epidermis proximal to the wound edge, at the wound edge and in the healing tongues during re-epithelialisation. In conclusion, this study exemplifies the versatility of combined dynamic and morphological analyses of wound healing in human skin, and adds to our understanding of melanocyte proliferation in normal skin under homeostatic conditions and during wound healing *in vitro*. By facilitating melanocyte proliferation and migration with subsequent activation of melanogenesis, enhanced treatment options could be designed for repigmentation of cutaneous scars and burn wounds.

Appendix A Additional Methods

A.1 Tissue Processing Schedule

Solution	Time Spent	Objective
Alcohol 70%	1.0 hours	Dehydration
Alcohol 70%	1.0 hours	Dehydration
Alcohol 96%	1.0 hours	Dehydration
Alcohol 96%	1.0 hours	Dehydration
Alcohol 96%	1.0 hours	Dehydration
Alcohol 100%	2.0 hours	Dehydration
Alcohol 100%	2.0 hours	Dehydration
Alcohol 100%	2.0 hours	Dehydration
Xylene 1	2.0 hours	Clearing
Xylene 2	2.0 hours	Clearing
Paraffin Wax 1	2.0 hours @60°C	Wax impregnation
Paraffin Wax 2	4.0 hours @60°C	Wax impregnation

A.2 Culture of Human Skin Explants

This protocol was obtained from Dr. John Common, A-Star Institute, Singapore (personal communication)

Normal human skin samples were collected from the surgeon, placed into sterile specimen bags and stored at 4°C until further processing. The skin samples were then immersed in dilute sodium hypochlorite solution for 2 mins to disinfect, followed by a rinse in PBS to remove the residual hypochlorite solution. The skin tissues were then placed in a petri dish containing 10 ml of RM+ culture medium* and 100µl of fungizone (amphotericin B, an antifungal polyene antibiotic).

Using sterile surgical tools, the adipose tissue and some dermal tissues were carefully excised to facilitate diffusion of the culture medium to the epidermis. Several punch biopsies (8 mm in diameter) were taken from the skin samples. An excisional cut (~2mm in width) to simulate a partial-thickness wound, was performed on each punch biopsy using sterile scissors. The wounded punches were placed in culture inserts at the air-liquid interface. The punches were incubated at 37°C in 5% v/v CO_2, and the medium was changed every day for the duration of the experiment. The punches were harvested at specific time-points and fixed in 10% neutral buffered formalin.

***RM+ Culture medium**

The RM+ medium consists of 1:3 mixture of Hams'-F12 (Gibco) and Dulbecco's modified Eagles' medium (DMEM, Invitrogen) supplemented with 10% w/v fetal bovine serum (FBS), 100 IU of penicillin/100µg/ml of streptomycin, L-glutamine and RM+ medium (hydrocortisone 0.4 µg/ml, insulin 5 µg/ml, adenine 1.8 x 10^{-4} M, epidermal growth factor 10ng/ml, cholera toxin 10 x 10^{-10} M, transferrin 5 µg/ml and lyothyronine 2 x 10^{-11} M).

A.3 Haematoxylin and Eosin Stain

Method:

1. Dewax sections by passing through two changes of xylene with intermittent agitation, 5 minutes in each

2. Sections are then passed through decreasing grades of ethyl alcohol for one minute in each: 3 changes of 100% ethyl alcohol; 2 changes of 96% ethyl alcohol; 1 change of 70% ethyl alcohol

3. Stain nuclei with Mayer's haematoxylin (progressive stain) for 5 minutes

4. Wash slides in running tap water for 1 minute

5. Blue nuclei in Scott's tap water for 1 minute

6. Wash in running tap water for 2 minutes

7. Counterstain with 1% eosin / phloxin stain for 4 minutes

8. Wash slides briefly in water and drain sections well

9. Dehydrate sections by rinsing briefly in 3 changes of 96% ethyl alcohol followed by 3 changes of 100% ethyl alcohol

10. Clear sections in 2 changes of xylene

11. Mount sections in Entellan™ mounting medium under a glass coverslip.

Results:

Nuclei: Blue
Muscle: deep pinkish-red
Collagen: pink
Red blood cells: orange-red
Cytoplasm: varying shades of pink to red

A.4 Optimised Protocol for Dual Immunostaining of FFPE sections

1. Dewax sections in xylene (2 X 10 mins)

Rehydrate through descending percentages of ethanol to water:

3 x3 mins of 100% ethanol; 3 x2 mins of 96% ethanol; 1 x 2 mins of 70% ethanol; 1x 1 min of 50% ethanol; 1 x 1 min of running tap water

2. Rinse slides in citrate buffer (pH 6.0) for 5 minutes

3. Perform antigen retrieval by heat-exposing epitopes using pressure cooker method i.e. 20 mins @ ~121°C + 10 mins cooling down. 3 x 5min PBST wash

4. Block non-specific binding in serum block @RT for 60 mins

5. For negative control: Leave on serum block instead of adding primary antibody

6. Pour off serum block (do not rinse) and add first primary (1º) Ab or 1º Ab cocktail at optimised concentration @RT for 60 mins, followed by O/N @4°C. 3 x 5min PBST wash

7. Add first fluorescent secondary (2º) Ab or 2ºAb cocktail at optimised concentration @RT for 120 mins in dark. 3 x 5min PBST wash

8. Add second 1º Ab at optimised concentration @RT for 60 mins in dark, followed by O/N @4°C. 3 x 5min PBST wash

9. Add second fluorescent 2º Ab at optimised concentration @RT for 120 mins in dark. 3 x 5min PBST wash

10. Counterstain with DAPI nuclear counterstain (diluted1:50 from aliquot) @RT for 20 mins in dark. 2 x 5min PBST wash

11. Mount sections under a coverslip with Mowiol (see Appendix A.6.3.5). Leave to set for 1 hr @RT in dark. Cover sections with aluminium foil to protect from light and refrigerate till viewing with fluorescent microscope.

Appendix B Solutions used

B.1 Phosphate Buffered Saline

(1x PBS, 0.14 M NaCl, 8.8 M Na2HPO4, 2.7 M KCl, 1.47 M KH2PO4, pH 7.4, 1 L)

Sodium chloride, NaCl	8 g
Disodium hydrogen phosphate, Na2HPO4	1.26 g
Potassium chloride, KCl	0.2 g
Potassium dihydrogen phosphate, KH2PO4	0.2 g
ddH2O	qs

Autoclave and store in aliquots at 4°C

B.2 Dulbecco's Modified Eagle's Medium (DMEM, pH 7.4, 1 L)

DMEM powder	27.06 g
Sodium hydrogen carbonate, NaHCO3	7.4 g
autoclaved ddH2O	qs

Adjust to pH 7.4. Mix well before use. Add 10% FCS and 100 IU of penicillin and 100µg/ml of streptomycin before use. Sterilise through a 0.2 µm filter and store in aliquots at 4°C.

Foetal Calf Serum (FCS)

FCS 500 ml

Heat inactivate by 20 min incubation in a 56°C water bath

Allow to cool, store aliquots at -20°C

Penicillin (100U/ml)/ Streptomycin (100µg/ml) (100x P/S, 500 ml)

Penicillin (1662U/mg)

Streptomycin (750U/mg)

ddH2O

Sterilise through a 0.2 µm filter and store in aliquots at -20°C

B.3 5-Bromo-2'-deoxyuridine (BrdU) solution

5 mM BrdU in DMEM solution. Mix well on a vortex mixer

B.4 10% Neutral buffered formaldehyde solution (w/v) (10% NBF)

Formaldehyde solution, 37-40%	100 ml
Sodium dihydrogen orthophosphate, monohydrate ($NaH_2PO4.H2O$)	4.0 g
Disodium hydrogen orthophosphate, anhydrous (Na_2HPO4)	6.5 g
ddH2O	900 ml

Dissolve on a magnetic stirrer; wear gloves and protective glasses and work in a fume hood. pH is 7.2 – 7.4.

B.5 4% formaldehyde solution from paraformaldehyde

Paraformaldehyde	4.0 g
1 x PBS (pH 7.4)	100 ml

Work in a fume hood. Place paraformaldehyde and PBS in a 250-ml measuring flask and heat to 50°C (whilst stirring on a magnetic stirrer) until milky white solution becomes clear.

Can add a few drops of saturated sodium hydroxide (NaOH) (111g in 100 ml of ddH2O) if solution does not dissolve completely. Adjust pH to 7.5 if necessary. Store at 4°C.

B.6 Mayer's Haematoxylin

Haematoxylin (CI 75290)	1.0 g
Sodium iodate	0.2 g
Aluminium potassium sulphate , dodecahydrate ($KAl_2(SO_4)_2.12\ H_2O$)	50 g
Chloral hydrate	30 g
Citric Acid	2.0 g
ddH2O	1000 ml

Dissolve the haematoxylin, potassium alum and sodium iodate in distilled water with gentle heat and stirring or leave to stand at RT overnight. Add chloral hydrate and citric acid, boil the mixture for 5 minutes. Cool and filter the solution. The stain is ready for use immediately. Store in a dark cupboard at room temperature.

B.7 Scott's tap water substitute

Sodium hydrogen carbonate	2 g
Magnesium sulphate. $7H_2O$	20 g
Tap water	1000 ml
Thymol	a pinch

Dissolve the salts in the water and add the thymol. Store at room temperature.

B.8 Eosin/phloxin stain

1% aqueous Eosin Y

Eosin Y (CI 45380)	1 g
ddH2O	100 ml

Mix well using a magnetic stirrer.

1% aqueous Phloxin B

Phloxin B (CI 45410)	1 g
ddH2O	100 ml

Mix well using a magnetic stirrer.

To make a working solution, take 100 ml of 1% aqueous Eosin Y and 10 ml of 1% aqueous Phloxin B. Mix the two solutions and allow to stand at room temperature for two weeks to ripen the stain. Dilute this mixture 1:1 with distilled water and allow to stand in a dark cupboard for a further two weeks; this step is important to prevent fading. The stain is now ready for use. Store at room temperature.

B.9 Phosphate buffered saline with Tween-20 (PBST)

Tween-20	0.5 ml
1 x PBS (pH 7.4)	1000 ml

Add Tween-20 to PBS. Mix well.

B.10 Citric acid buffer pH 6.0, 10 mM sodium citrate

Sodium citrate stock solution, 1 M:

Citric acid, anhydrous	48.03 g
ddH2O	150 ml

Mix to dissolve. Adjust pH to 6.0 with 10M NaOH (~60 ml). Adjust the final volume to 250ml with distilled water and recheck pH and adjust if necessary. Solution is stable at RT for 3 months or at 4º C for longer storage. For a 10 mM solution of sodium citrate pH 6.0, dilute the above stock solution 1:100 with distilled water.

B.11 Donkey Serum Block (10 % NDS)

Donkey serum, normal	0.5 ml
1% BSA in PBS	4.5 ml

Mix well with vortex mixer and refrigerate at 4ºC.

For 1% Bovine Serum Albumin (BSA) in PBS (w/v)

Bovine serum albumin fraction V	1 g
Tween-20	0.2 ml
Sodium azide	0.1 g
1X PBS pH 7.4	100 ml

Mix well with vortex mixer and pass through a 0.45 micrometre filter. Refrigerate at 4ºC.

B.12 2% donkey serum in 1% BSA/PBS solution

Donkey serum, normal	0.1 ml
1% BSA in PBS	4.9 ml

Mix well with vortex mixer and refrigerate at 4ºC.

B.13 4,6-Diamidino 2-phenylindole, Dihydrochloride (DAPI) nuclear counterstain

Aliquots (conc. 10mg) were previously dispensed into 1.5 ml Eppendorf tubes and glycerol was added 50:50 to facilitate long-term storage @-20ºC. From aliquot make a 1:50 dilution in PBS buffer, pH 7.4. Wrap in aluminium foil to protect from direct light and store in refrigerator.

B.14 Mowiol 4-88 Mounting medium pH 8.5

0.2 M Tris pH 8.5

0.2 M Tris(hydroxymethyl)-aminomethane	2.423 g

ddH2O	100 ml

Titrate to pH 8.5 with 6N HCl

Method:

1. To 6g of glycerol, slowly add 2.4g MOWIOL while mixing. (Add MOWIOL over the course of an hour.)
2. Add 6ml dH2O, mixing for 1min and let stand at room temp overnight, covered.
3. Heat 12ml of 0.2M Tris, pH 8.5 to 50°C in a water bath.
4. Add 12ml prewarmed 0.2M Tris (pH 8.5) and keep at 50°C for 10min. with occasional mixing. (Mixture can be kept at 50°C for 1hr with agitation every 10min. There will be undissolved mowiol left in the beaker.)
5. Clarify by centrifugation at 5000xg for 15min at 4°C.
6. Decant supernatant into a disposable conical centrifuge tube.
7. For fluorescence, add 1,4-diazobicyclo-[2.2.2]-octane (DABCO) to 2.5g/100ml to reduce fading. Mix gently by inversion.
8. Leave tube at 4°C for 15min to allow air bubbles to rise to the top.
9. Aliquot and store at -20°C.

Appendix C List of Reagents used

Name	Product number	Company
Aluminium potassium sulphate,	541A60647	Merck
Bovine serum albumin fraction V	10735086001	Roche
5-Bromo-2'-deoxyuridine	16880	Fluka
Chloral hydrate AR	SAAR1591500EM	Merck
Citric Acid, monohydrate	SAAR1605020EM	Merck
Coverslips, glass, 22 X 50 mm	GLAS2C29M2250REC	LASEC
DAPI - 4,6,Diamidino-2-Phenylindole,	D1306	Invitrogen
Donkey serum, normal	D9663	Sigma-Aldrich
Dulbecco's Modified Eagle's Medium	No.P02	Highveld
EDTA (ethylenediaminetetra-acetic acid)	E9884	Sigma-Aldrich
Eosin Y (CI 45380)	2186000CB	Merck
Entellan	1079610500	Merck
Ethanol, absolute	1.00983.2500	Merck
Formaldehyde, 40%	SAAR2436020LP	Merck
Glass microfibre filter paper, 0.45 µm	Whatman 1822-025	Merck
Glycerol	2676500LC	Merck
Haematoxylin (CI 75290)	2822000CB	Merck
HCl (hydrochloric acid, 37%)	SAAR3063054LCA	Merck
Isopropanol	SAAR5075040LC	Merck
Magnesium sulphate	SAAR4124000EM	Merck
Methanol	SAAR4164060LP	Merck
Microscope slides, glass, Superfrost Plus	GLAS54522M3000F	LASEC
Microscope slides, glass, frosted	GLAS54522M1000F	LASEC
Mowiol® 4-88	81381 ALDRICH	Sigma-Aldrich
Phloxin B (CI 45410)	115926	Merck
Potassium chloride (KCl)	SAAR5042000EM	Merck
Potassium dihydrogen orthophosphate	10203	BDH AnalaR
n-Propyl gallate	P3130	Sigma-Aldrich
Sodium azide	822335	Merck
Sodium chloride (NaCl)	SAAR5822320EM	Merck

Sodium dihydrogen orthophosphate	10245	BDH AnalaR
Sodium iodate	BDH 852600	Merck
Sodium hydrogen carbonate ($NaHCO_3$)	SAAR5822820EM	Merck
di-Sodium hydrogen phosphate (Na_2HPO_4)	1.06586.0500	Merck
di-Sodium hydrogen phosphate	1.06579.0500	Merck
Thymol	6018250DC	Merck
Tris(hydroxymethyl)-aminomethane	1083820500	Merck
Tween-20	SAAR6114500KF	Merck

Appendix D Ethics Approval

UNIVERSITY OF CAPE TOWN
IYUNIVESITHI YASEKAPA • UNIVERSITEIT VAN KAAPSTAD

FACULTY OF HEALTH SCIENCES
Human Research Ethics Committee

Annual Progress Report

Date	
HREC REF Number	
Protocol number (if applicable) & Protocol title	
Principal Investigator	
Department / Office Internal Mail Address	

List of documentation

[Please see attached Letter.]

RESEARCH ETHICS COMMITTEE
2011 -06- 20
HEALTH SCIENCES FACULTY
UNIVERSITY OF CAPE TOWN

HREC office use only (FWA00001637; IRB00001938)			
☑ Approved	This serves as notification of annual approval, including all documentation described above.		
☐ Not approved	See attached comments.		
Type of review	☑ Expedited	☐ Full committee	
Expiry date	28 JUNE 2012		
Signature Chairperson of the HREC	Signed by candidate	Date	21/6/2011

Department of Human Biology

Faculty of Health Sciences
University of Cape Town
Observatory Cape 7925
South Africa
Tel: + 27 21 406 6787
Fax: + 27 21 448 7226

June 2011

Attention : Professor Marc Blockman
Faculty of Health Sciences Research Ethics Committee
E52, Room 24
Old Main Building
Groote Schuur Hospital

Request to Extend Protocol : Registry of Skin Samples (REC REF : 493/2009)

Dear Prof Blockman and Committee Members

Permission for the above-mentioned protocol expired November 2010. The projects associated with the Skin Registry are however ongoing through 2011-12 and include a current Masters and PhD project under my supervision. I therefore request an extension of this protocol till the end of 2012.

If you and/or your committee feel that a progress report is necessary to further substantiate this request, I would gladly furnish you with one.

Looking forward to your response.

Regards,
Dr Lester M. Davids, Principal Investigator
Tel . 021-406 6787

Appendix E Data Tables

E.1 Number of sections examined at each time point

Time point	# samples	# sections per	Total # of
Day 0 (U)	1	4	4
Day 0 (W)	1	4	4
Day 1	2	4	8
Day 2	2	4	8
Day 5	2	4	8
Day 10	2	4	8
Day 12	2	4	8

U = unwounded skin W= wounded skin

E.2 Growth of epithelial tongues – Fig.3.12

Day 1	Day 2	Day 5	Day 10	Day 12
0,085	0,542	0,553	0,738	0,468
0,089	0,521	0,487	0,747	0,485
0,115	0,546	0,592	1,148	0,565
0,111	0,318	0,488	1,262	0,560
	0,329	0,676	1,286	0,510
	0,336	0,657	0,812	0,649
	0,797	0,729	0,783	0,634
	0,798	0,702	0,640	0,431
	0,793	0,702	0,621	0,437
	0,450	0,714	0,753	0,448
	0,424	0,634	0,880	
	0,448	0,637	0,854	
	0,450	0,583	0,812	

	0,723	0,564	0,783	
	0,694	0,476	0,643	
	0,770	0,564	0,650	
	0,716			

E.3 Length of epithelial outgrowths on LHS in mm – Fig.3.19 a

Day 1	Day 2	Day 5	Day 10	Day 12
0,013	0,453	1,027	0,992	1,530
0,013	0,444	1,067	1,012	1,631
0,014	0,291	1,124	1,523	1,484
0,035	0,306	1,047	1,553	1,584
	0,364	0,934	1,410	2,017
	0,282	0,921	1,145	2,135
	0,448	0,943		2,014
	0,434	0,908		1,889
				2,007
				2,013
				2,019

E.3 Length of epithelial outgrowths on RHS in mm – Fig.3.19 g

Day 1	Day 2	Day 5	Day 10	Day 12
0,0230	0,464	1,089	1,494	1,667
0,0270	0,420	1,162	1,511	1,789
0,0190	0,467	1,070	0,963	1,675
0,0090	0,484	1,058	0,941	1,813
	0,385	0,989	1,298	1,221
	0,370	1,123	1,504	1,383
	0,391	0,893		1,102
	0,406	0,864		1,819
				1,794

E.4 Width of epithelial tongue vs lateral outgrowth at days 10 & 12 – Fig.3.21

Day 10 Tongue	Day 10 Outgrowth	Day 12 Tongue	Day 12 Outgrowth
46,552	22,470	40,220	20,460
46,584	11,900	39,380	24,811
44,828	17,540	36,390	22,190
31,082	17,540	31,630	21,050
27,640	22,470	30,850	17,540
27,586	22,470	32,560	21,050
58,621	23,540	31,910	38,600
55,199	28,290	31,740	31,580
53,476	20,460	31,630	24,560

E.5 Average number of keratinocytes in cultured skin per mm (data extracted from table E.7 below) - Fig.3.24

Normal epidermis																
Day 0	15,84	17,07	12,82	14,76	6,50	9,26	19,42	19,97	12,96	12,85						
Day 1	8,85	9,95	2,50	6,60	6,88	8,74	9,28	5,69								
Day 2	4,80	7,45	8,03	7,04	10,32	18,34	6,23	6,20	5,62	5,02						
Day 5	5,12	9,00	4,65	5,23	8,75	8,29	3,60	7,03	15,36	9,70						
Day 10	3,68	9,34	9,50	9,58	9,86	7,15	10,51	13,03	10,75	5,04	3,40	19,49	6,85	2,82	3,93	6,13
Day 12	10,38	11,09	8,96	13,81	5,88	8,34	4,90	16,04	13,54	23,29	22,33	11,29	11,22	18,26	21,04	7,70
Healing tongues																
Day 0	0.00	0.00	0.00	0.00	0.00	0.00	0.00	0.00								

Day 1	0.00	0.00	0.00	0.00	0.00	0.00	0.00	0.00								
Day 2	16,95	24,86	10,05	9,12	18,96	24,45	6,87	10,98								
Day 5	43,38	46,96	41,25	44,70	45,32	43,19	30,81	21,45	34,46	29,85						
Day 10	8,08	22,99	22,32	29,80	23,90	29.41	20,36	28,50	25,89	25,44	19,25	44,91	40,27			
Day 12	22,73	16,39	37,62	27,72	38,85	17,24	31,70	31,70								

E.6 Average number of melanocytes in cultured skin per mm (data extracted from table E.7 below) - Fig.3.30

Normal epidermis																
Day 0	12,84	10,50	13,89	12,11	6,59	7,47	12,61	12,21	9,01	12,99						
Day 1	4,99	7,55	5,39	5,13	8,75	8,14	10,49	11,37								
Day 2	10,08	10,12	8,03	8,04	7,30	17,92	8,51	8,89	5,08	6,69						
Day 5	8,97	9,00	5,86	7,05	10,26	10,65	11,07	10,05	11,28	8,35						
Day 10	6,90	9,72	9,74	8,62	8,51	6,73	12,02	7,99	11,92	10,35	9,98	11,51	11,67	11,01	12,79	11,12
Day 12	9,82	9,81	8,59	11,61	10,53	8,92	8,94	10,49	15,50	13,92	12,02	14,17	15,80	13,49	8,84	8,63
Healing tongues																
Day 0	0.00	0.00	0.00	0.00	0.00	0.00	0.00	0.00	0.00	0.00	0.00	0.00	0.00	0.00	0.00	0.00

Day 1	0.00	0.00	0.00	0.00												
Day 2	0,00	0,00	1,83	1,52	2,37	2,72	6,87	0,00	1,10							
Day 5	4,21	1,74	4,27	0,00	1,51	1,66	4,20	1,40	0,00	4,07						
Day 10	2,87	4,18	1,36	2,82	0,00	3,82	1,30	0,00	1,59	3,61	1,73	1,34				
Day 12	0,00	4,10	3,96	1,91	2,66	5,76	0,00									

E.7 Data Table – raw data

Time	Sample #	epidermis proximal to WE on LHS			tongue LHS (incl. WE)			tongue RHS (incl. WE)			epidermis proximal to WE on RHS		
		BM L in µm	Ave #div KCs	Ave #MC	BM L in µm	Ave #div KCs	Ave #MC	BM L in µm	Ave #div KCs	Ave #MC	BM L in µm	Ave #div KCs	Ave #MC
Day 12	Sample 1	3564	(37) 10.38	(35) 9.82	1813	-	-	closed	-	-	4689	(52) 11.09	(46) 9.81
	Sample 2	5357	(48) 8.96	(46) 8.59	820	-	-	closed	-	-	3187	(44) 13.81	(37) 11.61
	Sample 3	4085	(24) 5.88	(43) 10.53	1599	-	-	closed	-	-	5156	(43) 8.34	(46) 8.92
	Sample 4	5703	(28) 4.90	(51) 8.94	474	-	-	closed	-	-	3242	(52) 16.04	(34) 10.49
	Sample 5	3840	(52) 13.54	(54) 15.5	396	(9) 22.73	(0) 0	244	(4) 16.39	(1) 4.10	3521	(82) 23.29	(49) 13.92
	Sample 6	3493	(78) 22.33	(42) 12.02	505	(14) 37.62	(2) 3.96	489	(19) 38.85	(1) 1.91	4516	5.76	(64) 14.17
	Sample 7	4366	(49) 11.22	(69) 15.80	376	(12) 31.91	(1) 2.66	290	(5) 17.24	(0) 0	3559	(65) 18.26	(48) 13.49
	Sample 8	3279	(69) 21.04	(29) 8.84	347	(11) 31.70	(2) 5.76	522	(9) 17.24	(0) 0	4283	(33) 7.70	(37) 8.63
Day 10	Sample 1	2173	(8) 3.68	(15) 6.90	-	-	-	closed	-	-	5248	(49) 9.34	(51) 9.72
	Sample 2	4314	(41) 9.50	(42) 9.74	696	(16) 22.99	(2) 2.87	717	(16) 22.32	(3) 4.18	3132	(30) 9.58	(27) 8.62
	Sample 3	4464	(44) 9.86	(38) 8.51	1485	-	-	closed			4757	(34) 7.15	(32) 6.73
	Sample 4	3995	(42) 10.51	(48) 12.02	738	(22) 29.80	(1) 1.36	710	(17) 23.90	(2) 2.82	3377	(44) 13.03	(27) 7.99
	Sample 5	4280	(46) 10.75	(51) 11.92	510	(15) 29.41	(0) 0	786	(16) 20.36	(3) 3.82	3767	(19) 5.04	(39) 10.35
	Sample 6	4708	(16) 3.40	(47) 9.98	772	(22) 28.50	(1) 1.30	734	(19) 25.89	(0) 0	4516	(44) 19.49	(52) 11.51
	Sample 7	3941	(27) 6.85	(46) 11.67	629	(16) 25.44	(1) 1.59	831	(16) 19.25	(3) 3.61	3905	(11) 2.82	(43) 11.01
	Sample 8	4067	(16) 3.93	(52) 12.79	579	(26) 44.91	(1) 1.73	745	(30) 40.27	(1) 1.34	4407	(27) 6.13	(49) 11.12
Day 5	Sample 1	3904	(20) 5.12	(35) 8.97	713	(31) 43.48	(3) 4.21	575	(27) 46.96	(1) 1.74	2890	(26) 9.0	(26) 9.0
	Sample 2	4945	(23) 4.65	(29) 5.86	703	(29) 41.25	(3) 4.27	559	(25) 44.7	(0) 0.0	4397	(23) 5.23	(31) 7.05
	Sample 3	3315	(29) 8.75	(34) 10.26	662	(30) 45.32	(1) 1.51	602	(26) 43.19	(1) 1.66	5069	(42) 8.29	(54) 10.65

	Sample 4	3613	(13) 3.60	(40) 11.07	714	(22) 30.81	(3) 4.2	699	(15) 21.45	(1) 1.4	2688	(19) 7.03	(27) 10.05
	Sample 5	3191	(49) 15.36	(36) 11.28	582	(20) 34.36	(0) 0.00	737	(22) 29.85	(3) 4.07	4431	(43) 9.70	(37) 8.35
Day 2	Sample 1	4166	(20) 4.8	(42) 10.08	413	(7) 16.95	(0) 0	362	(9) 24.86	(0) 0	5236	(39) 7.45	(53) 10.12
	Sample 2	3985	(32) 8.03	(32) 8.03	1094	(11) 10.05	(2) 1.83	658	(6) 9.12	(1) 1.52	4973	(35) 7.04	(40) 8.04
	Sample 3	3972	(41) 10.32	(29) 7.3	422	(8) 18.96	(1) 2.37	368	(9) 24.45	(1) 2.72	2399	(44) 18.34	(43) 17.92
	Sample 4	6579	(41) 6.23	(56) 8.51	582	(4) 6.87	(0) 0	911	(10) 10.98	(1) 1.1	4838	(30) 6.2	(43) 8.89
	Sample 5	3736	(21) 5.62	(19) 5.08	-	-	-	closed	-	-	5978	(30) 5.02	(40) 6.69
Day 1	Sample 1	2807	(24) 8.55	(14) 4.99	-	-	-	-	-	-	5430	(54) 9.95	(41) 7.55
	Sample 2	5199	(13) 2.5	(28) 5.39	-	-	-	-	-	-	2729	(18) 6.6	(14) 5.13
	Sample 3	6398	(44) 6.88	(56) 8.75	-	-	-	-	-	-	5035	(44) 8.74	(41) 8.14
	Sample 4	4958	(46) 9.28	(52) 10.49	-	-	-	-	-	-	5627	(32) 5.69	(64) 11.37
Day 0	Sample 1	10353	(164) 15.84	(133) 12.84									
	Sample 2	7145	(122) 17.07	(75) 10.50									
	Sample 3	10376	(144) 12.82	(133) 13.89									
	Sample 4	6773	(100) 14.76	(82) 12.11									
	Sample 5	10767	(70) 6.50	(71) 6.59									
	Sample 6	7233	(67) 9.26	(54) 7.47									
	Sample 7	4995	(97) 19.42	(63) 12.61									
	Sample 8	3605	(72) 19.97	(44) 12.21									
	Sample 9	6848	(88) 12.85	(89) 12.99									
	Sample 10	3550	(46) 12.96	(32) 9.01									

BM L = Basement Membrane Length; Ave # = Average number; KC = Keratinocyte/s; MC = Melanocyte/s; WE = Wound Edge

Please note: Cell counts in brackets are **actual counts** with the **calculated value** = actual counts divided by the length of BM/1000 to bring it to number of cells per mm basement membrane is outside the brackets.

The word ’Sample” as used in this table refers to a section that was analysed and may be a repeat. E.g. For day 0, Sample 1, 3 and 5 are repeat consecutive sections; Sample 2, 4 and 6 are different consecutive sections. Samples 7 and 9 are repeat consecutive sections and similarly, samples 8 and 9 are repeat consecutive sections.

Appendix F Published paper

TECHNICAL ARTICLE

Simultaneous Immunofluorescent Labeling Using Anti-BrdU Monoclonal Antibody and a Melanocyte-specific Marker in Formalin-fixed Paraffin-embedded Human Skin Samples

Morea Petersen, BTech, Lester M. Davids, PhD, and Susan H. Kidson, PhD

Abstract: Immunolabeling of tissue sections requires careful optimization of protocols in order to achieve accurate and consistent data. Multiple immunolabeling is desirable when determining the exact location and phenotype of cell populations in the same cellular compartment. 5-bromodeoxyuridine (BrdU)-immunolabeling is commonly used to assess cellular proliferation in vitro. However, the technical limitations of standard methods preclude multiple antigen immunolabeling. The aim was therefore to develop a robust protocol for simultaneous labeling using anti-BrdU and a melanocyte-specific marker in formalin-fixed paraffin-embedded (FFPE) skin samples. Human skin samples were obtained from patients undergoing elective plastic surgery. The tissue was incubated with BrdU, and a standard sample procedure for FFPE tissue was used. Heat-induced antigen retrieval was performed in a conventional pressure cooker, followed by immunolabeling with anti-BrdU and anti-Melan A/MART-1 antibodies. Fluorescent-conjugated secondary antibodies were used for signal detection. We have demonstrated both proliferating cells (BrdU-immunopositive) and melanocytes (Melan A/MART-1-immunopositive) in the basal compartment of the epidermis in our skin samples. Successful double labeling requires heat-induced epitope retrieval to replace the harsh pretreatment protocols of standard BrdU immunolabeling methods. We have optimized a robust protocol for the double labeling of proliferating cells and cells bearing melanocyte-specific antigens (melanocytes and/or melanoblasts) in FFPE human skin samples.

Key Words: immunohistochemistry, immunofluorescent labeling, multiple labeling, FFPE, BrdU, Ki-67, Melan A/MART-1

(*Appl Immunohistochem Mol Morphol* 2012;20:614–617)

Received for publication November 24, 2011; accepted February 8, 2012.
From the Faculty of Health Sciences, University of Cape Town, Cape Town, South Africa.
Supported in part by the National Research Foundation of South Africa (S.H.K.); the Medical Research Council of South Africa Senior Career Award grant (L.M.D.), and the University of Cape Town (M.P.).
The authors declare no conflict of interest.
Reprints: Lester M. Davids, PhD, Faculty of Health Sciences, University of Cape Town, Anzio Road, Cape Town, Western Cape 7925, South Africa (e-mail: lester.davids@uct.ac.za).

Immunohistochemical techniques are widely used in both clinical and research applications as an aid to obtain information regarding disease processes and to elucidate the mechanism of cellular events and interactions. However, careful optimization of the immunohistochemical protocol needs to be conducted to achieve accurate and consistent data. Prepared sections of frozen tissue are commonly used in immunohistochemical techniques as the best demonstration of cellular antigens with negligible effect on native protein conformation. The clinical availability and associated limitations of frozen section technique, however, necessitates the need for alternative methods. One such alternative is formalin-fixed paraffin-embedded (FFPE) tissues. The main drawback of this type of fixation, however, is its masking effect on antigenic epitopes in the tissue sections. If FFPE sections are therefore to be successfully used for the localization of cellular antigens, the protocol has to include some form of antigen retrieval.[1] Common antigen retrieval methods include the use of proteolytic enzymes, for example trypsin, ficin, and pepsin,[2] or heat-induced epitope retrieval (HIER) that involves a combination of wet heat and steaming, autoclaving or microwaving at high temperatures (~121°C) in either sodium citrate buffer at pH 6.0 or EDTA buffer at pH 8.0.[1,3,4] To date, HIER has been shown to consistently be the best method of exposing antigenic determinants in FFPE tissues.[3–5]

Because of the inherent difficulties associated with multiple labeling of FFPE tissues[6] and the complicated 3-dimensional architecture of human skin, few studies use multiple antigen immunostaining techniques on FFPE human skin in normal and diseased states. Although it is understandable that Ki-67 remains the "gold standard" for proliferating cell detection in pathologic samples,[7,8] molecularly this stain includes the entire cell cycle, and thus, even cells that are perhaps cytostatic in the tissues examined will provide a positive signal leading to elevated cell numbers. In contrast, immunolabeling of the halogenated pyrimidine, 5-bromodeoxyuridine (BrdU), only highlights S-phase dividing cells and thus represents a more definitive picture of proliferating cells ex vivo.[9] However, standard BrdU immunolabeling techniques on FFPE tissue use a harsh DNA denaturation step, necessary to reveal the BrdU epitopes.[10] In addition, the

References

AARABI, S., LONGAKER, M. T. & GURTNER, G. C. 2007. Hypertrophic scar formation following burns and trauma: new approaches to treatment. *PLoS Med,* 4**,** e234.

ADZICK, N. S. & LORENZ, H. P. 1994. Cells, matrix, growth factors, and the surgeon. The biology of scarless fetal wound repair. *Annals of Surgery,* 220**,** 10-18.

ALALUF, S., ATKINS, D., BARRETT, K., BLOUNT, M., CARTER, N. & HEATH, A. 2002. Ethnic variation in melanin content and composition in photoexposed and photoprotected human skin. *Pigment Cell Research / sponsored by the European Society for Pigment Cell Research and the International Pigment Cell Society,* 15**,** 112-118.

ANDO, H., NIKI, Y., ITO, M., AKIYAMA, K., MATSUI, M. S., YAROSH, D. B. & ICHIHASHI, M. 2012. Melanosomes are transferred from melanocytes to keratinocytes through the processes of packaging, release, uptake, and dispersion. *J Invest Dermatol,* 132**,** 1222-9.

AROCA, P., SOLANO, F., SALINAS, C., GARCIA-BORRON, J. C. & LOZANO, J. A. 1992. Regulation of the final phase of mammalian melanogenesis. The role of dopachrome tautomerase and the ratio between 5,6-dihydroxyindole-2-carboxylic acid and 5,6-dihydroxyindole. *Eur J Biochem,* 208**,** 155-63.

BANERJEE, J. & SEN, C. K. 2015. microRNA and Wound Healing. *Advances in experimental medicine and biology,* 888**,** 291-305.

BASRUR, V., YANG, F., KUSHIMOTO, T., HIGASHIMOTO, Y., YASUMOTO, K., VALENCIA, J., MULLER, J., VIEIRA, W. D., WATABE, H., SHABANOWITZ, J., HEARING, V. J., HUNT, D. F. & APPELLA, E. 2003. Proteomic analysis of early melanosomes: identification of novel melanosomal proteins. *J Proteome Res,* 2**,** 69-79.

BAYNASH, A. G., HOSODA, K., GIAID, A., RICHARDSON, J. A., EMOTO, N., HAMMER, R. E. & YANAGISAWA, M. 1994. Interaction of endothelin-3 with endothelin-B receptor is essential for development of epidermal melanocytes and enteric neurons. *Cell,* 79**,** 1277-85.

BEMENT, W. M., FORSCHER, P. & MOOSEKER, M. S. 1993. A novel cytoskeletal structure involved in purse string wound closure and cell polarity maintenance. *J Cell Biol,* 121**,** 565-78.

BETZ, P., NERLICH, A., WILSKE, J., TUBEL, J., PENNING, R. & EISENMENGER, W. 1993. The time-dependent localization of Ki67 antigen-positive cells in human skin wounds. *Int J Legal Med,* 106**,** 35-40.

BIRLEA, S. A., COSTIN, G. E., ROOP, D. R. & NORRIS, D. A. 2016. Trends in Regenerative Medicine: Repigmentation in Vitiligo Through Melanocyte Stem Cell Mobilization. *Med Res Rev*.

BOENISCH, T. 2006. Heat-induced antigen retrieval: what are we retrieving? *The journal of histochemistry and cytochemistry : official journal of the Histochemistry Society,* 54**,** 961-964.

BOISSY, R. E., SAKAI, C., ZHAO, H., KOBAYASHI, T. & HEARING, V. J. 1998. Human tyrosinase related protein-1 (TRP-1) does not function as a DHICA oxidase activity in contrast to murine TRP-1. *Experimental dermatology,* 7**,** 198-204.

BORENA, B. M., MARTENS, A., BROECKX, S. Y., MEYER, E., CHIERS, K., DUCHATEAU, L. & SPAAS, J. H. 2015. Regenerative Skin Wound Healing in Mammals: State-of-the-Art on Growth Factor and Stem Cell Based Treatments. *Cellular Physiology and Biochemistry,* 36**,** 1-23.

BOROVANSKY, J. & RILEY, P. A. 2011. *Melanins and Melanosomes:Biosynthesis, Biogenesis, Physiological, and Pathological Functions,* Weinheim, Germany, Wiley-Blackwell.

BRANCATO, S. K. & ALBINA, J. E. 2011. Wound macrophages as key regulators of repair: origin, phenotype, and function. *Am J Pathol,* 178**,** 19-25.

BREATHNACH, A. S. 1960. Melanocytes in Early Regenerated Human Epidermis *. *Journal of Investigative Dermatology,* 35**,** 245-251.

BUSAM, K. J. & JUNGBLUTH, A. A. 1999. Melan-A, a new melanocytic differentiation marker. *Adv Anat Pathol,* 6**,** 12-8.

CHADWICK, S., HEATH, R. & SHAH, M. 2012. Abnormal pigmentation within cutaneous scars: A complication of wound healing. *Indian J Plast Surg,* 45**,** 403-11.

CHEN, K., MANGA, P. & ORLOW, S. J. 2002. Pink-eyed dilution protein controls the processing of tyrosinase. *Mol Biol Cell,* 13**,** 1953-64.

CHOU, W. C., TAKEO, M., RABBANI, P., HU, H., LEE, W., CHUNG, Y. R., CARUCCI, J., OVERBEEK, P. & ITO, M. 2013. Direct migration of follicular melanocyte stem cells to the epidermis after wounding or UVB irradiation is dependent on Mc1r signaling. *Nat Med,* 19**,** 924-9.

CICHOREK, M., WACHULSKA, M., STASIEWICZ, A. & TYMINSKA, A. 2013. Skin melanocytes: biology and development. *Postepy Dermatol Alergol,* 30**,** 30-41.

COMPANJEN, A. R., VAN DER WEL, L. I., WEI, L., LAMAN, J. D. & PRENS, E. P. 2001. A modified ex vivo skin organ culture system for functional studies. *Arch Dermatol Res,* 293**,** 184-90.

COX, P. M., DHILLON, A. P., HOWE, S., PITTILO, R. M. & RODE, J. 1989. Repopulation of guinea-pig skin by melanocytes during wound healing: a morphometric study. *British journal of experimental pathology,* 70**,** 679-689.

DAS, T., SAFFERLING, K., RAUSCH, S., GRABE, N., BOEHM, H. & SPATZ, J. P. 2015. A molecular mechanotransduction pathway regulates collective migration of epithelial cells. *Nat Cell Biol,* 17**,** 276-87.

DE MAZIERE, A. M., MUEHLETHALER, K., VAN DONSELAAR, E., SALVI, S., DAVOUST, J., CEROTTINI, J. C., LEVY, F., SLOT, J. W. & RIMOLDI, D. 2002. The melanocytic protein Melan-A/MART-1 has a subcellular localization distinct from typical melanosomal proteins. *Traffic,* 3**,** 678-93.

DESMOULIERE, A. 1995. Factors influencing myofibroblast differentiation during wound healing and fibrosis. *Cell Biol Int,* 19**,** 471-6.

DORSKY, R. I., MOON, R. T. & RAIBLE, D. W. 1998. Control of neural crest cell fate by the Wnt signalling pathway. *Nature,* 396**,** 370-3.

DORSKY, R. I., MOON, R. T. & RAIBLE, D. W. 2000. Environmental signals and cell fate specification in premigratory neural crest. *Bioessays,* 22**,** 708-16.

EISINGER, M. & MARKO, O. 1982. Selective proliferation of normal human melanocytes in vitro in the presence of phorbol ester and cholera toxin. *Proceedings of the National Academy of Sciences of the United States of America,* 79**,** 2018-2022.

ERICKSON, C. A. 1993. From the crest to the periphery: control of pigment cell migration and lineage segregation. *Pigment Cell Research / sponsored by the European Society for Pigment Cell Research and the International Pigment Cell Society,* 6**,** 336-347.

FAHS, F., BI, X., YU, F.-S., ZHOU, L. & MI, Q.-S. 2015. New insights into microRNAs in skin wound healing. *IUBMB Life,* 67**,** 889-896.

FAROOQUI, R. & FENTEANY, G. 2005. Multiple rows of cells behind an epithelial wound edge extend cryptic lamellipodia to collectively drive cell-sheet movement. *Journal of cell science,* 118**,** 51-63.

FENTEANY, G., JANMEY, P. A. & STOSSEL, T. P. 2000. Signaling pathways and cell mechanics involved in wound closure by epithelial cell sheets. *Curr Biol,* 10**,** 831-8.

FITZPATRICK, T. B. & BREATHNACH, A. S. 1963. The Epidermal Melanin Unit System. *Dermatologische Wochenschrift,* 147**,** 481-489.

FUCHS, E. & HORSLEY, V. 2008. More than one way to skin. *Genes & development,* 22**,** 976-985.

FUCHS, E. & RAGHAVAN, S. 2002. Getting under the skin of epidermal morphogenesis. *Nature reviews.Genetics,* 3**,** 199-209.

GAO, F. L., JIN, R., ZHANG, L. & ZHANG, Y. G. 2013. The contribution of melanocytes to pathological scar formation during wound healing. *Int J Clin Exp Med,* 6**,** 609-13.

GARCIN, C. L., ANSELL, D. M., HEADON, D. J., PAUS, R. & HARDMAN, M. J. 2016. Hair Follicle Bulge Stem Cells Appear Dispensable for the Acute Phase of Wound Re-epithelialization. *Stem Cells,* 34**,** 1377-85.

GAUGLITZ, G. G. 2013. Management of keloids and hypertrophic scars: current and emerging options. *Clin Cosmet Investig Dermatol,* 6**,** 103-14.

GONZALEZ, A. C., COSTA, T. F., ANDRADE, Z. A. & MEDRADO, A. R. 2016. Wound healing - A literature review. *An Bras Dermatol,* 91**,** 614-620.

GORDON, P. R., MANSUR, C. P. & GILCHREST, B. A. 1989. Regulation of human melanocyte growth, dendricity, and melanization by keratinocyte derived factors. *J Invest Dermatol,* 92**,** 565-72.

GOSAIN, A., JONES, S. B., SHANKAR, R., GAMELLI, R. L. & DIPIETRO, L. A. 2006. Norepinephrine modulates the inflammatory and proliferative phases of wound healing. *J Trauma,* 60**,** 736-44.

GRICHNIK, J. M. 2006. Kit and Melanocyte Migration. *Journal of Investigative Dermatology,* 126**,** 945-947.

GUO, H., XING, Y., LIU, Y., LUO, Y., DENG, F., YANG, T., YANG, K. & LI, Y. 2016. Wnt/beta-catenin signaling pathway activates melanocyte stem cells in vitro and in vivo. *J Dermatol Sci,* 83**,** 45-51.

GURTNER, G. C., WERNER, S., BARRANDON, Y. & LONGAKER, M. T. 2008. Wound repair and regeneration. *Nature,* 453**,** 314-321.

HAASS, N. K. & HERLYN, M. 2005. Normal Human Melanocyte Homeostasis as a Paradigm for Understanding Melanoma. *Journal of Investigative Dermatology Symposium Proceedings,* 10**,** 153-163.

HALABAN, R. 2000. The Regulation of Normal Melanocyte Proliferation. *Pigment Cell Res,* 13**,** 4-14.

HALABAN, R., LANGDON, R., BIRCHALL, N., CUONO, C., BAIRD, A., SCOTT, G., MOELLMANN, G. & MCGUIRE, J. 1988. Basic fibroblast growth factor from human keratinocytes is a natural mitogen for melanocytes. *J Cell Biol,* 107**,** 1611-9.

HALABAN, R., TYRRELL, L., LONGLEY, J., YARDEN, Y. & RUBIN, J. 1993. Pigmentation and proliferation of human melanocytes and the effects of melanocyte-stimulating hormone and ultraviolet B light. *Ann N Y Acad Sci,* 680**,** 290-301.

HARA, M., YAAR, M. & GILCHREST, B. A. 1995. Endothelin-1 of keratinocyte origin is a mediator of melanocyte dendricity. *J Invest Dermatol,* 105**,** 744-8.

HARRISON, C. A., HEATON, M. J., LAYTON, C. M. & MAC NEIL, S. 2006. Use of an in vitro model of tissue-engineered human skin to study keratinocyte attachment and migration in the process of reepithelialization. *Wound Repair Regen,* 14**,** 203-9.

HEARING, V. J. 2011. Determination of Melanin Synthetic Pathways. *Journal of Investigative Dermatology,* 131, Supplement 3**,** E8-E11.

HEATH, R. L., THOMLINSON, A. M. & SHAH, M. 2009. Melanocytes and burn wound healing. *Burns,* 35**,** S44.

HEMESATH, T. J., STEINGRIMSSON, E., MCGILL, G., HANSEN, M. J., VAUGHT, J., HODGKINSON, C. A., ARNHEITER, H., COPELAND, N. G., JENKINS, N. A. & FISHER, D. E. 1994. microphthalmia, a critical factor in melanocyte development, defines a discrete transcription factor family. *Genes Dev,* 8**,** 2770-80.

HENG, M. C. 2011. Wound healing in adult skin: aiming for perfect regeneration. *Int J Dermatol,* 50**,** 1058-66.

HIROBE, T. 1988. Developmental changes of the proliferative response of mouse epidermal melanocytes to skin wounding. *Development,* 102**,** 567-74.

HOASHI, T., WATABE, H., MULLER, J., YAMAGUCHI, Y., VIEIRA, W. D. & HEARING, V. J. 2005. MART-1 is required for the function of the melanosomal matrix protein PMEL17/GP100 and the maturation of melanosomes. *J Biol Chem,* 280**,** 14006-16.

ILINA, O. & FRIEDL, P. 2009. Mechanisms of collective cell migration at a glance. *J Cell Sci,* 122**,** 3203-8.

ITO, M., LIU, Y., YANG, Z., NGUYEN, J., LIANG, F., MORRIS, R. J. & COTSARELIS, G. 2005. Stem cells in the hair follicle bulge contribute to wound repair but not to homeostasis of the epidermis. *Nat Med,* 11**,** 1351-4.

ITO, S. & WAKAMATSU, K. 2003. Quantitative analysis of eumelanin and pheomelanin in humans, mice, and other animals: a comparative review. *Pigment Cell Research / sponsored by the European Society for Pigment Cell Research and the International Pigment Cell Society,* 16**,** 523-531.

JANIS, J. E. & HARRISON, B. 2014. Wound healing: part I. Basic science. *Plast Reconstr Surg,* 133**,** 199e-207e.

JIMBOW, K., HUA, C., GOMEZ, P. F., HIROSAKI, K., SHINODA, K., SALOPEK, T. G., MATSUSAKA, H., JIN, H. Y. & YAMASHITA, T. 2000a. Intracellular vesicular trafficking of tyrosinase gene family protein in eu- and pheomelanosome biogenesis. *Pigment Cell Research / sponsored by the European Society for Pigment Cell Research and the International Pigment Cell Society,* 13 Suppl 8**,** 110-117.

JIMBOW, K., PARK, J. S., KATO, F., HIROSAKI, K., TOYOFUKU, K., HUA, C. & YAMASHITA, T. 2000b. Assembly, target-signaling and intracellular transport of tyrosinase gene family proteins in the initial stage of melanosome biogenesis. *Pigment Cell Research / sponsored by the European Society for Pigment Cell Research and the International Pigment Cell Society,* 13**,** 222-229.

KATARANOVSKI, M. & KARADAGLIC, D. 1999. Skin organ culture: A review. *Acta Dermatovenerologica APA,* 8**,** 131-140.

KATARINA JANSSON, G. K. A. A. H. 1996. Characterization of a New in vitro Model for Studies of Reepithelialization in Human Partial Thickness Wounds. *In Vitro Cellular & Developmental Biology. Animal,* 32**,** 534- 540.

KAWAKAMI, Y., BATTLES, J. K., KOBAYASHI, T., ENNIS, W., WANG, X., TUPESIS, J. P., MARINCOLA, F. M., ROBBINS, P. F., HEARING, V. J., GONDA, M. A. & ROSENBERG, S. A. 1997. Production of recombinant MART-1 proteins and specific antiMART-1 polyclonal and monoclonal antibodies: use in the characterization of the human melanoma antigen MART-1. *J Immunol Methods,* 202**,** 13-25.

KAWAKAMI, Y., ROBBINS, P. F. & ROSENBERG, S. A. 1996. Human melanoma antigens recognized by T lymphocytes. *Keio J Med,* 45**,** 100-8.

KESWELL, D., DAVIDS, L. M. & KIDSON, S. H. 2012. Migration of human melanocytes into keratinocyte monolayers in vitro. *Journal of Dermatological Science,* 66**,** 160-163.

KESWELL, D., KIDSON, S. H. & DAVIDS, L. M. 2015. Melanocyte migration is influenced by E-cadherin-dependent adhesion of keratinocytes in both two- and three-dimensional in vitro wound models. *Cell Biol Int,* 39**,** 169-76.

KIDSON, S. H., RICHARDS, P. D., RAWOOT, F. & KROMBERG, J. G. 1993. An ultrastructural study of melanocytes and melanosomes in the skin and hair bulbs of rufous albinos. *Pigment Cell Res,* 6**,** 209-14.

KIERSZENBAUM, A. L., & TRES, L. L. 2012. *Histology and cell biology: An introduction to pathology,* Philadelphia, PA, Elsevier Saunders.

KIPPENBERGER, S., BERND, A., BEREITER-HAHN, J., RAMIREZ-BOSCA, A. & KAUFMANN, R. 1997. Melanocytes in vitro: how do they undergo mitosis? *Pigment Cell Res,* 10**,** 85-7.

KLEIN-PARKER, H. A., WARSHAWSKI, L. & TRON, V. A. 1994. Melanocytes in human skin express bcl-2 protein. *J Cutan Pathol,* 21**,** 297-301.

KLESZCZYNSKI, K. & FISCHER, T. W. 2012. Development of a short-term human full-thickness skin organ culture model in vitro under serum-free conditions. *Arch Dermatol Res,* 304**,** 579-87.

KOBAYASHI, T., URABE, K., WINDER, A., JIMENEZ-CERVANTES, C., IMOKAWA, G., BREWINGTON, T., SOLANO, F., GARCIA-BORRON, J. C. & HEARING, V. J. 1994. Tyrosinase related protein 1 (TRP1) functions as a DHICA oxidase in melanin biosynthesis. *The EMBO journal,* 13**,** 5818-5825.

KORNER, A. & PAWELEK, J. 1982. Mammalian tyrosinase catalyzes three reactions in the biosynthesis of melanin. *Science,* 217**,** 1163.

KUBIC, J. D., YOUNG, K. P., PLUMMER, R. S., LUDVIK, A. E. & LANG, D. 2008. Pigmentation PAX-ways: The role of Pax3 in melanogenesis, melanocyte stem cell maintenance, and disease. *Pigment cell & melanoma research,* 21**,** 627-645.

LARS STEINSTRAESSER, A. R., KAI GEVERS, MICHAEL SORKIN, TOBIAS HIRSCH, MARCO KESTING, MICHAEL SAND, SAMMY AL-BENNA, STEFAN LANGER, HANS-ULRICH STEINAU, AND FRANK JACOBSEN 2009. A Human Full-Skin Culture System for Interventional Studies. *Eplasty,* 9.

LE POOLE, I. C., VAN DEN WIJNGAARD, R. M., WESTERHOF, W., DORMANS, J. A., VAN DEN BERG, F. M., VERKRUISEN, R. P., DINGEMANS, K. P. & DAS, P. K. 1994. Organotypic culture of human skin to study melanocyte migration. *Pigment Cell Research / sponsored by the European Society for Pigment Cell Research and the International Pigment Cell Society,* 7**,** 33-43.

LEBONVALLET, N., JEANMAIRE, C., DANOUX, L., SIBILLE, P., PAULY, G. & MISERY, L. 2010. The evolution and use of skin explants: potential and limitations for dermatological research. *Eur J Dermatol,* 20**,** 671-84.

LEE, H. O., LEVORSE, J. M. & SHIN, M. K. 2003. The endothelin receptor-B is required for the migration of neural crest-derived melanocyte and enteric neuron precursors. *Dev Biol,* 259**,** 162-75.

LEIF, R. C., STEIN, J. H. & ZUCKER, R. M. 2004. A short history of the initial application of anti-5-BrdU to the detection and measurement of S phase. *Cytometry.Part A : the journal of the International Society for Analytical Cytology,* 58**,** 45-52.

LEVY, C., KHALED, M. & FISHER, D. E. 2006. MITF: master regulator of melanocyte development and melanoma oncogene. *Trends Mol Med,* 126**,** 406-414.Epub 2006.

LEVY, V., LINDON, C., ZHENG, Y., HARFE, B. D. & MORGAN, B. A. 2007a. Epidermal stem cells arise from the hair follicle after wounding. *The FASEB Journal,* 21**,** 1358-1366.

LEVY, V., LINDON, C., ZHENG, Y., HARFE, B. D. & MORGAN, B. A. 2007b. Epidermal stem cells arise from the hair follicle after wounding. *FASEB J,* 21**,** 1358-1366.

LI, G., SCHAIDER, H., SATYAMOORTHY, K., HANAKAWA, Y., HASHIMOTO, K. & HERLYN, M. 2001. Downregulation of E-cadherin and Desmoglein 1 by autocrine hepatocyte growth factor during melanoma development. *Oncogene,* 20**,** 8125-35.

LI, L., FUKUNAGA-KALABIS, M., YU, H., XU, X., KONG, J., LEE, J. T. & HERLYN, M. 2010. Human dermal stem cells differentiate into functional epidermal melanocytes. *Journal of Cell Science,* 123**,** 853-860.

LIN, J. Y. & FISHER, D. E. 2007. Melanocyte biology and skin pigmentation. *Nature,* 445**,** 843-850.

LORENZ, H. P. & ADZICK, N. S. 1993. Scarless skin wound repair in the fetus. *The Western journal of medicine,* 159**,** 350-355.

LUO, S., YUFIT, T., CARSON, P., FIORE, D., FALANGA, J., LIN, X., MAMAKOS, L. & FALANGA, V. 2011. Differential keratin expression during epiboly in a wound model of bioengineered skin and in human chronic wounds. *Int J Low Extrem Wounds,* 10**,** 122-9.

MARGADANT, C., CHARAFEDDINE, R. A. & SONNENBERG, A. 2010. Unique and redundant functions of integrins in the epidermis. *FASEB J,* 24**,** 4133-52.

MARKS, M. S. & SEABRA, M. C. 2001. The melanosome: membrane dynamics in black and white. *Nat Rev Mol Cell Biol,* 2**,** 738-48.

MARKS, R. & NISHIKAWA, T. 1973. Active epidermal movement in human skin in vitro. *Br J Dermatol,* 88**,** 245-8.

MARTIN, P. 1997. Wound healing--aiming for perfect skin regeneration. *Science (New York, N.Y.),* 276**,** 75-81.

MARTIN, P. & LEWIS, J. 1992. Actin cables and epidermal movement in embryonic wound healing. *Nature,* 360**,** 179-83.

MASUNAGA, T., SHIMIZU, H., YEE, C., BORRADORI, L., LAZAROVA, Z., NISHIKAWA, T. & YANCEY, K. B. 1997. The extracellular domain of BPAG2 localizes to anchoring filaments and its carboxyl terminus extends to the lamina densa of normal human epidermal basement membrane. *J Invest Dermatol,* 109**,** 200-6.

MEDIC, S. & ZIMAN, M. 2010. PAX3 expression in normal skin melanocytes and melanocytic lesions (naevi and melanomas). *PLoS One,* 5**,** e9977.

MENDOZA-GARCIA, J., SEBASTIAN, A., ALONSO-RASGADO, T. & BAYAT, A. 2015. Optimization of an ex vivo wound healing model in the adult human skin: Functional evaluation using photodynamic therapy. *Wound Repair Regen,* 23**,** 685-702.

MESZAROS, A. J., REICHNER, J. S. & ALBINA, J. E. 2000. Macrophage-induced neutrophil apoptosis. *J Immunol,* 165**,** 435-41.

MINWALLA, L., ZHAO, Y., LE POOLE, I. C., WICKETT, R. R. & BOISSY, R. E. 2001. Keratinocytes play a role in regulating distribution patterns of recipient melanosomes in vitro. *The Journal of investigative dermatology,* 117**,** 341-347.

MITCHISON, T. J. & CRAMER, L. P. 1996. Actin-Based Cell Motility and Cell Locomotion. *Cell,* 84**,** 371-379.

MORT, R. L., JACKSON, I. J. & PATTON, E. E. 2015. The melanocyte lineage in development and disease. *Development,* 142**,** 620-32.

MURAWALA, P., TANAKA, E. M. & CURRIE, J. D. 2012. Regeneration: the ultimate example of wound healing. *Semin Cell Dev Biol,* 23**,** 954-62.

NISHIMURA, E. K. 2011. Melanocyte stem cells: a melanocyte reservoir in hair follicles for hair and skin pigmentation. *Pigment Cell & Melanoma Research,* 24**,** 401-410.

OETTING, W. S. & SETALURI, V. 2007. The Tyrosinase Gene Family. *The Pigmentary System.* Blackwell Publishing Ltd.

OLCZYK, P., MENCNER, L. & KOMOSINSKA-VASSEV, K. 2014. The role of the extracellular matrix components in cutaneous wound healing. *Biomed Res Int,* 2014**,** 747584.

OPDECAMP, K., NAKAYAMA, A., NGUYEN, M. T., HODGKINSON, C. A., PAVAN, W. J. & ARNHEITER, H. 1997. Melanocyte development in vivo and in neural crest cell cultures: crucial dependence on the Mitf basic-helix-loop-helix-zipper transcription factor. *Development,* 124**,** 2377-86.

PAJEROWSKI, J. D., DAHL, K. N., ZHONG, F. L., SAMMAK, P. J. & DISCHER, D. E. 2007. Physical plasticity of the nucleus in stem cell differentiation. *Proc Natl Acad Sci U S A,* 104**,** 15619-24.

PANOUSOPOULOU, E., HOBBS, C., MASON, I., GREEN, J. B. & FORMSTONE, C. J. 2016. Epiboly generates the epidermal basal monolayer and spreads the nascent mammalian skin to enclose the embryonic body. *J Cell Sci,* 129**,** 1915-27.

PANZELLA, L., NAPOLITANO, A. & D'ISCHIA, M. 2011. Is DHICA the key to dopachrome tautomerase and melanocyte functions? *Pigment Cell Melanoma Res,* 24**,** 248-9.

PATEL, G. K., WILSON, C. H., HARDING, K. G., FINLAY, A. Y. & BOWDEN, P. E. 2006. Numerous Keratinocyte Subtypes Involved in Wound Re-Epithelialization. *Journal of Investigative Dermatology,* 126**,** 497-502.

PEPPER, F. J. 1954. The epithelial repair of skin wounds in the guinea-pig with special reference to the participation of melanocytes. *Journal of Morphology,* 95**,** 471-499.

PETERS, E. M., MAURER, M., BOTCHKAREV, V. A., JENSEN, K., WELKER, P., SCOTT, G. A. & PAUS, R. 2003. Kit is expressed by epithelial cells in vivo. *The Journal of investigative dermatology,* 121**,** 976-984.

PETERSEN, M., DAVIDS, L. M. & KIDSON, S. H. 2012. Simultaneous immunofluorescent labeling using anti-BrdU monoclonal antibody and a melanocyte-specific marker in formalin-fixed paraffin-embedded human skin samples. *Applied Immunohistochemistry & Molecular Morphology,* 20**,** 614-617.

PETIT, V. & LARUE, L. 2016. Any route for melanoblasts to colonize the skin! *Experimental Dermatology,* 25**,** 669-673.

PILCHER, B. K., SUDBECK, B. D., DUMIN, J. A., WELGUS, H. G. & PARKS, W. C. 1998. Collagenase-1 and collagen in epidermal repair. *Arch Dermatol Res,* 290 Suppl**,** S37-46.

PINCELLI, C. & MARCONI, A. 2010. Keratinocyte stem cells: friends and foes. *J Cell Physiol,* 225**,** 310-5.

POLAK, J. M. & VAN NOORDEN, S. 1997. *Introduction to immunocytochemistry,* Oxford, BIOS Scientific Publishers in association with the Royal Microscopical Society.

POWELL, A. M., SAKUMA-OYAMA, Y., OYAMA, N. & BLACK, M. M. 2005. Collagen XVII/BP180: a collagenous transmembrane protein and component of the dermoepidermal anchoring complex. *Clin Exp Dermatol,* 30**,** 682-7.

RAPOSO, G. & MARKS, M. S. 2007. Melanosomes – dark organelles enlighten endosomal membrane transport. *Nature reviews. Molecular cell biology,* 8**,** 786-797.

RAPOSO, G., TENZA, D., MURPHY, D. M., BERSON, J. F. & MARKS, M. S. 2001. Distinct protein sorting and localization to premelanosomes, melanosomes, and lysosomes in pigmented melanocytic cells. *J Cell Biol,* 152**,** 809-24.

RICHARDSON, R., SLANCHEV, K., KRAUS, C., KNYPHAUSEN, P., EMING, S. & HAMMERSCHMIDT, M. 2013. Adult zebrafish as a model system for cutaneous wound-healing research. *J Invest Dermatol,* 133**,** 1655-65.

RITTIE, L. 2016. Cellular mechanisms of skin repair in humans and other mammals. *J Cell Commun Signal,* 10**,** 103-20.

ROMRELL, R. 1989. *Histology: A Text and Atlas*.

SAFFERLING, K., SUTTERLIN, T., WESTPHAL, K., ERNST, C., BREUHAHN, K., JAMES, M., JAGER, D., HALAMA, N. & GRABE, N. 2013. Wound healing revised: a novel reepithelialization mechanism revealed by in vitro and in silico models. *J Cell Biol,* 203**,** 691-709.

SCHEPSKY, A., BRUSER, K., GUNNARSSON, G. J., GOODALL, J., HALLSSON, J. H., GODING, C. R., STEINGRIMSSON, E. & HECHT, A. 2006. The microphthalmia-associated transcription factor Mitf interacts with beta-catenin to determine target gene expression. *Mol Cell Biol,* 26**,** 8914-27.

SCHIAFFINO, M. V. & TACCHETTI, C. 2005. The ocular albinism type 1 (OA1) protein and the evidence for an intracellular signal transduction system involved in melanosome biogenesis. *Pigment Cell Research,* 18**,** 227-233.

SCHOLZEN, T. & GERDES, J. 2000. The Ki-67 protein: from the known and the unknown. *J Cell Physiol,* 182**,** 311-22.

SEIJI, M., FITZPATRICK, T. B. & BIRBECK, M. S. C. 1961. The Melanosome: A Distinctive Subcellular Particle of Mammalian Melanocytes and the Site of Melanogenesis1. *Journal of Investigative Dermatology,* 36**,** 243-252.

SHAW, T. J. & MARTIN, P. 2009. Wound repair at a glance. *J Cell Sci,* 122**,** 3209-13.

SHILO, S., ROY, S., KHANNA, S. & SEN, C. K. 2007. MicroRNA in cutaneous wound healing: a new paradigm. *DNA Cell Biol,* 26**,** 227-37.

SIMPSON, C. L., PATEL, D. M. & GREEN, K. J. 2011. Deconstructing the skin: cytoarchitectural determinants of epidermal morphogenesis. *Nat Rev Mol Cell Biol,* 12**,** 565-80.

SITARAM, A. & MARKS, M. S. 2012. Mechanisms of protein delivery to melanosomes in pigment cells. *Physiology (Bethesda),* 27**,** 85-99.

SNELL, R. S. 1963. A study of the melanocytes and melanin in a healing deep wound. *Journal of Anatomy,* 97**,** 243-253.

SNYDER, M. L. & PAULINO, A. F. 2002. Melan-A as a useful diagnostic immunohistochemical stain for the diagnosis of primary sinonasal melanomas. *Head Neck,* 24**,** 52-5.

SOLANO, F. & GARCÍA-BORRÓN, J. C. 2007. Enzymology of Melanin Formation. *The Pigmentary System.* Blackwell Publishing Ltd.

SPRITZ, R. A., HO, L., FURUMURA, M. & HEARING, V. J., JR. 1997. Mutational analysis of copper binding by human tyrosinase. *J Invest Dermatol,* 109**,** 207-12.

STEEL, K. P., DAVIDSON, D. R. & JACKSON, I. J. 1992. TRP-2/DT, a new early melanoblast marker, shows that steel growth factor (c-kit ligand) is a survival factor. *Development,* 115**,** 1111-9.

SZABO, G. 1954. The number of melanocytes in human epidermis. *British medical Journal,* 1**,** 1016.

TADOKORO, T., KOBAYASHI, N., ZMUDZKA, B. Z., ITO, S., WAKAMATSU, K., YAMAGUCHI, Y., KOROSSY, K. S., MILLER, S. A., BEER, J. Z. & HEARING, V. J. 2003. UV-induced DNA damage and melanin content in human skin differing in racial/ethnic origin. *Faseb j,* 17**,** 1177-9.

TAI, G., REID, B., CAO, L. & ZHAO, M. 2009. Electrotaxis and wound healing: experimental methods to study electric fields as a directional signal for cell migration. *Methods Mol Biol,* 571**,** 77-97.

TAMMI , R., JANSEN, C. T. & SANTTI, R. 1979. Histometric analysis of human skin in organ culture. *Journal of Investigative dermatology,* 73**,** 138-140.

TANG, A., ELLER, M. S., HARA, M., YAAR, M., HIROHASHI, S. & GILCHREST, B. A. 1994. E-cadherin is the major mediator of human melanocyte adhesion to keratinocytes in vitro. *J Cell Sci,* 107 (Pt 4)**,** 983-92.

TAYLOR, K. L., LISTER, J. A., ZENG, Z., ISHIZAKI, H., ANDERSON, C., KELSH, R. N., JACKSON, I. J. & PATTON, E. E. 2011. Differentiated melanocyte cell division occurs in vivo and is promoted by mutations in Mitf. *Development,* 138**,** 3579-89.

TAYLOR, S. C. 2002. Skin of color: biology, structure, function, and implications for dermatologic disease. *J Am Acad Dermatol,* 46**,** S41-62.

THONG, H. Y., JEE, S. H., SUN, C. C. & BOISSY, R. E. 2003. The patterns of melanosome distribution in keratinocytes of human skin as one determining factor of skin colour. *The British journal of dermatology,* 149**,** 498-505.

USUI, M. L., UNDERWOOD, R. A., FLECKMAN, P. & OLERUD, J. E. 2013. Parakeratotic corneocytes play a unique role in human skin wound healing. *J Invest Dermatol,* 133**,** 856-8.

VELANGI, S. S. & REES, J. L. 2001. Why are scars pale? An immunohistochemical study indicating preservation of melanocyte number and function in surgical scars. *Acta Derm Venereol,* 81**,** 326-8.

VITICCHIE, G., LENA, A. M., CIANFARANI, F., ODORISIO, T., ANNICCHIARICO-PETRUZZELLI, M., MELINO, G. & CANDI, E. 2012. MicroRNA-203 contributes to skin re-epithelialization. *Cell Death Dis,* 3**,** e435.

VOLLMAR, B., EL-GIBALY, A. M., SCHEUER, C., STRIK, M. W., BRUCH, H. P. & MENGER, M. D. 2002. Acceleration of cutaneous wound healing by transient p53 inhibition. *Lab Invest,* 82**,** 1063-71.

WEHRLE-HALLER, B. 2003. The role of Kit-ligand in melanocyte development and epidermal homeostasis. *Pigment Cell Res,* 16**,** 287-96.

WHITEMAN, D. C., PARSONS, P. G. & GREEN, A. C. 1999. Determinants of melanocyte density in adult human skin. *Archives of Dermatological Research,* 291**,** 511-516.

WOLFF, K. & STINGL, G. 1983. The Langerhans Cell. *The Journal of investigative dermatology,* 80**,** 17s-21s.

XIONG, X., WU, T. & HE, S. 2013. Physical forces make rete ridges in oral mucosa. *Med Hypotheses,* 81**,** 883-6.

XU, W., JONG HONG, S., JIA, S., ZHAO, Y., GALIANO, R. D. & MUSTOE, T. A. 2012. Application of a partial-thickness human ex vivo skin culture model in cutaneous wound healing study. *Lab Invest,* 92**,** 584-99.

XUE, M. & JACKSON, C. J. 2015. Extracellular Matrix Reorganization During Wound Healing and Its Impact on Abnormal Scarring. *Advances in Wound Care,* 4**,** 119-136.

YAAR, M. & GILCHREST, B. A. 1991. Human melanocyte growth and differentiation: a decade of new data. *J Invest Dermatol,* 97**,** 611-7.

YAMAGUCHI, Y., BRENNER, M. & HEARING, V. J. 2007. The regulation of skin pigmentation. *J Biol Chem,* 282**,** 27557-61.

YANG, X., WANG, J., GUO, S.-L., FAN, K.-J., LI, J., WANG, Y.-L., TENG, Y. & YANG, X. 2011. miR-21 Promotes Keratinocyte Migration and Re-epithelialization During Wound Healing. *International Journal of Biological Sciences,* 7**,** 685-690.

ZABIEROWSKI, S. E., FUKUNAGA-KALABIS, M., LI, L. & HERLYN, M. 2011. Dermis-derived stem cells: a source of epidermal melanocytes and melanoma? *Pigment Cell Melanoma Res,* 24**,** 422-9.

ZAIDI, Z. & LANIGAN, S. W. 2010. Skin: Structure and Function. 1-15.

ZHAO, M. 2009. Electrical fields in wound healing-An overriding signal that directs cell migration. *Semin Cell Dev Biol,* 20**,** 674-82.